Chair of Ferrous Metallurgy

Doctoral Thesis

Investigation on thermal plasma pyrolysis of methane for hydrogen gas and solid carbon production

Dipl.-Ing. Oday Daghagheleh

September 2024

AFFIDAVIT

I declare on oath that I wrote this thesis independently, did not use any sources and aids other than those specified, have fully and truthfully reported the use of generative methods and models of artificial intelligence, and did not otherwise use any other unauthorized aids.

I declare that I have read, understood and complied with the "Good Scientific Practice" of the Montanuniversität Leoben.

Furthermore, I declare that the electronic and printed versions of the submitted thesis are identical in form and content.

Date 09.09.2024

_____
Signature Author
Oday Daghagheleh

Abstract

As an intermediate step toward phasing out fossil fuels, natural gas can be cracked into hydrogen with solid carbon as a valuable byproduct, preventing atmospheric carbon release. This study explores the innovative concept of cracking natural gas into hydrogen and solid carbon via plasma pyrolysis. Initial feasibility testing shows high-efficiency potential, though process optimization is essential. A statistical parameter study highlights the significant influence of parameters such as plasma gas, power input, and arc length on process outcomes. Experiments are conducted using a thermal plasma reactor with a variable gas mixture of Ar and CH_4 to form a DC-transferred plasma arc. The product gas is analyzed, and the plasma arc is recorded with a camera on the top lid. Images reveal carbon formation and growth, leading to disruptive interruptions and reduced process efficiency. Despite this, a high H_2 yield of 67% to 100% is achieved. Higher CH_4 content and extended arc lengths disturb the plasma arc, lowering the H_2 yield, while increased power input and a wider reaction zone improve it. Characterization of the produced carbon shows distinct microstructural differences between samples from the gas filter and reaction chamber. SEM analyses reveal finer textures in the former and larger dendritic particles in the latter. Raman spectroscopy confirms crystalline graphite-like structures with low defect concentrations. XRD supports these findings, indicating graphitic crystalline structures. EDS and ICP-MS analyses confirm high-purity carbon. BET surface area analysis shows significant variations, with filter-collected samples ranging from 40 to 170 m²/g compared to 7 to 30 m²/g for chamber-collected samples, correlating with smaller particle size and higher defect numbers. Establishing a new plasma testing facility is the next crucial step, providing a platform for data production and validation, paving the way for commercial-scale implementation.

Kurzfassung

Als ein Zwischenschritt zum Ausstieg aus fossilen Brennstoffen kann Erdgas in Wasserstoff umgewandelt werden, wobei fester Kohlenstoff als wertvolles Nebenprodukt entsteht und eine Freisetzung von Kohlenstoff in die Atmosphäre verhindert wird. Diese Studie untersucht das innovative Konzept der Umwandlung von Erdgas in Wasserstoff und festen Kohlenstoff mittels Plasmapyrolyse. Erste Machbarkeitsstudien zeigen ein hohes Effizienzpotenzial, obwohl eine Prozessoptimierung notwendig ist. Eine statistische Parameterstudie hebt den signifikanten Einfluss von Parametern wie dem Plasmagas, der Leistungsaufnahme und der Lichtbogenlänge auf die Prozessergebnisse hervor. Experimente werden mit einem thermischen Plasmareaktor durchgeführt, der ein variables Gasgemisch aus Ar und CH_4 verwendet, um einen DC-übertragenen Lichtbogen zu erzeugen. Das Produktgas wird analysiert und der Lichtbogen mit einer Kamera im Deckel aufgezeichnet. Bilder zeigen die Bildung und das Wachstum von Kohlenstoff, was zu störenden Unterbrechungen und verminderter Prozesseffizienz führt. Trotz dieser Probleme wird eine hohe H_2-Ausbeute von 67% bis 100% erreicht. Höhere CH_4-Gehalte und verlängerte Lichtbogenlängen stören den Lichtbogen und verringern die H_2-Ausbeute, während erhöhte Leistungsaufnahme und ein breiterer Reaktionsbereich diese verbessern. Die Charakterisierung des erzeugten Kohlenstoffs zeigt deutliche mikrostrukturelle Unterschiede zwischen den Proben aus dem Gasfilter und der Reaktionskammer. SEM-Analysen zeigen feinere Texturen in ersteren und größere, dendritische Partikel in letzteren. Raman-Spektroskopie bestätigt kristalline, graphitartige Strukturen mit geringen Defektkonzentrationen. XRD unterstützt diese Ergebnisse und weist auf graphitische kristalline Strukturen hin. EDS- und ICP-MS-Analysen bestätigen hochreinen Kohlenstoff. BET-Oberflächenanalyse zeigt signifikante Unterschiede, wobei Filterproben Werte von 40 bis 170 m²/g im Vergleich zu 7 bis 30 m²/g für Kammerproben

aufweisen, was mit kleineren Partikelgrößen und höheren Defektzahlen korreliert. Der Aufbau einer neuen Plasmatestanlage ist der nächste entscheidende Schritt und bietet eine Plattform für die Datenerfassung und Validierung, wodurch der Weg für die kommerzielle Umsetzung geebnet wird.

Acknowledgment

I want to primarily thank my dear supervisor and Professor, Johannes Schenk, for being such a supportive person not only in my professional pathway but also in my personal life. His personality and genuine care for others have been inspiring for me.

My gratitude also goes to my mentor and Professor, Markus Lehner, for his support and wise consultation during my thesis work. I appreciate all my colleagues for their help. Without them, this work could not be accomplished. I want to mention some of those who are highlighted in my mind: Susanne Michelic for promoting me; the coordinator of the project, Robert Obenaus-Emler; my colleague and friend Michael Zarl, for his tips and support; Manuel Farkas, for his help in the laboratory; my students with their assistance; Andreas Sprung, who always makes things easier than they look; my previous mentor, Daniel Spreitzer for believing in me; and Heng Zheng, my buddy, during these years.

My heart is filled with love towards my parents, Walid and Zeynab, making me keep carrying on in any situation. All I have and would achieve come from them and their sacrifices. To them, I dedicate this book. Having my sister Naghmeh, with her heartwarming energy sent over from overseas, has always cheered me. I want to thank Naghmeh and my brother-in-law, Habib, for taking care of our parents back home. I appreciate my other sister, Haleh, and brother, Asad, who made me feel like I was not away from my family.

In 2016, I started a new chapter in Leoben. I think Leoben and the whole community of Austria at large, which I have become a part of now, have given me a chance to build a new life with a better version of myself. I appreciate you all from the bottom of my heart.

Table of Contents

List of Figures

List of Tables

Nomenclature

ΔH°	[kJ/mol]	Standard enthalpy
$C_{V,Ar}$	[vol. %]	Gas concentration of Ar in product gas
C_{V,H_2}	[vol. %]	Gas concentration of H_2 in product gas
I	[A]	Electric current
t_{cyc}	[min]	Time of a measuring cycle
V	[V]	Electric voltage
V_{Ar}	[Nl]	Gas volume of Ar
$V_{H_{2-produced}}$	[Nl]	Gas volume of H_2 produced
$V_{CH_{4-in}}$	[Nl]	Gas volume of CH_4 input
$\dot{V}_{Ar}$	[Nl/min]	Gas volume flow rate of Ar
$\dot{V}_{CH_{4-in}}$	[Nl/min]	Gas volume flow rate of CH_4 input

Abbreviations

AC	Alternating Current
BET	Brunauer Emmett Teller
CB	Carbon Black
CCS	Carbon Capture and Storage
CCU	Carbon Capture and Utilization
CNT	Carbon Nanotube
CVD	Chemical Vapor Deposition
DBD	Dielectric Barrier Discharge
DC	Direct Current
EDS	Energy Dispersive Spectroscopy
FCEV	Fuel Cell Electric Vehicle
GAD	Gliding Arc Discharge
GD	Glow Discharge
GHG	Greenhouse Gas
ICP-MS	Inductively Coupled Plasma Mass Spectrometry
ICE	Internal Combustion Engine
IEA	International Energy Agency

MUL	Montanuniversität Leoben
MW	Microwave
NG	Natural Gas
NTP	Non-thermal Plasma
NZE	Net Zero Emission
PEC	Photoelectrochemical
PEM	Polymer Electrolyte Membrane
POX	Partial Oxidation
PTP	Point-To-Point
RF	Radiofrequency
RSA	Rotating Sliding Arc
SEM	Scanning Electron Microscopy
SLM	Standard Liters per Minutes
SMR	Steam Methane Reforming
SSA	Specific Surface Area
TC	Thermochemical
TP	Thermal Plasma
TPP	Thermal Plasma Pyrolysis
TPPM	Thermal Plasma Pyrolysis of Methane
TSC	Turbostratic Carbon
XRD	X-ray Diffractometry

"We are those who revel in the wine without a cup,

Every morning we are illuminated, and every evening we are delighted.

They say you have no conclusion,

We are those who are happy without any conclusion."

Rumi

1. Introduction

In this section, after discussing the background and the necessity of taking actions toward problem solving, the work frame is extensively described in different work packages, where we learn the structure of this thesis.

1.1 Background and motivation

The escalating energy demand, driven by the growing global population and the expansion of industry and technology, necessitates the exploration of further energy sources. Conventional fossil resources like oil, coal, and natural gas (NG) are not only depleting but also have detrimental environmental impacts [1]. Statistical analyses underscore the significant role of the energy sector in CO_2 and SO_2 emissions, contributing 46% and 82%, respectively [2,3]. Forecasts suggest a concerning rise in CO_2 emissions from 50% in 2030 to 80% in 2050 [2].

The European Green Deal, a set of policies approved by the European Commission, has set a goal for Europe to achieve net-zero greenhouse gas (GHG) emissions by 2050 [4–6]. The Austrian Federal Government has targeted for climate neutrality in 2040 [7]. Moreover, there is a push to provide 100% of Austrian national electricity consumption from renewable sources by 2030 [7]. This shift towards sustainable energy sources emphasizes the need to transition away from fossil fuels. Hydrogen gas (H_2) has emerged as a promising solution in this transition, offering the potential for a reduction in dependency on imported fossil fuels and contributing to an environmental friendly energy supply [7]. Concurrently, climate-neutral H_2 can be an important sustainable option for a secure energy supply in Austria in the future [7].

However, the widespread adoption of H_2 production faces challenges related to production, storage, and transportation [2]. The majority of H_2 utilized in industrial applications is still mostly derived from fossil fuels [2]. Despite the sustainability of electrolysis of water, which currently accounts for only 4% of H_2 production, economic and energy-related constraints hinder its broader implementation [2,8].

A study from 1995 envisioned a future where 100% clean hydrogen would serve as the predominant energy source, named "the age of energy gases". An updated analysis of this prediction, coupled with the growing global population curve, is presented in Figure 1 [1,9,10]. The study indicates a transition from liquid and solid energy sources to gaseous resources such as methane gas (CH_4) and H_2, a trend projected to persist. The increasing demand for CH_4 as a fuel stems from its superior combustion efficiency and reduced pollutant emissions compared to traditional sources like oil and coal [2]. However, the direct utilization of CH_4 in the energy sector results in a significant increase in GHG emissions, unlike H_2. Urgent measures are necessary to mitigate the dangers of global warming and halt the growth of GHGs. This imperative entails accelerating the adoption of H_2, requiring the conversion of CH_4 to H_2 and ultimately transitioning entirely to "green hydrogen" production, potentially utilizing seawater as a source and leaving behind all fossil fuels.
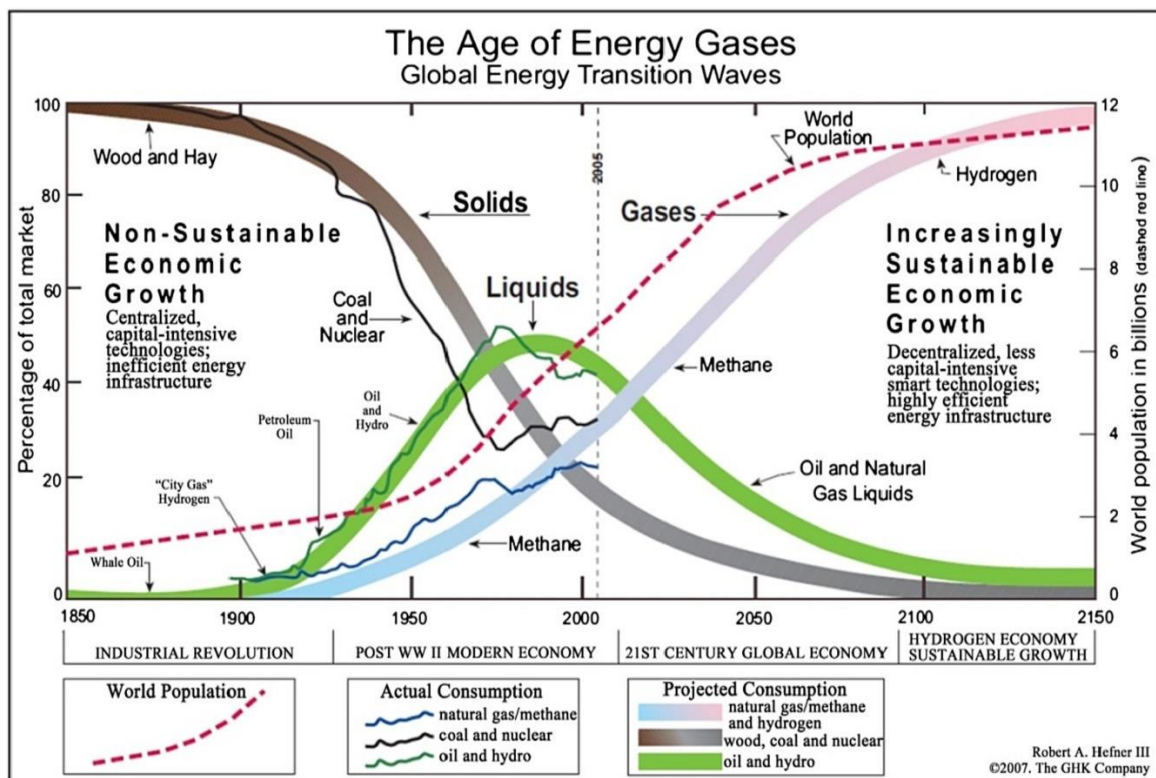
Figure 1. The Age of Energy Gases: Forecasting the global transition to H_2 in response to population growth [1].

In conclusion, considering the current infrastructure and challenges associated with electrolysis, hydrocarbons are expected to remain the primary hydrogen feedstock in the immediate future, serving as a midterm solution. Presently, steam methane reforming (SMR) dominates H_2 production, constituting approximately half of the global production of H_2 from CH_4 [3]. Additionally, other methods such as oil reforming and coal gasification contribute to H_2 production using diverse feed materials. Unfortunately, all these methods release CO_2 into the atmosphere, hindering efforts to reduce emissions. Specifically, SMR results in the production of approximately 10 kg of CO_2 for every kg of H_2 produced [3].

In this case, methane pyrolysis presents an alternative method with significant advantages. This process converts CH_4 into H_2 and valuable solid carbon, without releasing carbon oxides into the atmosphere. Moreover, pyrolysis demands 38 kJ of energy per mole of produced H_2, making it a significantly more efficient process compared to electrolysis, which requires seven times more energy, amounting to 285 kJ/mol H_2 [11].

H_2 serves not only as an energy carrier but also finds application in various industries, including steelmaking. Currently, steel production accounts for 7 to 9% of CO_2 emissions due to the use of fossil fuels such as coal in conventional steelmaking processes [12]. The widespread adoption of H_2 and its availability at low costs will accelerate the industry's transition to environmentally friendly practices. In the steel industry, H_2 can serve as a reductant agent for steel production. Several processes are under development for achieving 100% hydrogen-based steelmaking, including the HYFOR® process [13,14], and the HyREX® process [15], both utilizing the principle of fluidized bed reduction, along with the SuSteel project [16], which employs hydrogen plasma in a carbon-neutral steel production process.

As an alternative energy source, H_2 is increasingly drawing attention, driven by governmental and social pressures pushing industries to adopt sustainable and eco-friendly practices. There is a notable competition within the industry to meet these sustainability targets sooner. Projections suggest that demand will surge from 90 million tons in 2020 to over 150 million tons by 2030 [6]. Forecasts further reveal that 70 million tons are expected to be low-emission hydrogen [6]. Given that approximately 75% by weight of methane is converted into solid carbon, this process could produce a considerable amount of high-value solid carbon. Therefore, addressing the major carbon markets is imperative for optimizing the H_2 production process and compensating for the associated costs.

Methane pyrolysis, which occurs at temperatures exceeding 1200 °C, can be powered by various means, including electrical heating furnaces, solar furnaces, and plasma formation using electricity [3]. Various methods have been proposed for methane pyrolysis, with plasma technology being one of the intriguing options [17–25]. Plasma offers advantages, as it can

provide the necessary energy for the process and can be turned on and off without additional heating or processing steps [26]. This is particularly useful for on-site applications like the mentioned hydrogen-based steelmaking since it allows for immediate adjustments in hydrogen supply, eliminating the need for long-term storage. Furthermore, plasma operates at extremely high temperatures, reaching up to 10000 °C, that abolishes the need for catalysts [27]. This is significant because catalysts can pose problems such as carbon buildup and concerns about product purity. The use of plasma in carbon production is relatively new and enables the production of novel grades of carbon with high purity, along with the flexibility to adjust parameters [28]. Adding to these features, if the electricity for plasma is sourced from renewable sources and the resulting carbon is fully utilized in other sectors, the process achieves the goal of zero carbon footprint.

Given the recent advancements in plasma technology, there arises a necessity to develop a comprehensive process concept that can offer scientific insights into the principle of thermal plasma pyrolysis of methane (TPPM). This will enhance our understanding of the process, enabling improvements in both the process itself and the quality of the products. However, it is important to note that comprehending plasma technology can be intricate and often relies on experimental validation additional to theoretical calculations.

1.2 Objectives and framework

This work represents a comprehensive research and experimental endeavor focused on the noble concept of TPPM. The overarching aim is to formulate and refine the process concept, thereby providing valuable knowledge for scaling up the process and enhancing its efficiency.

To facilitate the explanation of the thesis structure, a framework is illustrated in Figure 2, highlighting the core focus of the study. Following the introduction of the theory of methane pyrolysis and a literature review on related research areas, Chapters 2 and 3, experimental work is presented, as indicated by the different pentagons in Figure 2.

Two crucial factors aimed at enhancing the process efficiency are ensuring a stable and continuous process with the highest possible H_2 yield and productivity. Another interconnected aspect represented by a pentagon in the figure is the quality of the produced material, namely solid carbon. Through experiments conducted using a lab-scale plasma furnace, a technical feasibility study and a parameter optimization study are carried out. The methodology and results of these experiments are presented in Chapters 4 and 5. Subsequently, an investigation on the produced carbon utilizing various methods is reported in Chapter 6.

Finally, drawing from the insights gained through the experiments and based on the conclusions derived, a new design for the concept is formulated in Chapter 7.
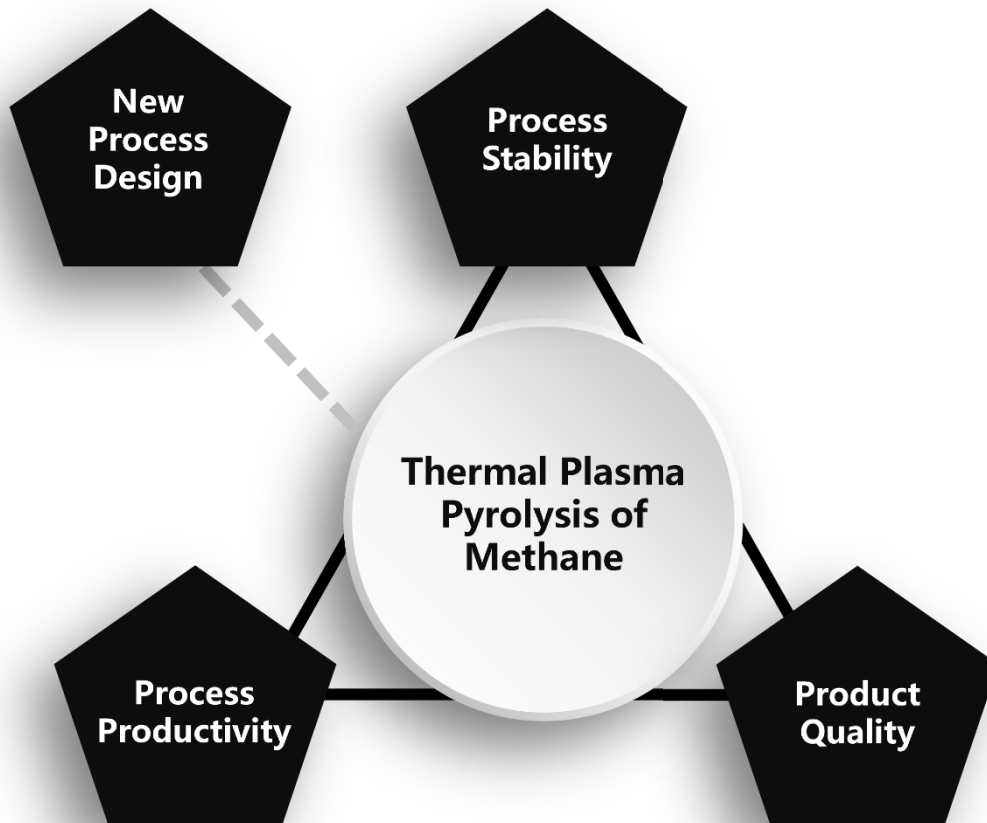
Figure 2. Framework illustration: Core components of the current study.

To achieve the defined goals, various work packages have been delineated as follows and are summarized in Table 1:

- **Work package 1: Literature review – Chapters 2-3**

Aim: Illuminating the concept of methane pyrolysis and conducting a comprehensive review of related published works with a focus on TPPM.

Execution: Due to the relative immaturity of the idea of TPPM, accessing detailed experimental works and research studies proved challenging. However, efforts were focused on tracking publications in publicly available libraries and journals to gather relevant knowledge and information to support the study.

- **Work package 2: Experimental analysis of TPPM – Chapters 4-5**

Aim: Testing the feasibility of the process, as well as determining and evaluating selected influencing factors on process stability and productivity.

Execution: Various trials were conducted to systematically study the process and the relationship between process parameters and both process stability and productivity using a lab-scale plasma furnace.

- **Work package 3: Investigation of produced solid carbon – Chapter 6**

Aim: Determining the characteristics of the produced solid carbon.

Execution: The solid carbon produced from the tests was collected and characterized using various methods.

- **Work package 4: Design and development of a concept for a new testing facility – Chapter 7**

Aim: Establishing a new thermal plasma facility for methane pyrolysis.

Execution: Specification of a process concept and communication with potential suppliers for a pilot plant should be initiated. Design and development of a new plasma plant for methane pyrolysis were undertaken, enabling trials with a wide range of process parameters.

Table 1. Summary of the various work packages in this thesis, along with their corresponding chapters.

Work package	Name	Chapter
1	Literature review	2-3
2	Experimental analysis of TPPM	4-5
3	Investigation of produced solid carbon	6
4	Design and development of a concept for a new testing facility	7

2 Methane pyrolysis: Hydrogen and Carbon

This chapter delves into the fundamentals of methane pyrolysis, focusing on its primary products: hydrogen and carbon. Additionally, it includes characterizations of these products along with intriguing facts about their properties. Finally different techniques and the current status of methane pyrolysis processes are listed and described in details.

2.1 Thermodynamic fundamentals

The principle of methane pyrolysis, known also as methane decarbonization, methane decomposition, and methane cracking, is the simple reaction of breaking the bonds on CH_4 molecoules and formation of 2 moles of H_2 and a solid carbon molecule. This lead to a mass-balance of 4 g of H_2 and 12 g of carbon.

This reaction is endothermic and requires energy input. The overall reaction and the standard enthalpy (at 25 °C and 1 atm) are shown in Equation 2-1. Figure 3 illustrates the thermodynamic aspects of CH_4 pyrolysis at temperatures from 0 up to 1300 °C and in a pressure range of 1 to 10 bar, as calculated using the FactSage 8.2 software with the FactPS database. For each mole of H_2 produced 37.8 kJ energy is required. The complete decomposition occurs at temperatures above 1200 °C. Higher pressures elevate the required temperature because the reaction produces two moles of gas for every mole of the original substance.

$$CH_4 \rightarrow C_{(s)} + 2H_2 \qquad \Delta H^{\circ}_{298} = 75.6 \, kJ/mol \qquad \text{2-1}$$
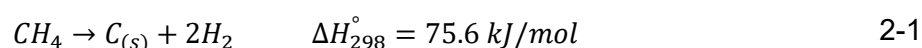
From the reaction equation with the corresponding thermodynamic data, it is evident that high temperatures and low pressures shift the equilibrium to the right side, making them desirable.
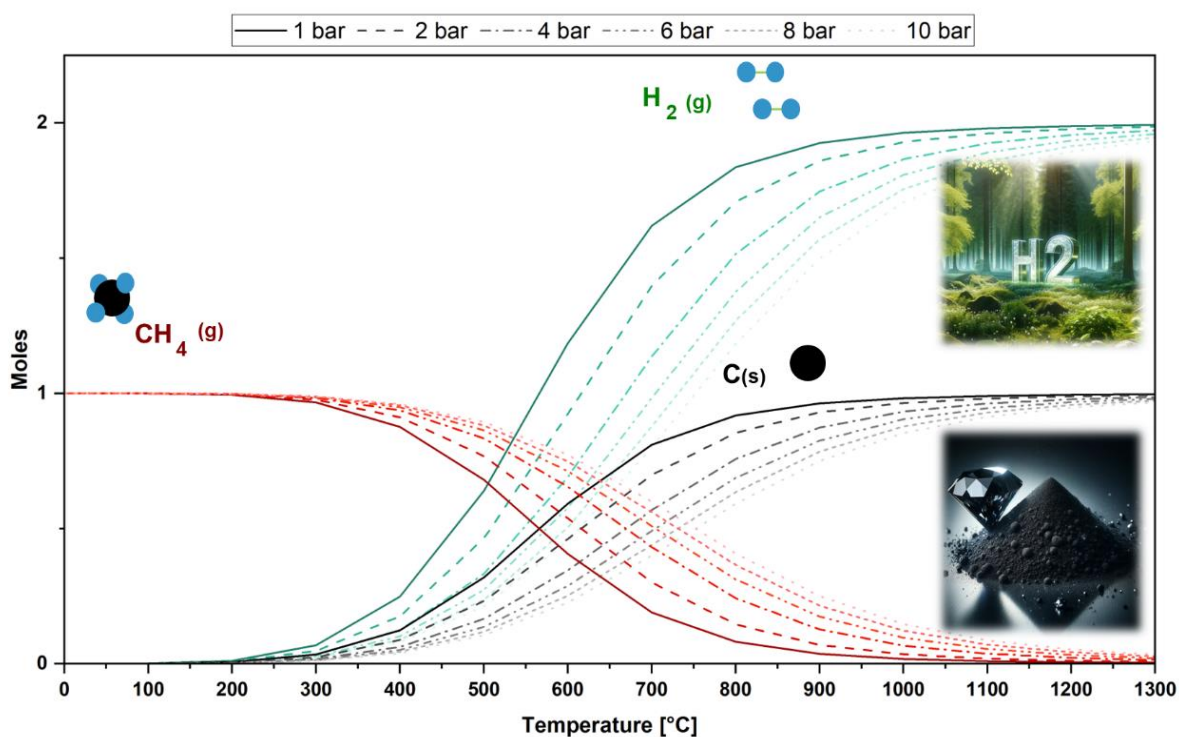
Figure 3. Overall reaction of methane pyrolysis and production of H_2 and solid carbon, calculated for a pressure range of 1 to 10 bar using FactSage 8.2 software.

Methane pyrolysis yields not only H_2 and carbon but also involves a complex interplay of kinetic constraints and decomposition mechanisms influenced by factors such as temperature, pressure, and reaction medium. Hydrocarbons rely on two primary bond types: carbon-carbon (C-C) and carbon-hydrogen (C-H). C-C bonds possess a lower energy of dissociation, rendering them weaker and more susceptible to breakage [29]. Consequently, thermal splitting of these bonds results in the formation of lighter hydrocarbons. Overall, the cracking process of hydrocarbons entails a series of simultaneous endothermic dissociations and exothermic recombination reactions within the reaction medium [30]. While CH_4, consisting of a single carbon atom, cannot be fractionated into lighter hydrocarbons, it can form higher unsaturated hydrocarbons. CH_4 exhibits instability compared to H_2 at temperatures exceeding 527 °C but remains the most stable hydrocarbon up to 1027 °C, beyond which Benzene (C_6H_6) becomes more stable than CH_4 [31]. Acetylene (C_2H_2), also known as ethyne, and ethylene (C_2H_4), also known as ethene, are the next stable hydrocarbons at start temperature of 1227 °C [29]. However, these products become unstable at elevated temperatures, and given a sufficiently

long reaction time, the final products revert to H_2 and C. To prevent the decomposition of C_2H_4 and C_2H_2, it is imperative to quench them [29,31]. Minimizing the reaction time enables the attainment of intermediate products from methane pyrolysis [31]. Figure 4 illustrates ten gas species in equilibrium, calculated from thermodynamic data by Gueret et at. [29], with carbon excluded as a product. The figure depicts the mole fraction at a total pressure of 1 bar and an H/C ratio of 4 [31].
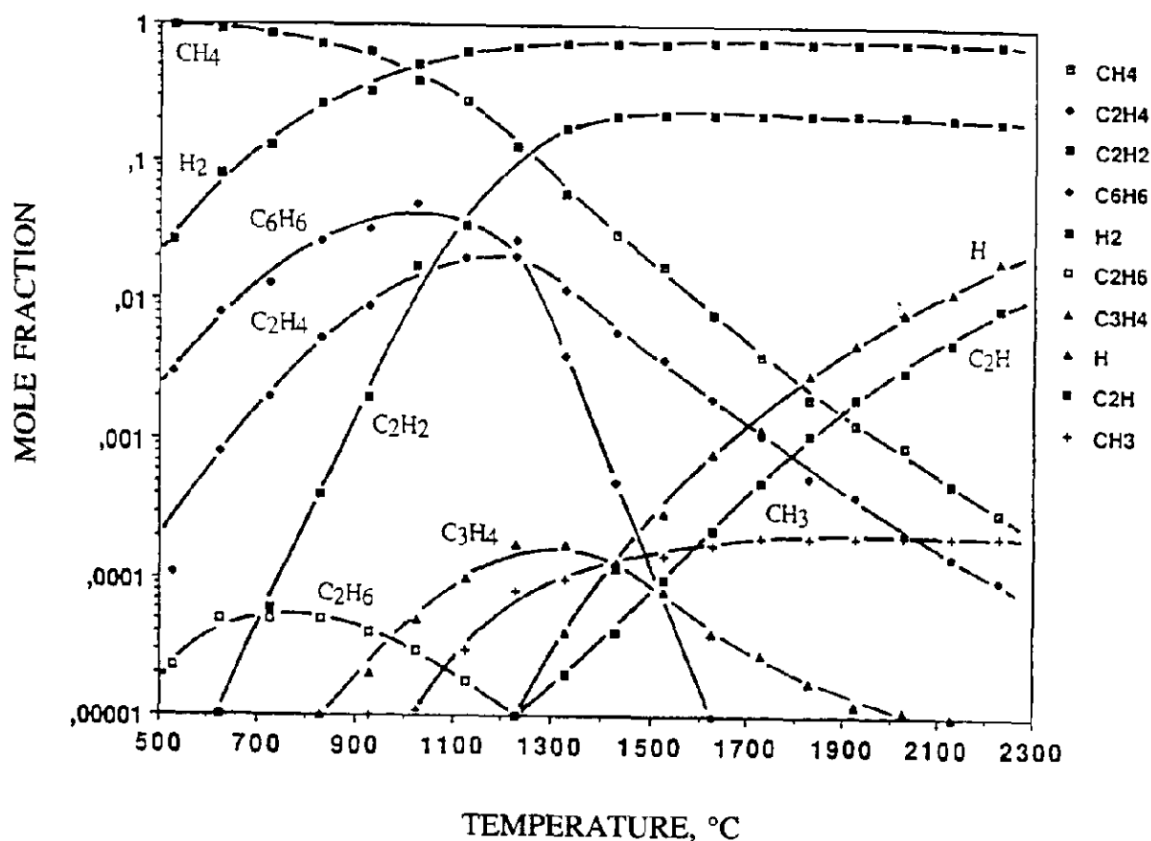
Figure 4. Equilibrium composition of methane decomposition calculations at a total pressure of 1 bar and an H/C ratio of 4 [29].

Numerous studies have been conducted to elucidate the detailed formation of hydrogen and carbon [29–34]. The stepwise reaction of methane decomposition can be described as follows [31]:

$$2CH_4 \rightarrow C_2H_6 + H_2 \qquad\qquad 2\text{-}2$$

$$C_2H_6 \rightarrow C_2H_4 + H_2 \qquad\qquad 2\text{-}3$$

$$C_2H_4 \rightarrow C_2H_2 + H_2 \qquad\qquad 2\text{-}4$$

$$C_2H_2 \rightarrow 2C + H_2 \qquad\qquad 2\text{-}5$$

In conclusion the overall reaction can be written as, where in each step a mole of H_2 is released [31]:

$$2CH_4 \rightarrow C_2H_6 \rightarrow C_2H_4 \rightarrow C_2H_2 \rightarrow 2C + H_2 \qquad\qquad 2\text{-}6$$
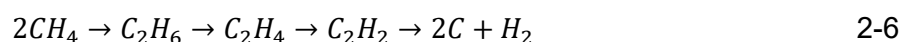
Incorporating solid carbon into the calculations reveals that the stable products are H_2 and solid carbon within temperature ranges of 1000 to 2500 °C, with the highest selectivity observed in the range of 1027 to 1927 °C (Figure 5) [35,36].
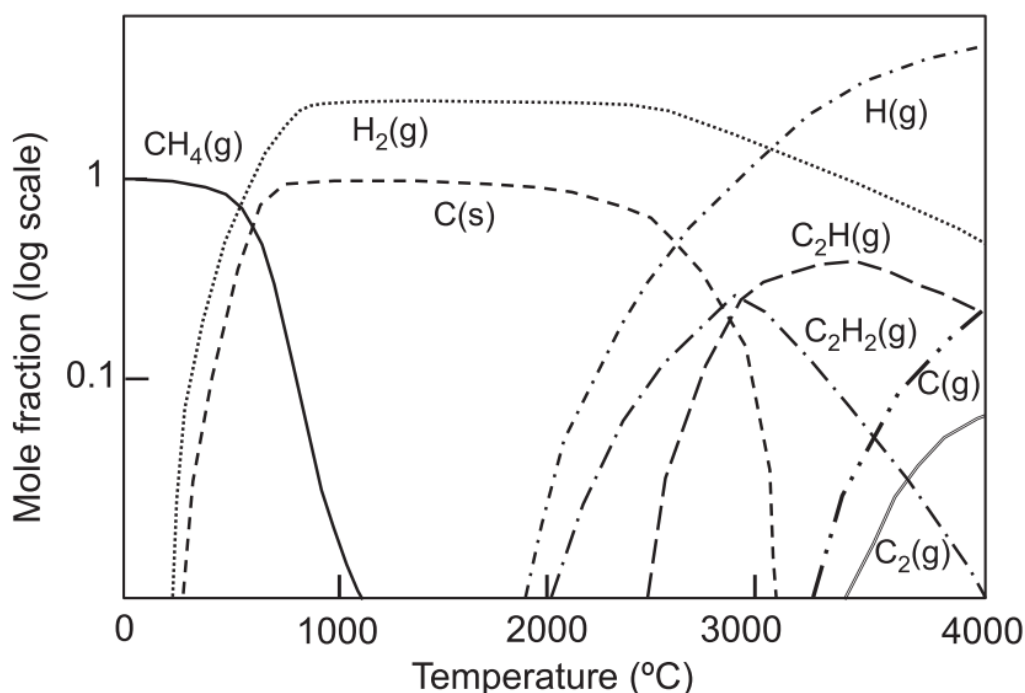
Figure 5. Simplified equilibrium of 1 mol methane pyrolysis and the different products in a temperature range up to 4000 °C [36].

2.2 Hydrogen, the future power

Hydrogen, a transparent, odorless, and flavourless element, comprises a single proton in its nucleus, encircled by a solitary electron. This elemental simplicity positions it as the lightest constituent on the periodic table. While it dominates the cosmos, constituting approximately 75% of its elemental mass, pure hydrogen is relatively uncommon on Earth due to its inclination to bond with other elements. It accounts for approximately 14% of the Earth's crust [37,38].

Today, hydrogen remains a fundamental component of stars, including our Sun, where nuclear fusion processes continuously generate energy by converting hydrogen into helium [39]. Though primarily found in molecular form in the universe, hydrogen also plays vital roles

within living organisms, including humans. It is a key component of water (H_2O), which constitutes approximately 60% of the human body by weight, serving as a critical solvent for biochemical reactions, amounting to around 10% of the human body's mass [38].

Highly reactive, hydrogen readily forms compounds with most elements, participating in various chemical reactions, such as combustion, oxidation, and reduction [37]. It boasts the lowest density of all gases at room temperature and exists as a diatomic, non-polar molecule, with a boiling point of -252.87 °C and a melting point of -259.16 °C [37].

Despite its highly flammable nature, burning in concentrations ranging from 4 to 75% by volume, hydrogen boasts a relatively high auto-ignition temperature of 585 °C, rendering it safer to handle compared to other fuels. Its thermal activation energy required to ignite a stoichiometric H_2/O_2 mixture is merely 0.02 mJ [37].

In summary, hydrogen's remarkable attributes, extensive cosmic presence, essential role in sustaining life, and wide-ranging applications underscore its significance as one of the universe's fundamental elements. Its potential as a clean and sustainable energy carrier holds promise for addressing critical environmental challenges and shaping the future of energy production and consumption.

2.2.1 Hydrogen production

The demand for H_2 is on the rise and is projected to escalate further, reaching 150 million tons by 2030 and over 430 million tons by 2050, as per the Net Zero Emissions by 2050 (NZE) scenario outlined by the International Energy Agency (IEA) (Figure 6) [40]. The NZE scenario lays out a model pathway for the global energy sector to achieve net zero CO_2 emissions by 2050. Notably, H_2 production must be accomplished using low-emission or zero-emission technologies [40].
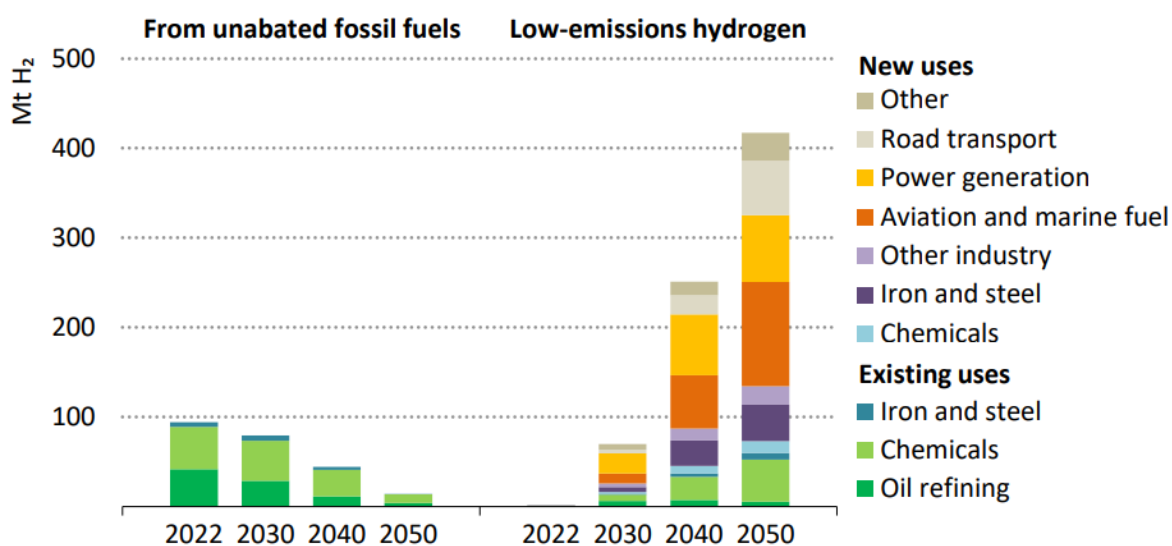
Figure 6. Global H_2 demand forecast, according to NZE Scenario in the years 2022 - 2050 [40].

H_2 production entails diverse methods and employs various feedstock options. These options encompass a spectrum of sources, including solar, nuclear, and wind energies, as well as electrolysis and conversion methods utilizing biomass, wood, coal, or NG [41]. Figure 7 illustrates a summary of the feedstocks utilized in H_2 production across various sources.
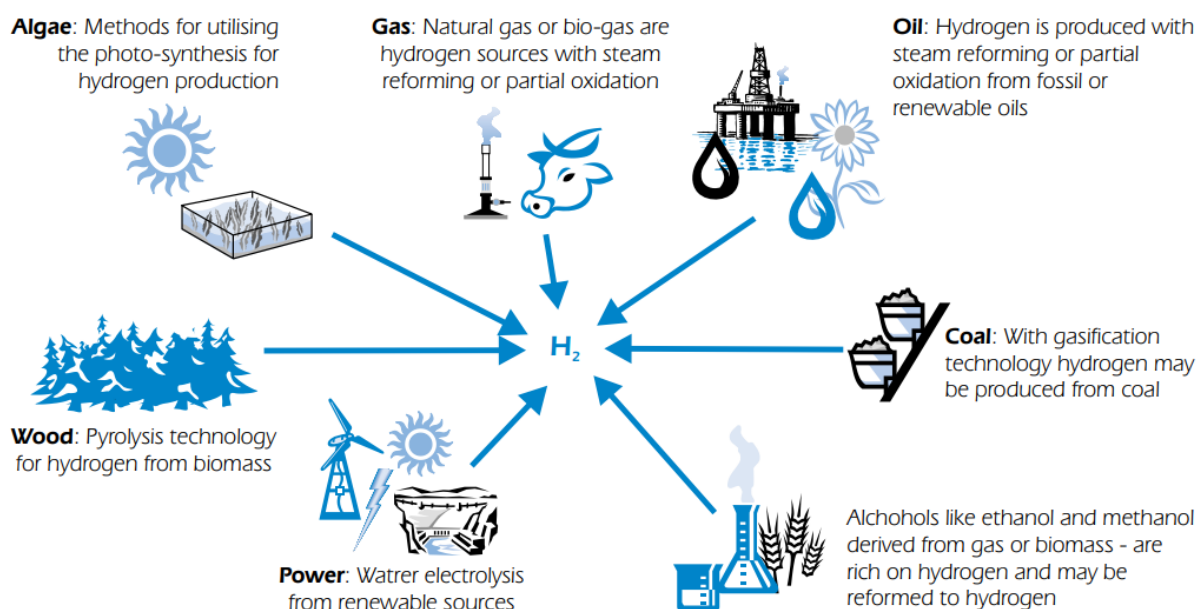
Figure 7. Feedstock varieties for H_2 Production [42].

Various pathways exist to convert these feedstocks into the final product of H_2. Figure 8 illustrates the different routes to H_2 production, highlighting TPPM in dark blue, which is the focus of the current work [43]. Examining the current global production of H_2, which was 95

million tonnes in 2022, fossil fuels hold the majority share in its production. The main methods include SMR from NG, coal gasification, and by-product hydrogen obtained at refineries and in the petrochemical industry during naphtha reforming, as depicted in Figure 9 [44]. Low-emission hydrogen production has a minimal share. The production methods are discussed in the following subsections.
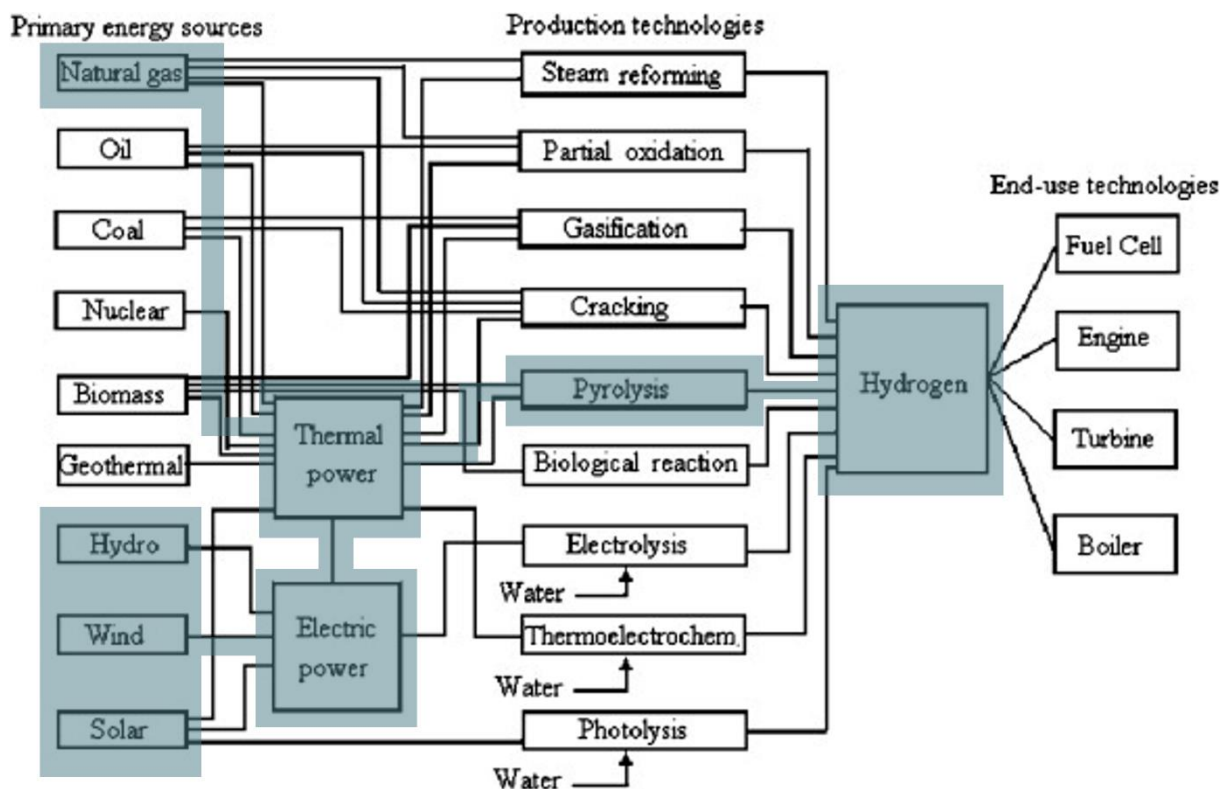
Figure 8. H$_2$ production routes, adapted and edited from [43].
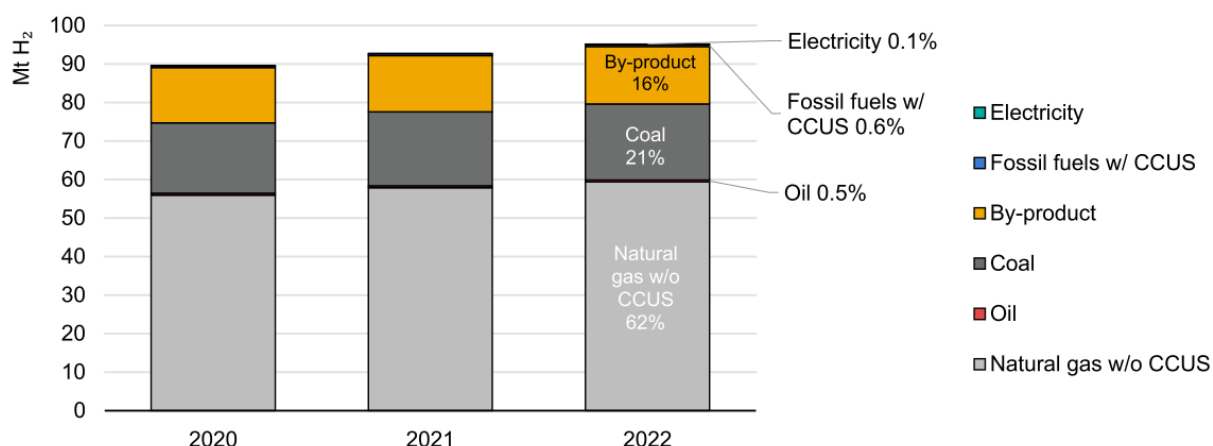
Note: CCUS= carbon capture, utilisation and storage.

Figure 9. Hydrogen production share by different technologies in the years 2020-2022 [44].

- **Steam methane reforming (SMR) process:**

SMR necessitates high temperatures, typically achieved by burning NG, to provide the required heat [42]. In SMR, steam (H_2O) reacts with CH_4 in the presence of a catalyst, typically nickel, at temperatures ranging from 700 to 1100 °C.

In the SMR process, steam reforming of NG (or CH_4 from other sources) leads to the production of a hydrogen-rich gas. This gas typically consists of approximately 70–75% H_2 on a dry basis, accompanied by smaller amounts of CH_4 (2–6%), carbon monoxide (CO) (7–10%), and CO_2 (6–14%) [42].

The SMR process involves a three-step sequence to produce H_2. Initially, CH_4 undergoes catalytic reforming at high temperatures and pressures, resulting in a syngas mixture composed of H_2 and CO. Following this, a catalytic shift reaction occurs, combining CO with H_2O to produce the desired H_2 product. Lastly, the H_2 product is purified via adsorption. The reforming step in gaseous state at standard conditions (25 °C and 1 atm) is described by the following reaction [42].

$$CH_4 + H_2O \leftrightarrow CO + 3H_2 \qquad \Delta H^{\circ}_{298} = +206 \ kJ/mol \qquad \text{2-7}$$
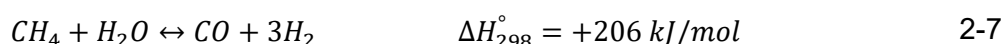
- **Partial oxidation (POX) of hydrocarbons:**

This method entails the partial oxidation of hydrocarbons, such as CH_4 or naphtha, using oxygen (O_2) or H_2O. By regulating the amounts of O_2 and H_2O, the reaction remains exothermic and does not necessitate external energy.

Similar to SMR, POX results in a syngas mixture comprising H_2 and carbon oxides, which can subsequently undergo further processing to yield pure H_2. An example reaction involving iso-octane is as follows [42]:

$$2C_8H_{18} + 2H_2O + 9O_2 \rightarrow 12CO + 4CO_2 + 20H_2 \qquad \text{2-8}$$

- **Coal gasification:**

H_2 can also be derived from coal through a process known as gasification. In this method, syngas (composed of CO and H_2) is produced from coal and can be further enriched with hydrogen [42]:

$$Coal(carbon \ source) + H_2O \rightarrow CO + H_2 + impurities \qquad \text{2-9}$$
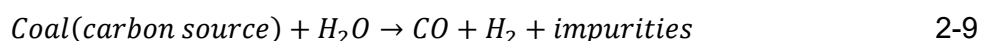
H_2O can then be shifted to produce additional H_2 by adjusting reaction conditions accordingly [42]:

$$CO + H_2O \rightarrow H_2 + CO_2 \qquad \text{2-10}$$

It is important to note that H_2 derived from coal accounts for only 18% of the world's hydrogen production. The complex and costly gasification process presents a significant drawback for its widespread production [42].

- **Biomass gasification:**

Biomass gasification involves the conversion of biomass feedstocks, such as agricultural residues or organic waste, into a syngas mixture containing H_2, CO, CO_2 and nitrogen (N_2). This process occurs through high-temperature, oxygen-limited reactions. The main reaction of biomass gasification is as follow [42]:

$$Gasification\ of\ biomass \rightarrow H_2 + CO_2 + CO + N_2 \qquad \text{2-11}$$
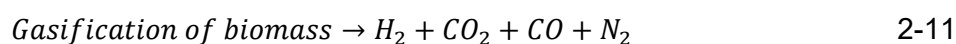
The syngas produced can undergo further processing to isolate H_2, offering the advantage of utilizing renewable biomass feedstocks.

It is worth noting that all these methods, mentioned above, contribute to GHG emissions.

- **Electrolysis:**

Electrolysis, a well-established method, involves the decomposition of water into H_2 and O_2 using electricity. This process offers a sustainable approach to H_2 production, particularly when powered by renewable energy sources.

Electrolysis involves two primary types of water electrolysers: those with an alkaline electrolyte and those with a polymer electrolyte membrane (PEM) [42]. Both types operate within temperature ranges typically between 70-130 °C [42]. Alkaline water electrolysis, a conventional method, has been in use for decades with efficiencies averaging around 70–80% [42]. The overall reaction can be described as follows:

$$H_2O \rightarrow H_2 + 1/2O_2 \qquad \text{2-12}$$

Other water splitting methods, such as Thermochemical (TC) Water Splitting, High Temperature Electrolysis (HTE) and Photoelectrochemical (PEC) Water Splitting are beyond the scope of the current work and will not be further described [9,42].

- **Methane pyrolysis:**

Finally, methane pyrolysis, the primary focus of this study, that is introduced and its principle is outlined at the beginning of this chapter. Various existing methods and techniques for methane pyrolysis are extensively discussed in section 2.4.

2.2.2 Classification of hydrogen

H_2 can be classified based on colour codes and the method of its production, as well as its environmental impact. These variations are described further using the colour codes and shown in Figure 10 [44,45]:

- **Green Hydrogen:**

Definition: H_2 produced using renewable energy sources, such as solar, wind, or hydroelectric power, to power the electrolysis process, which splits water molecules into hydrogen and oxygen.

Environmental Impact: Considered environmentally friendly and sustainable since it relies on renewable energy sources and produces no GHG emissions during production.

- **Blue Hydrogen:**

Definition: H_2 produced from NG through SMR, where the CO_2 emissions generated are captured and stored (carbon capture and storage, or CCS).

Environmental Impact: While the H_2 production process itself generates CO_2 emissions, capturing and storing these emissions mitigates its environmental impact. However, the overall environmental benefits depend on the efficiency of the CCS process.

- **Grey Hydrogen:**

Definition: H_2 produced from fossil fuels, typically NG, through processes like SMR or coal gasification, without CCS.

Environmental Impact: Considered the least environmentally friendly option as it relies on fossil fuels and results in the release of CO_2 emissions, contributing to climate change and air pollution.

- **Turquoise Hydrogen:**

Definition: Similar to blue hydrogen, turquoise hydrogen is produced from NG through SMR, but with the additional utilization of carbon capture and utilization (CCU) technologies to convert CO_2 emissions into useful products or chemicals. The H_2 produced through methane pyrolysis is also categorized under this color code.

Environmental Impact: Aims to reduce the net carbon footprint by capturing and utilizing CO_2 emissions, potentially offering environmental benefits compared to traditional blue hydrogen.

- **Pink Hydrogen:**

Definition: H_2 produced through electrolysis using electricity generated from nuclear power plants.

Environmental Impact: While it doesn't directly produce GHG emissions during production, it raises concerns regarding nuclear waste disposal and potential environmental impacts associated with nuclear energy production.

- **White Hydrogen:**

Definition: H_2 that is harvested from the geological deposits.

Environmental Impact: Similar to pink hydrogen, it avoids direct GHG emissions. However, the feasibility and commercial viability of extracting white hydrogen are still under investigation.
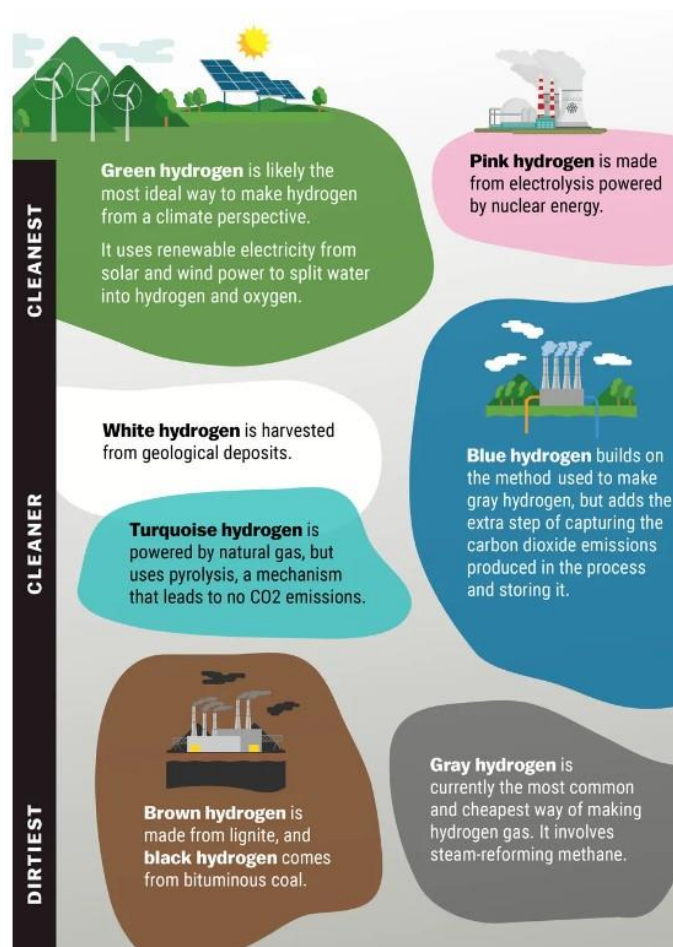
Figure 10. The hydrogen colour palette [46].

As efforts to decarbonize the energy sector intensify, there is a growing focus on scaling up production of green hydrogen while exploring methods to reduce the environmental footprint of other production routes.

2.2.3 Hydrogen application

H_2 integration across various sectors, including transportation, power generation, and mobility, holds substantial promise [45]. Furthermore, H_2 can be efficiently stored and transported, offering versatility in energy distribution [47]. Moreover, H_2 serves as an effective energy storage and grid stabilization solution, especially when coupled with renewable energy sources like solar and wind power. Excess electricity generated during periods of low demand can be used to produce H_2 via electrolysis, which can then be stored and converted back to electricity as needed [37].

Widely utilized across diverse industries such as petroleum refining, chemical production, and metal processing, H_2 finds applications in various processes, including ammonia (NH_3)

synthesis for fertilizer production, petroleum product refining via hydrocracking, and the production of chemicals like methanol [47]. Notably, NH_3 production for fertilizer accounts for approximately half of the H_2 produced today, representing its primary industrial use [48].

The utilization of H_2 as a fuel for transportation and stationary applications is gaining significant attention both technically and from a policy standpoint. H_2 is being explored for use in internal combustion engines (ICEs) and fuel cell electric vehicles (FCEVs). Projections suggest that by 2040, the adoption of H_2 in fuel cell-powered cars and light trucks could potentially replace the consumption of 18.3 million barrels of petroleum per day [40–42,44,49]. Figure 11 shows a prediction of H_2 utilization in year 2050, compared to the status of year 2019.
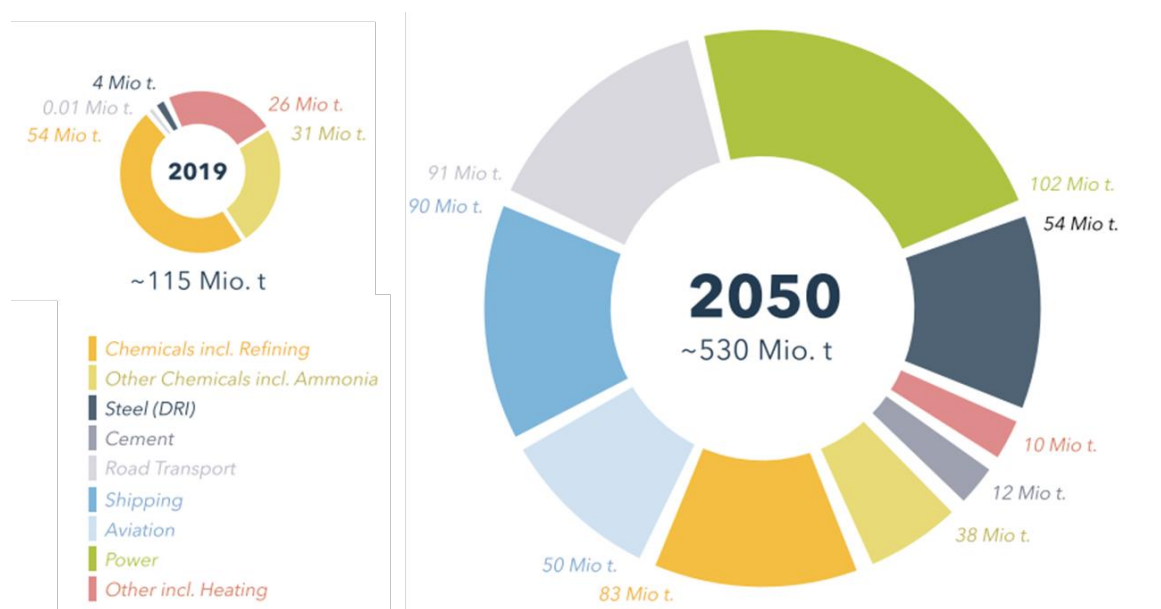
Figure 11. Evolution of H_2 utilization from 2019 to 2050 [49].

2.3 Carbon, the black diamond

Carbon, a non-metallic element essential to life on Earth, is present in a wide array of compounds. Renowned as the "building block of life," carbon's versatility stems from its capacity to form long chains and intricate structures [50]. Due to its significance, it is poetically referred to as the "black diamond" here.

Carbon ability to bond with other elements in various configurations gives rise to a spectrum of materials with vastly different properties. From the brilliance of diamonds to the softness of

graphite in pencils, carbon comes in various forms, each offering unique characteristics and applications [51,52].

Crucially, carbon plays an indispensable role in organic chemistry, serving as the foundation of all living organisms. It is a fundamental component of carbohydrates, proteins, fats, and nucleic acids, essential molecules for life. Comprising approximately 18% of our body weight, carbon ranks as the second most abundant element by mass in the human body, surpassed only by O_2 [53].

Carbon's conductivity, driven by its unique atomic structure, underpins its critical role in modern electronics, energy storage, and materials science. These properties arise from the delocalized π-electrons within carbon's sp² hybridized bonds, facilitating efficient charge transport [51].

Understanding carbon's properties and behaviours is crucial for advancing scientific knowledge and developing innovative solutions in areas such as energy and environmental sustainability.

In its pure state, carbon can exist in various allotropes, including graphite, diamond, and fullerene. Figure 12 provides a comprehensive list of different carbon allotropes, which will be further discussed in detail.
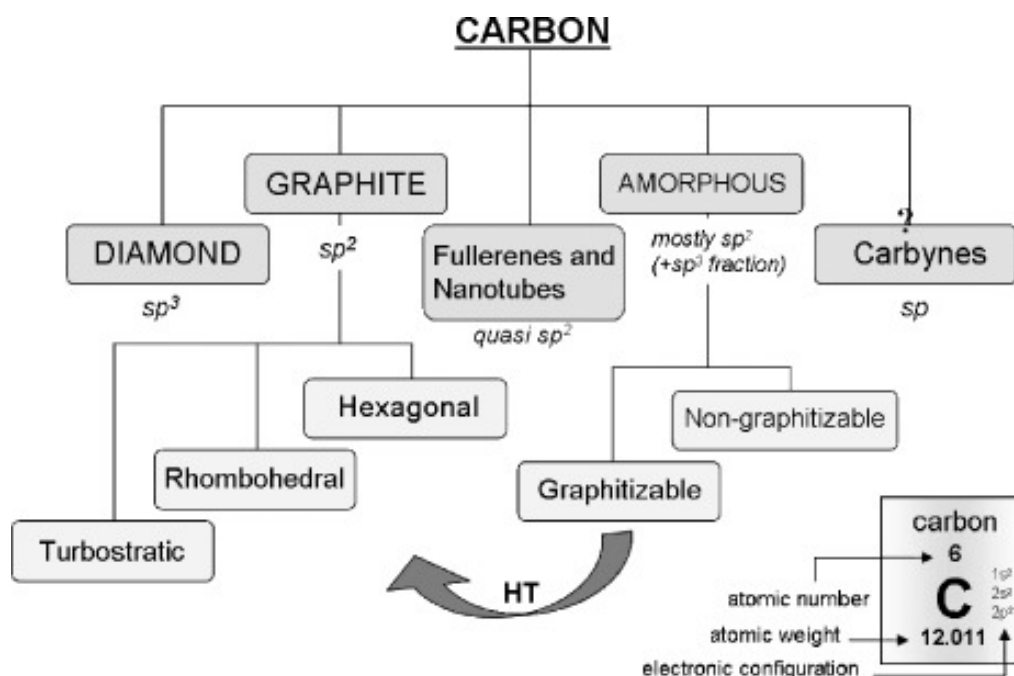
Figure 12. Varieties of carbon allotropes [51].

Carbon-based materials can be categorized based on their structure, which significantly influences their properties and uses. Here are some common classifications, summarized later, in Figure 15.

- **Diamond:**

Diamonds are composed of carbon atoms arranged in a tetrahedral lattice structure, with each carbon atom covalently bonded to four others (Figure 13). This structure is characterized by sp^3-hybridized bonding, where each carbon atom forms covalent bonds with three surrounding atoms, creating a three-dimensional arrangement of tetrahedra. The angle between these bonds measures 109.5 °, resulting in the diamond structure, which corresponds to a specific cubic unit cell. This arrangement produces an exceptionally strong and rigid material with excellent thermal conductivity [51]. Diamonds typically crystallize in a cubic structure, and industrial production has been achieved. They are also found in a less common hexagonal form, which exhibits lower hardness [51]. Diamonds are renowned for their unparalleled hardness, making them valuable for cutting tools, jewellery, and various industrial applications where hardness and durability are essential.
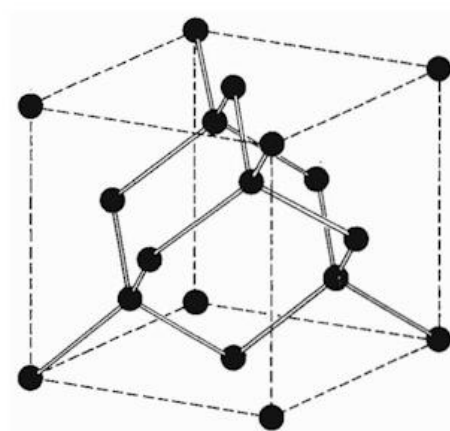
Figure 13. The tetrahedral lattice structure of diamond [54].

- **Graphene:**

Graphene comprises a single layer of carbon atoms arranged in a two-dimensional hexagonal lattice of sp^2-hybridized carbon atoms. While it serves as the fundamental building block of other carbon allotropes like graphite, its distinctive properties distinguish it. Remarkably strong, lightweight, and flexible, graphene also demonstrates exceptional electrical and thermal conductivity [51].

- **Graphite:**

In contrast to diamonds, graphite possesses a layered structure in which carbon atoms form flat, hexagonal sheets stacked on top of each other. Within these layers, carbon atoms are covalently bonded using sp^2-hybridized bonds [51]. Weak van der Waals forces hold the layers together, enabling easy sliding past one another and enhancing both electrical and thermal conductivity. The crystal structure of graphite is hexagonal, with graphene layers stacked in a regular ABABAB sequence, resulting in a defined interlayer distance of 3.354 Å (Figure 14) [51,55].

However, the structure of graphite can deviate from its ideal form. Turbostratic carbon (TSC) is a notable variant where graphene layers lack ordered stacking, instead displaying relative rotations and translations between adjacent layers. It is crucial to distinguish TSC from graphite, as the former exhibits an expanded interlayer distance compared to hexagonal graphite. Nonetheless, it is important to note that this distinctive property alone should not be the sole basis for differentiating between graphite and TSC [51].

Graphite is renowned for its lubricating properties and electrical conductivity, making it valuable in a variety of applications, including pencils, lubricants, electrodes, and as a component in composite materials [51,52].
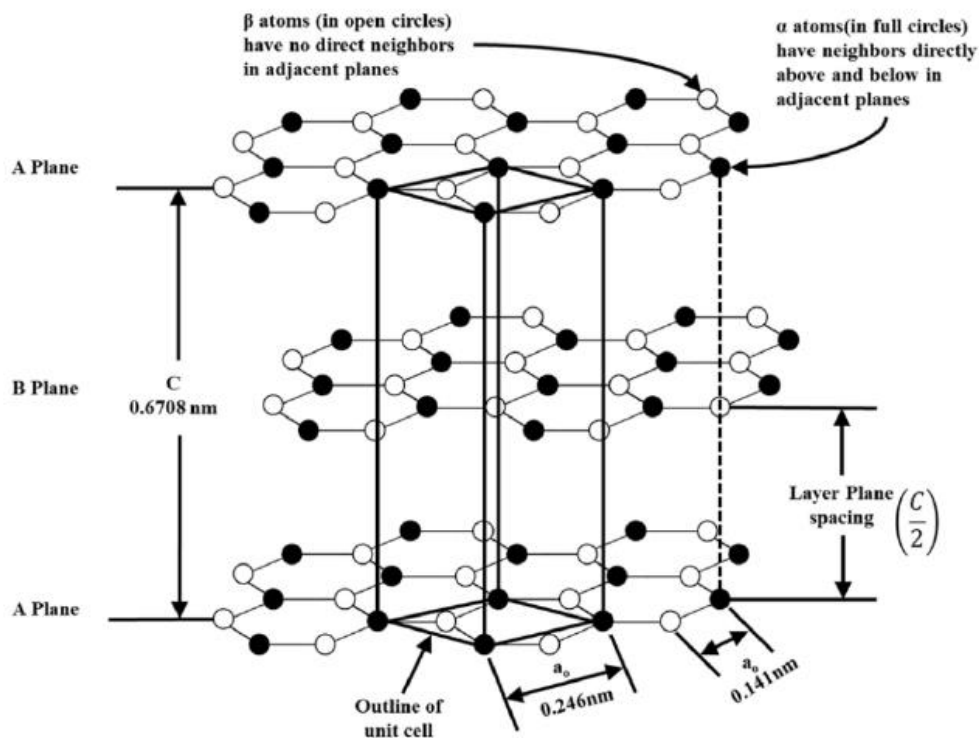
Figure 14. Crystal structure of graphite showing the stacking sequence and the layer plane spacing [55].

- **Fullerenes and Carbon Nanotubes (CNTs):**

Fullerenes are hollow, cage-like structures composed of carbon atoms arranged in pentagonal and hexagonal rings. They possess unique properties, including high chemical reactivity, and are being investigated for various applications such as drug delivery, superconductors, and nanotechnology [56,57].

CNTs are cylindrical structures formed by rolled-up graphene sheets. They can exist in single-walled or multi-walled configurations and exhibit exceptional strength, stiffness, and electrical conductivity. CNTs find applications across diverse fields including electronics, aerospace, materials science, and nanotechnology [56,57].
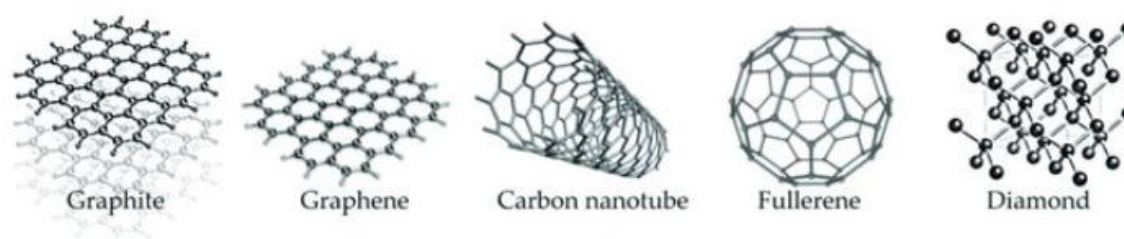
Figure 15. Various structure schemas of carbon allotropes [56].

Some carbon materials are not crystallized and are identified by their random structure, which cannot be categorized under the mentioned structural types. These are known as amorphous carbon.

- **Amorphous Carbon:**

Unlike crystalline carbon structures, amorphous carbon lacks long-range order in its atomic arrangement. It encompasses materials like carbon black (CB), charcoal, coal, soot, and activated carbon. Amorphous carbon materials exhibit diverse properties depending on their production methods and can be utilized in filters, pigments, and electrodes. For example, activated carbon, often referred to as porous carbons, undergoes chemical or physical activation processes. Through activation, these carbons achieve exceptionally high surface areas, ranging from approximately 500 to 3000 m^2/g, and may also exhibit well-developed microporosity [51].

Another significant form is industrial CB, distinguished from common soot by its deliberate production, whereas soot is an unintended and undesirable by-product of combustion. Industrial CB comprises spherical carbon particles that aggregate into particles of varying sizes [58]. Initial electron micrographs portrayed CB particles as separate, spherical entities prone to

clustering or linking together in chains. However, advancements in microscopy revealed that the particles in most CBs were fused, forming a cohesive and continuous solid carbon structure [28].

CB ranks among the oldest manufactured products, with historical usage as a pigment in inks and mural paints traced back to ancient Chinese and Egyptians [28].

The pivotal moment that significantly influenced the utilization of CB was the discovery of its remarkable reinforcing properties when incorporated into natural rubber [28,58].

CB finds diverse applications across several industries, including mobility, plastics, and agriculture. Its uses span steelmaking, plastics manufacturing, fuel production, and electronics, with particular importance in tire industry where it serves as a reinforcement, enhancing mechanical and dynamic properties [58,59].

A market analysis indicates a 5.75% increase in the carbon black market size, growing from 22.79 USD billion in 2024 to 30.15 USD billion in 2029 [60].

- **Carbyne:**

Carbyne is a theoretical one-dimensional form of carbon, comprising an infinitely long chain of carbon atoms with alternating single and triple bonds. It is anticipated to exhibit remarkable mechanical, electrical, and thermal properties. However, experimental synthesis of carbyne has not yet been achieved due to its extreme reactivity and the challenges involved in stabilization. Nevertheless, it is envisioned to have potential applications in nanoelectronics and materials science [51].

These classifications offer only a glimpse into the diverse world of carbon-based materials. Each structure presents unique properties that can be customized for specific applications, fostering innovation across various industries. Some carbon materials may exhibit properties overlapping multiple classifications and cannot be definitively categorized under a specific group.

2.3.1 Carbon production

Carbon occurs naturally in fossil fuels like coal, petroleum, and NG. These carbon-rich hydrocarbons undergo thermal decomposition or refining processes to extract carbonaceous materials such as coke, CB, and activated carbon for various industrial applications.

Additionally, biomass-derived carbon sources such as wood, agricultural residues, and organic waste can be converted into biochar, charcoal, or syngas through pyrolysis, gasification, or combustion processes.

Synthetic processes for the production of carbon materials are further elaborated below:

- **Coal and biomass Gasification:**

These processes, previously described for the production of H_2 and CO, yield a product gas that can undergo further processing to generate solid carbon products like coke, biochar, activated carbon, or carbon fibers [61].

- **Carbonization:**

Carbonization entails heating organic precursors, such as coal, wood, or synthetic polymers, in an oxygen-free environment to create carbon-rich materials like charcoal, coke, or carbon fibers. Typically conducted at elevated temperatures (> 500 °C), this process drives off volatile components and transforms the precursor into a stable carbonaceous product [61].

- **Graphitization:**

Graphitization is a thermal treatment process that converts amorphous carbon materials, such as CB or carbon fibers, into crystalline graphite structures with organized atomic arrangements. This process entails annealing carbon materials at temperatures exceeding 2000 °C in inert atmospheres. Through this treatment, graphitic carbon growth is induced, leading to enhanced structural alignment and conductivity [61].

- **Chemical Vapor Deposition (CVD):**

CVD is a method for depositing thin films of carbon nanomaterials, such as CNTs and graphene layers, onto substrate surfaces. During CVD, precursor gases containing carbon, like CH_4 or C_2H_4, undergo thermal decomposition or dissociation in the presence of a catalyst at elevated temperatures (> 600 °C) [62].

- **Electrochemical Processes:**

Electrolysis offers a means to produce carbon-based materials such as graphite, graphene, or CNTs from carbon-containing electrolytes or precursor solutions. Through electrochemical deposition or exfoliation techniques, these carbon nanostructures can be carefully synthesized

and assembled on electrode surfaces or in solution. This approach allows for the customization of properties and morphologies, catering to diverse applications in electronics, energy storage, and catalysis [63].

- **Pyrolysis:**

Biomass Pyrolysis: Biomass, such as wood, agricultural residues, or organic waste, undergoes pyrolysis, a thermochemical decomposition process in the absence of oxygen, to produce solid carbon. This process involves heating biomass feedstocks to temperatures typically ranging from 300 to 800 °C in a controlled environment. As a result, organic compounds break down to form solid char, biochar, or activated carbon [64].

Plastic Pyrolysis: Plastic waste, comprising polyethylene, polypropylene, polystyrene, and other polymers, can be thermally decomposed via pyrolysis to yield solid carbonaceous residues, oils, and gases. Typically, plastic pyrolysis entails heating plastic waste to elevated temperatures exceeding 400 °C in the absence of air to minimize combustion and generate carbon-rich char or CB [65].

Methane pyrolysis: Under varying process conditions, different types of solid carbon are observed, including amorphous or TSC, CNTs, nanofibers, graphite-like carbon, and CB. A literature review explores the distinctions between these carbon forms generated from methane pyrolysis, considering factors such as process temperature and the use of different catalyst types and summarizes them, as shown in Figure 16 [66].
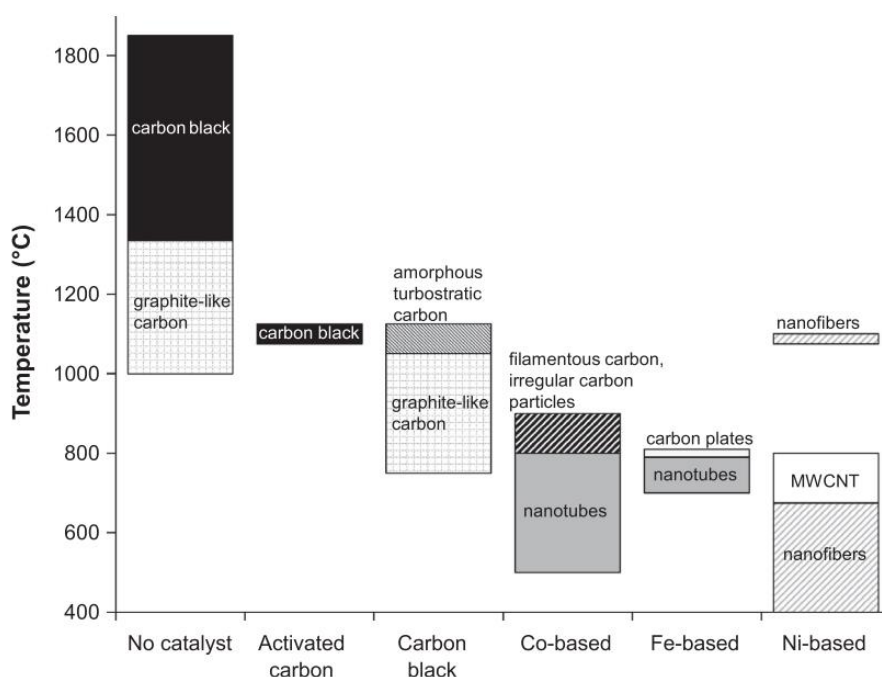
Figure 16. Different carbon products derived from various methane pyrolysis processes with and without the use of catalysts [66].

Although CB is often cited as the product of methane pyrolysis, as seen the solid carbon resulting from pyrolysis does not always meet the precise specifications of commercial CB.

2.3.2 Carbon applications

- **Tire and rubber industry:**

CB enhances the durability, strength, and wear resistance of rubber compounds, making them suitable for use in tires, conveyor belts, automotive parts, and industrial products [58].

Carbon fibers, derived from carbon-rich precursors such as polyacrylonitrile or pitch, are used as reinforcement materials in high-performance tires and rubber products. Carbon fibers impart strength, stiffness, and lightweight properties to rubber composites, improving their mechanical performance and fuel efficiency in automotive applications.

- **Agriculture:**

Biochar and activated carbon serve as valuable soil amendments, enhancing soil quality, fertility, and crop productivity. Biochar, derived from biomass through pyrolysis, improves soil water retention, nutrient retention, and microbial activity, thereby fostering better plant growth and yield. Meanwhile, activated carbon, renowned for its high surface area and adsorption

capacity, effectively removes contaminants and toxins from soil, water, and agricultural inputs [61].

Agriculture plays a pivotal role in carbon sequestration, which involves capturing and storing atmospheric CO_2 in soils and vegetation. Practices such as no-till farming, cover cropping, and agroforestry facilitate carbon sequestration by bolstering soil organic carbon levels and curbing greenhouse gas emissions from agricultural activities. Carbon sequestration in agricultural soils not only helps mitigate climate change but also enhances soil health and boosts ecosystem resilience [61,67].

- **Energy storage:**

Graphite and CNTs find widespread application as electrodes in lithium-ion batteries and various rechargeable battery technologies. Renowned for their high conductivity, stability, and energy storage capacity, these materials play indispensable roles in powering portable electronics, electric vehicles, and grid-scale energy storage systems [56,57].

Meanwhile, activated carbon and graphene feature prominently in supercapacitors, devices designed to store electrical energy via electrostatic charge separation at the electrode-electrolyte interface [68]. Supercapacitors offer rapid charging and discharging rates, high power density, and prolonged cycle life, making them ideal for applications requiring swift energy storage and delivery, such as hybrid vehicles, renewable energy installations, and electronic gadgets [68].

- **Water treatment:**

Activated carbon is extensively employed in water treatment procedures to eliminate organic contaminants, pollutants, and impurities from drinking water, wastewater, and industrial effluents. Utilized within activated carbon filters, this material adsorbs dissolved organic compounds, chlorine, volatile organic compounds, and other harmful substances, thereby enhancing water quality and taste [69].

CNTs and graphene oxide are currently under investigation for their potential in water purification and desalination applications. These nanomaterials boast high surface area, porosity, and adsorption capacity, facilitating efficient removal of contaminants and salt ions from water through processes like membrane filtration, adsorption, and catalysis [70].

- **Healthcare and biomedical applications:**

Carbon-based materials are used in various medical devices and implants due to their biocompatibility, mechanical strength, and corrosion resistance. Carbon fibers, CNTs, and graphene are employed in orthopedic implants, prosthetics, dental composites, and tissue engineering scaffolds to enhance structural integrity, durability, and biological performance [71].

Figure 17. Various examples of carbon application [72].

2.4 Methane pyrolysis techniques

Methane pyrolysis processes can be classified in various ways, considering the utilization of different reactors, energy sources, catalysts, and operating conditions. Initially, the distinction between catalytic and non-catalytic pyrolysis is outlined. Subsequently, a classification approach is employed to delineate the available processes.

2.4.1 Catalytic pyrolysis

Catalytic pyrolysis is a decomposition process where a catalyst is employed to reduce the temperature required for methane pyrolysis. While temperatures exceeding 1200 °C are

typically needed for efficient methane pyrolysis, the use of a catalyst, such as metals, can lower operating temperatures to below 1000 °C. These catalysts can exist in liquid or solid form, depending on the furnace and method used [73,74].

Solid catalysts comprise various materials, including metals such as nickel (Ni), cobalt (Co), iron (Fe), gallium (Ga), Rhenium (Re), ruthenium (Ru), rhodium (Rh), iridium (Ir), platinum (Pt), tin (Sn), magnesium (Mg), bismuth (Bi), tellurium (Te), tungsten (W), palladium (Pd), molybdenum (Mo) and copper (Cu), either in pure or alloy form. Additionally, non-metals like carbon are used. These metals can be supported on carriers, with aluminium (Al) oxide and silicon (Si) oxide being the preferred choices. Ni is widely used due to its high activity, followed by Co, Ru, Rh, Pt, Re, Ir, Pd, W, Fe, Mo, in descending order [21,66,75,76].

The primary advantage of catalytic pyrolysis is its ability to lower the required operating temperature and saving energy. However, adding a catalyst during the reaction can lead to coking, where carbon solidifies on the catalyst surface and reduces its activity. Separating heterogeneous catalysts from carbon and recovering them is challenging, resulting in the inability to recover some catalysts.

In contrast to metal catalysts, carbon-based catalysts exhibit lower activity and deactivation rates. However, the resulting carbon is amorphous with various morphologies, whereas valuable CNTs are produced with metal catalysts [66,75]. Carbon-based catalysts do not require separation or regeneration; instead, the deactivated catalyst with deposited carbon can be removed, and fresh catalyst added [75].

2.4.2 Non-catalytic pyrolysis

Non-catalytic processes operate at temperatures above 1200 °C, eliminating the need for catalysts. However, certain techniques, such as thermal plasma, can be tested both with and without catalysts. In thermal plasma, catalysts can be employed in the form of molten or solid metals to enhance efficiency.

2.4.3 Classification of the pyrolysis techniques based on the type of reactor used

The following subsections introduce a classification of the different approaches to methane pyrolysis based on the type of reactor used, along with an example of each process. This approach is illustrated in Figure 18, which delineates between catalytic and non-catalytic

reactor types, highlighting instances where certain reactors can function either with or without catalysts.
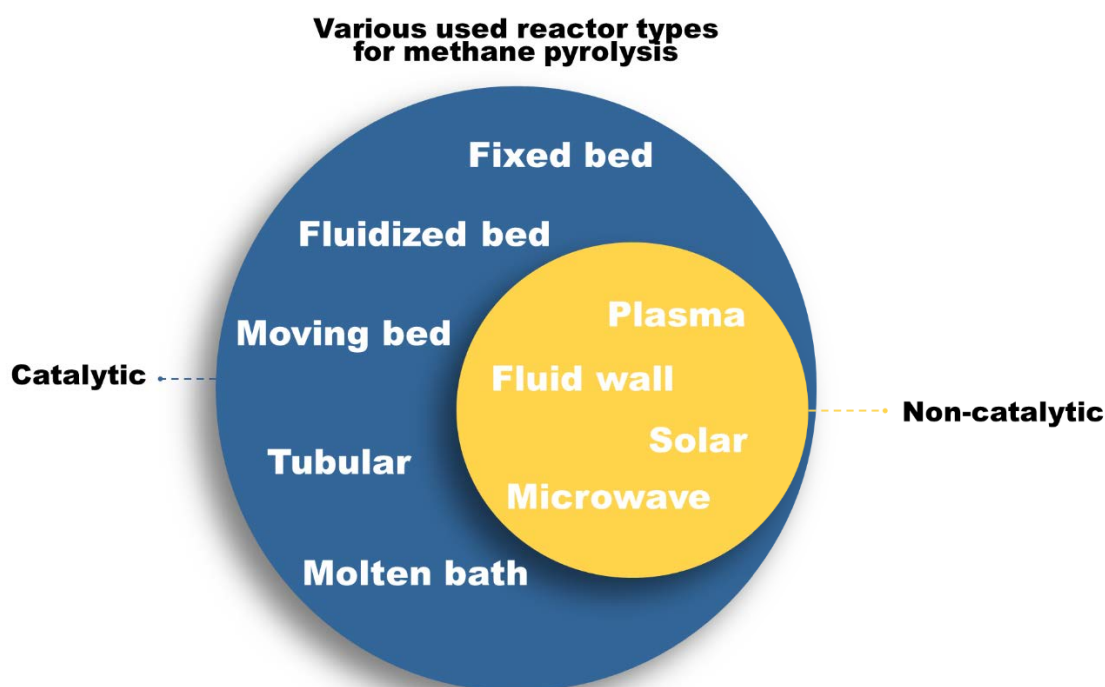
Figure 18. Grouping of the various catalytic and non-catalytic reactor types employed in experimental methane pyrolysis works.

2.4.3.1 Fluidized-bed reactor – Catalytic pyrolysis

Fluidized-bed reactors represent a significant advancement in gas-solid reactions by facilitating enhanced contact between the two phases, good mixing, and elevated rates of mass and heat transfer [77,78]. These reactors are exclusively employed for catalytic methane pyrolysis, given their operational temperatures below 1000 °C. The principle revolves around utilizing fine particles of catalyst, predominantly metal-based (such as Fe and Ni) or carbon-based, to catalyze pyrolysis at reduced temperatures [77].

While these reactors has the advantageous of producing high value carbon material such as CNTs, they face challenges related to catalyst deactivation and regeneration, as well as issues stemming from the fluidization behaviour caused by catalyst swelling due to carbon formation [76,77].

An exemplary process illustrating this approach is the HAZER® process developed by an Australian company, which patented a fluidized bed system utilizing fine iron ores as catalysts (Figure 19). By adjusting parameters such as pressure, temperature, and mass flow within the

reactor, the fluidized behaviour and, consequently, the H_2 yield and carbon characteristics can be tailored. Schematics of the process further elucidate its operational intricacies [79].

Operating parameters

Process temperature	850 °C
Methane feed	0.01 l min^{-1} (at 20 °C and 1 atm)
Methane conversion	92 %
Catalyst	Fe_2O_3 / Fe_3O_4
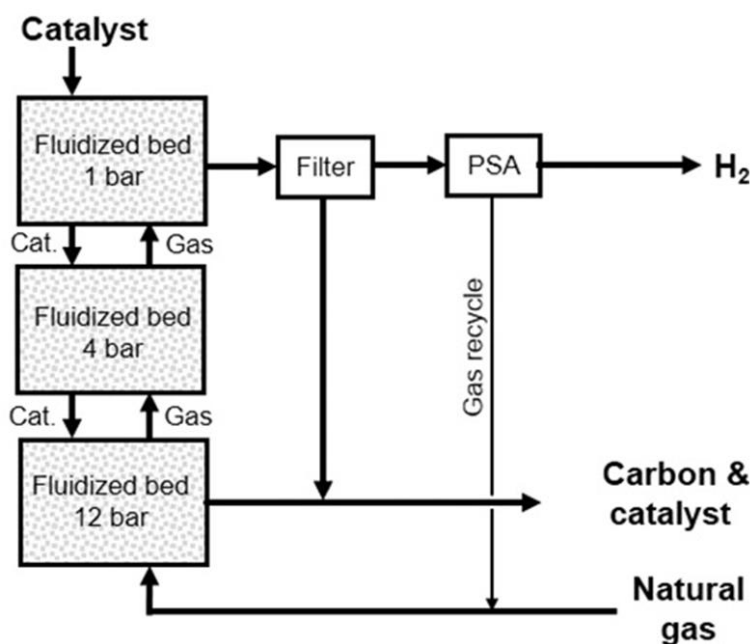
Figure 19. Operating parameters and a scheme of the HAZER® process [79].

2.4.3.2   Fixed bed reactor – Catalytic pyrolysis

Fixed-bed reactors are commonly employed as a fundamental tool for catalyst screening and evaluating operational parameters such as temperature and space velocity, particularly in the context of kinetic measurements and H_2 yield. Typically utilized at the experimental scale, these reactors encounter limitations during testing due to the accumulation of carbon produced during pyrolysis, ultimately resulting in reactor tube blockage. Consequently, catalysts must be periodically removed along with the carbon deposits. However, the subsequent technique introduced offers continuous discharge of products, eliminating the necessity for process sequencing [73].

2.4.3.3   Moving bed reactor – Catalytic pyrolysis

A prominent example of the moving bed pyrolysis process is developed by BASF Process Catalysts GmbH in Germany for research purposes. In this setup, carbon catalysts in the form

of granules are transported in counterflow to the gas phase at temperatures reaching up to 1400 °C. The H_2 exits the reactor along with any unreacted CH_4. As solid carbon accumulates on the catalysts, they tend to increase in size. Within the reaction zone, electrodes directly heat the catalysts, promoting pyrolysis reactions primarily at their surfaces [73]. This assumption is supported by the observed growth of carbon granule particles passing through the reactor [79].

Using a moving carbon bed for methane pyrolysis offers several advantages. Firstly, the solid carbon particles deposit directly onto the surface of the carbon bed granules, which are made of a similar material. This eliminates the need for mechanical or chemical separation from a different medium. Secondly, the process does not require a specialized or expensive medium since carbon serves as the primary medium for transferring heat to the methane gas [73].

Figure 20 illustrates the operating parameters and provides a schematic representation of the BASF process.

Operating parameters
Process temperatures   1000 - 1400 °C
Natural gas feed   10 m³ h⁻¹ (at 20 °C and 1 atm)
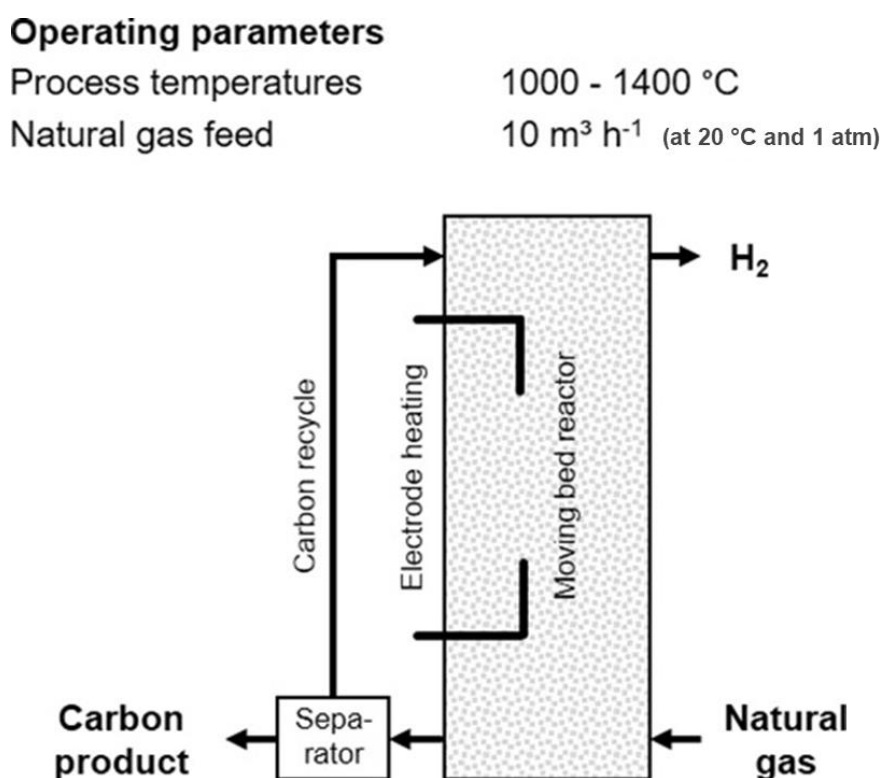
Figure 20. Schematic representation illustrating the principle of moving bed methane pyrolysis [79].

2.4.3.4 Molten bath reactor – Catalytic pyrolysis

This technique involves heating and melting a catalyst, which could be either metals or a salt bath. Other variations focus on different methods of introducing methane gas into the melt,

such as through an immersed lance or from the bottom using gas purging plugs, or a combination of both. Additionally, efficiency can be increased by employing mechanical or magnetic stirring. The primary objective is to prolong the lifetime of CH_4 gas bubbles and enhance the gas residence time within the melt, thereby increasing reactivity and improving the conversion rate [74,80,81].

Molten metals are generally effective heat transfer media for directly heating CH_4. They offer advantages such as carbon insolubility, allowing for easier separation of carbon products, and the lower density of carbon particles compared to molten metals, facilitating their flotation on top [73,74].

One advantage of using molten metal bubble column systems is the ability to reuse the molten metal for future reactions, making the process more cost-efficient compared to catalytic processes with solid catalysts. However, challenges include molten metal corrosion when in contact with other metals, which complicates separating molten metal contamination from carbon product particles, as well as high impurities from the catalysts in the produced carbon [73,79].

The Department of Nonferrous Metallurgy at Montanuniversität Leoben (MUL) has devised a concept for a molten metal pyrolysis process using an experimental-scale induction furnace and a graphite crucible filled with molten metal alloys, operating at temperatures of up to 1300 °C. CH_4, at rates of up to 4 standard liters per minute (SLM), is introduced through an alumina lance positioned at the top of the furnace. N_2 flushing is employed to increase gas flow volume and prevent carbon agglomeration in the product gas piping. During operation, carbon predominantly exits the reactor with the product gas, where it is collected in a designated carbon container and subsequently separated from the gas stream using a ceramic filter. Any remaining carbon is deposited on the catalyst surface. Ongoing research at Montanuniversität Leoben (MUL) aims to scale up the process for commercialization. A detailed process scheme is depicted in Figure 21 [80,81].
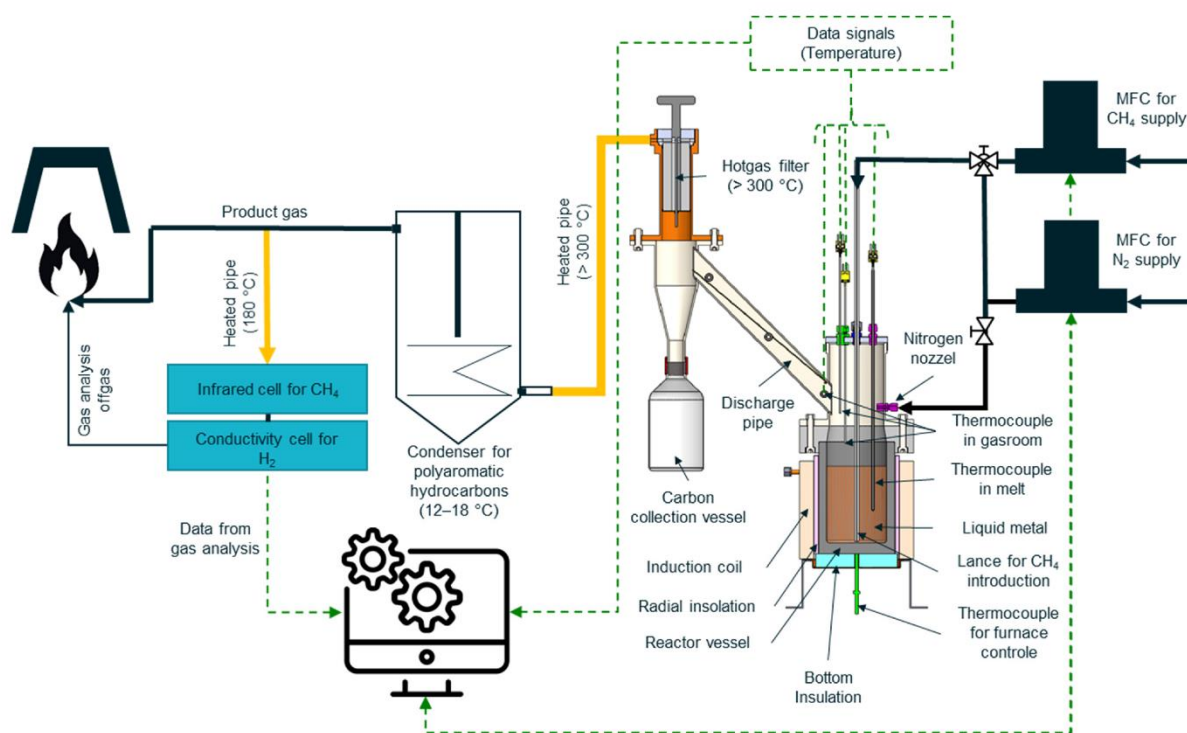
Figure 21. Overview of the molten metal reactor process by Montanuniversität Leoben (MUL) [81].

2.4.3.5 Tubular reactor – Catalytic pyrolysis

In these reactor configurations, solid carbon deposition commonly occurs on the inner surfaces downstream of the reaction area, particularly in tubes with diameters ranging from 3 to 6 mm. Tubular reactors offer potential for scalability in large-scale methane pyrolysis processes. However, their effective operation requires elevated reaction temperatures exceeding 1000 °C, as well as specialized surface treatments on the reactor walls to reduce solid carbon buildup within the reaction zone [73].

2.4.3.6 Fluid wall reactor – Catalytic and non-catalytic pyrolysis

Fluid wall reactors are engineered to withstand high temperatures, reaching up to 1300 °C, facilitated by electric heaters [73]. In these setups, CH_4 is directed through a tube, such as an alumina tube. Within the fluid wall-flow reactor design, a preheated inert gas is introduced radially through the porous reactor wall to deter the deposition of solid carbon on the reactor walls [82]. However, the necessity to filter H_2 from the inert gas, solid carbon, and unconverted CH_4 adds complexity to the overall process [82].

An illustration of an experimental-scale fluid wall reactor for methane pyrolysis is provided in Figure 22. In this design, the heating gas traverses through the porous wall driven by the pressure difference, serving the dual purpose of supplying heat for the endothermic reaction

and potentially preventing carbon deposition within and on the porous ceramic structure. The porous section is securely affixed downstream using high-temperature adhesive [82].
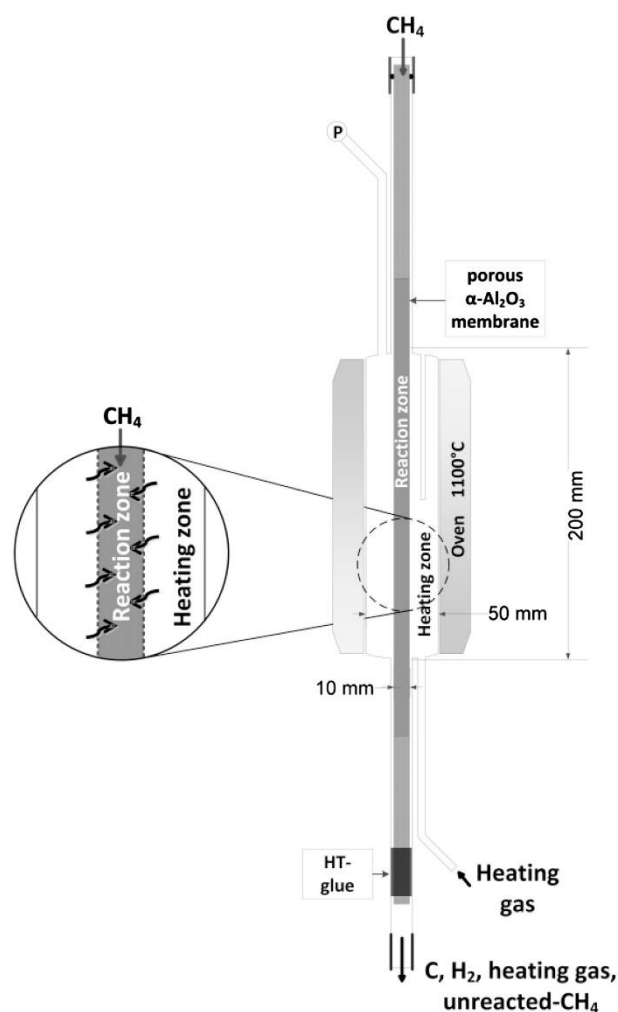
Figure 22. Drawing of a fluid wall reactor [82].

2.4.3.7 Microwave reactor – Catalytic and non-catalytic pyrolysis

Microwave reactors utilize electromagnetic waves in the microwave frequency range to rapidly heat the feedstock, inducing pyrolysis. The high-intensity microwave energy disrupts chemical bonds within the feedstock. Notably, microwave technology heats the material from within, a key distinction from conventional heating methods. CH_4 is typically fed into a microwave reactor and subjected to a microwave frequency of 2450 Hz. It then passes through a bed of coal char catalyst inside a quartz tube, where it decomposes into H_2, with solid carbon being deposited on the catalyst surface [73,83].

One advantage of microwave heating is the generation of small hot spots or microplasmas within the catalytic bed, which enhances the conversion rate of CH_4. However, the presence

of these hot spots or microplasmas can lead to uneven heating and temperature distribution, resulting in uncertainty in temperature measurements and control within the reactor [73].

This technology can also be combined with the formation of plasma, a method known as microwave plasma. However, a detailed discussion of plasma technology is presented later in subsequent subsections [73].

Regarding scalability, microwave pyrolysis technology is still in its early stages of development.

2.4.3.8 Solar reactor – Catalytic and non-catalytic pyrolysis

The fundamental principle involves concentrating solar radiation onto a reactor containing CH_4, typically employing a solar concentrator. In these reactor types, solar energy is harnessed in two distinct manners, categorized by how the reactants are heated via solar radiation: direct and indirect heating [84].

In directly-irradiated solar reactors, radiative heat is absorbed either through an open aperture or a closed transparent window (e.g., quartz). However, these windowed reactors are prone to fracture when the window becomes contaminated with carbon and overheated due to local heat concentration [84].

In contrast, indirect solar heating reactors receive solar radiation through an intermediate opaque wall. Heat is then transferred to the reactants through infrared reradiation, conduction, and convection. The presence of a window is no longer a concern in this setup. However, this type of reactor is associated with higher radiative losses because of the elevated temperature of the absorbing wall compared to the reaction zone. Sometimes, to enhance process efficiency, carbon is co-fed into the reactor for its catalytic effect and to enhance solar radiation absorption. Nevertheless, heat transfer from the reactor wall to the gas remains relatively low [84].

Both direct and indirect solar reactors are depicted in Figure 23 (a) and (b), respectively [84].
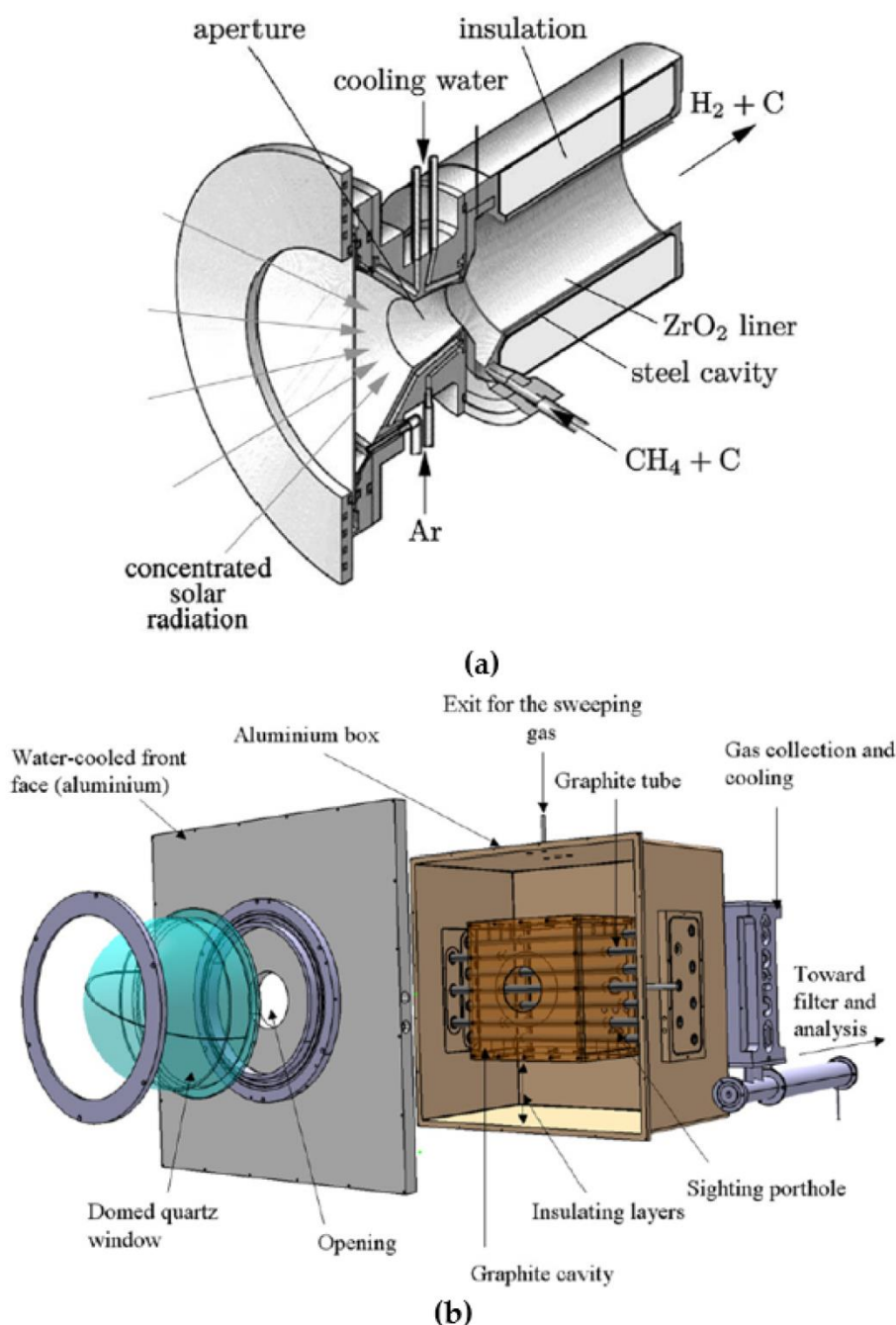
Figure 23. Direct (a) and indirect (b) heated solar reactors [84].

2.4.3.9 Plasma pyrolysis – Catalytic and non-catalytic

Plasma pyrolysis can be conducted across a wide temperature spectrum, ranging from room temperature to several thousand degrees Celsius. This variability depends on various discharge parameters, including frequency, pressure, voltage, input power, distinguishing between various types of plasmas. Subsequent chapters delve into the distinctions between hot or thermal and cold or non-thermal plasma processes [85–87].

Plasma converts electrical energy into chemo-physical energy, generating highly active species within a reactive environment, thereby facilitating the dissociation of bonds within substances like CH_4. Numerous plasma methods have been employed for methane pyrolysis, including dielectric barrier discharge (DBD), microwave (MW) discharge, gliding arc discharge (GAD), point-to-point (PTP) configurations such as high-frequency pulsed plasma, radio frequency (RF) discharge, alternating current (AC) discharge, direct current (DC) discharge, spark discharge, corona discharge, hollow cathode plasma, electron beam, and high-frequency captive techniques. These methods vary in structural design, plasma temperature, generation mode, discharge power, electric field value, power supply configuration, operating pressure, and energy density. Consequently, different reactor types and approaches lead to diverse CH_4 reforming routes [85–87].

Here, a concise overview and two examples of both non-thermal plasma (NTP) and thermal plasma (TP) pyrolysis are provided. However, as the focus of this work pertains to plasma pyrolysis, the subsequent chapter aims to offer an extended survey of all available technology types related to this process.

In thermal plasma pyrolysis (TPP), a plasma torch is utilized to heat CH_4, causing its decomposition into H_2 and C at exceedingly high temperatures, reaching up to 10,000 °C within the plasma arc region [87]. On the contrary, NTP processes typically operate at much lower temperatures, with some methods like DBD barely exceeding 1000 °C and often remaining at room temperature [87].

An illustrious example of TPP applied to methane is exemplified in the Monolith process. In 2012, Monolith Materials, a US-based company, embarked on a project aimed at producing CB as its primary output via plasma pyrolysis [79,88]. This process is introduced in Section 3.4.1.2 in details An illustration of the process with its operating parameters is presented in Figure 24.

Operating parameters Seaport-plant

Temperature reaction zone   2100 °C
Natural gas feed   144 m³ h⁻¹ (NTP)
Methane conversion   94 %
Plasma power (electr.)   0.85 MW

**Operating parameters Olive-Creek-plant
(under construction)**
Carbon black output   10 - 15 kt a⁻¹
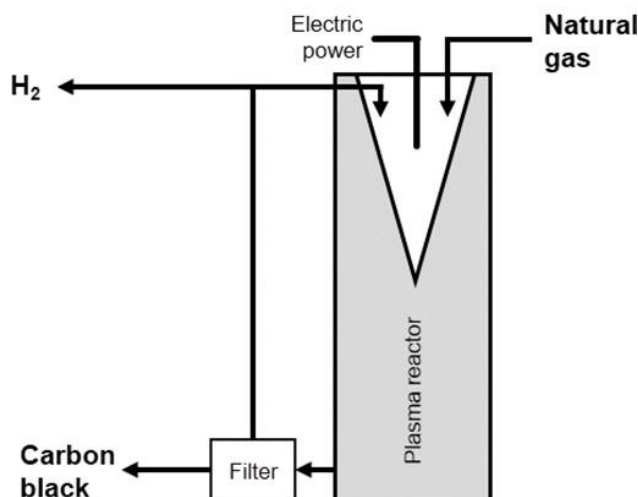
Figure 24. Operating parameters and the principle of the Monolith process [79].

NTPs function by inducing electronic excitations, prompting electrons to accelerate and collide with CH_4 molecules. Compared to the NTPs, TPs have demonstrated superior methane conversion efficiencies, attributed to their homogeneous discharge space [21].

Although NTPs generally do not require catalysts for methane pyrolysis, some studies have explored the use of metal-based catalysts in configurations such as DBD or GAD plasmas. However, the introduction of catalysts presents challenges as they may interfere with the discharge performance and overall plasma behaviour [87].

A notable advantage of plasma pyrolysis lies in its ability to generate high-quality carbon particles with exceptional purity compared to alternative methane pyrolysis methods [59,87]. Nonetheless, further comprehension of plasma dynamics is imperative for enhancing performance and efficiency.

Table 2 summarizes the various reactor types for methane pyrolysis, pointing out their respective advantages and challenges.

Table 2. Summary of different reactor types for methane pyrolysis with their advantages and challenges.

Reactor type	Catalytic	Non-catalytic	Advantages	Challenges
Fluidized-bed	✓	✗	• enhanced gas-solid contact • high-value carbon products	• catalyst deactivation • fluidization behaviour
Fixed bed	✓	✗	• suitable for kinetic measurments of H_2 yield	• catalyst deactivation • carbon accumulation and reactor blockage
Moving bed	✓	✗	• continuous discharge of material	• catalyst-carbon seperation
Molten bath	✓	✗	• flexible gas input methods • high heat transfer • reusabilitty of the molten metal	• corrosion issues • imputries from catalysts in carbon product
Tubular	✓	✗	• potential for scalability	• high temperatures (over 1000 °C) required • carbon deposition on the inner reactor wall
Fluid wall	✓	✓	• avoiding carbon deposition on reactor wall through inert gas	• inert gas – H_2 seperation
Microvawe	✓	✓	• rapid heating	• uneven heating
Solar	✓	✓	• direct and indirect use of solar energy	• transparent window prone to fracture • low heat transfer
Plasma	✓	✓	• wide temperature ranges, up to 10000 °C • pure carbon products (in non-catalytic process) • simple and compact design	• complex nature of plasma

2.5 Summary

H_2, as an energy carrier, serves as a key alternative to fossil fuels. However, its environmentally friendly production encounters challenges in production, storage, and transport. Moreover, transitioning to eco-friendly H_2 entails adapting to new technologies, which may face initial resistance. Nonetheless, there is a growing understanding of the necessity to protect our planet by curbing GHG emissions, evident from individual choices like

opting for liquid deodorants over spray canes to larger-scale shifts such as transitioning to 100% H_2 in the steelmaking sector.

We learned that our current infrastructure does not allow immediate avoidance of fossil fuels entirely, so it is necessary to take what we have and come up with some mid-term solutions. The study offers methane pyrolysis as that solution. Via methane pyrolysis we take the energy deposited in available CH_4, that its direct using releases CO_2, and store it in form of clean H_2. Another advantage of this concept is the production of carbon, a valuable element with high functionality in the modern world, without it reacting with oxygen to form CO_2.

Different production routes and the feedstocks for both H_2 and C were discussed, after introducing them individually and learn about their properties. The aim is to produce and utilize them in a circular manner, ensuring they do not disrupt the natural balance. The ultimate goal for H_2 is to produce it from seawater, allowing it to cycle back into the environment after use, returning as water or rain. Additional measures involve discontinuing conventional carbon processing methods that co-produce carbon oxides.

A general overview of the studied pyrolysis methods and the techniques used was provided, mostly involving catalysts. The advantages and disadvantages of each method were discussed. For example, it is widely acknowledged that catalysts are prone to carbonization, causing them to lose functionality over time and deactivate. Furthermore, separating the produced carbon from catalysts can be challenging, and their regeneration might lead to CO_2 emissions, potentially undermining the entire process.

The study concludes that TPP offers significant potential, yielding the purest carbon product and high H_2 yield in the absence of catalysts.

3 A literature review on plasma pyrolysis of methane

In this chapter, following a brief introduction to plasma and its fundamental properties, a comprehensive literature review is conducted on the subject of plasma pyrolysis of methane, with a particular focus on TPP. This review aims to illuminate the current status of research in this area, elucidate existing knowledge gaps, and delineate the opportunities for further investigation.

3.1 Plasma: Beyond material

Plasma* is formed by infusing a gas with adequate energy. Unlike solids, liquids, and gases, plasma represents the fourth state of matter for a substance [87].

---

*   In the mid-19th century, Czech physiologist Jan Evangelista Purkinje introduced the Greek term "plasma" (meaning "formed or molded") to describe the clear fluid remaining after removing all cellular material from blood [85]. Nearly half a century later, in 1922, American scientist Irving Langmuir proposed a similar term, "plasma" to describe the state of electrons, ions, and neutrals in an ionized gas. Langmuir likened these constituents to corpuscular material entrained in a fluid-like medium, though unlike blood plasma, there is no actual "fluid medium" entraining these particles in ionized gas. Consequently, plasma scientists have often had to clarify to friends and acquaintances that they are not studying medicine [85].

In a standard plasma chemical reaction, electrons receive energy from an electric field and transform into high-energy electrons. Subsequently, these high-energy electrons transfer their energy to all other components of the plasma through collisions. This energy transfer fuels various processes including ionization, excitation, dissociation, attachment, and scattering of these components [87].

Take H_2 as an example for plasma gas. When H_2 is exposed to high temperatures, it undergoes a transformation into a fourth state of matter. In this state, H_2 transcends its molecular structure, giving rise to a mixture of electrons, ions, atoms, and other particles. It is important to note that plasma maintains electrical neutrality, regardless of whether it is partially or completely ionized. Figure 25 illustrates how the different states of matter vary with changes in temperature and pressure [87].
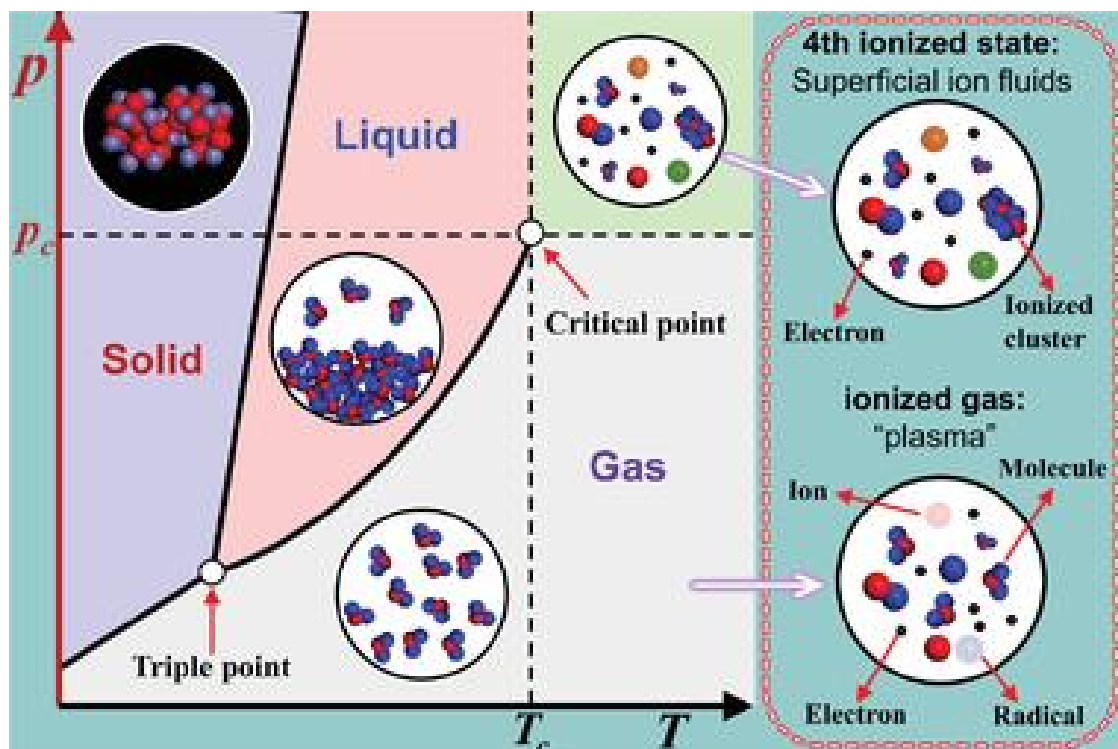
Figure 25. Different states of matter as function of temperature and pressure [87].

3.2 Classification of Plasmas

Plasma, typically described as gas that is either fully or partially ionized, can be broadly classified into two main types based on temperature: high-temperature plasma (such as corona or stellar plasma) and low-temperature plasma [87]. As mentioned before, low-temperature plasma can be further divided into thermal and non-thermal categories, depending on the

average temperature of the plasma system. In NTP, the absence of equilibrium results in electrons possessing significantly higher energies compared to ions and neutrals. Collisions between electrons and gas molecules give rise to the formation of free radicals and particles in excited states [87]. A typical NTP consists of mercury vapor gas inside a fluorescent lamp, which can be touched while operating due to its lower temperature [87].

Although not as intense as TP, NTP (cold plasma) offers significant advantages for applications involving gaseous chemical reactions, such as pyrolysis of methane. The term "non-thermal" refers to the temperature of the bulk gas stream, which typically remains lower, similar to ambient room temperature [89].

Conversely, TP, alternatively referred to as hot plasma, exhibits thermal equilibrium among its constituent particles — electrons, ions, and neutrals — resulting in similar kinetic energies. TP systems, characterized by high temperatures, efficiently dissociate or ionize the reaction gas due to the equilibrium state within the plasma zone. Additionally, TP demonstrates high enthalpy, electron density, energy density, and chemical reactivity, leading to elevated collision rates among particles [85,87]. TP is extensively utilized in the decomposition of hazardous chemicals featuring robust bonds and in facilitating reactions involving solid particle systems, such as nano-carbon synthesis. This type of plasma harbors highly energetic components capable of disrupting stable or resilient chemical bonds within compounds. Specific variants like thermal-arc, torch plasma, or supersonic plasma are adept at handling high input flow rates while ensuring very short reaction times [36]. Figure 26 illustrates the typical ranges of electron temperature and density for both TPs and NTPs [90].
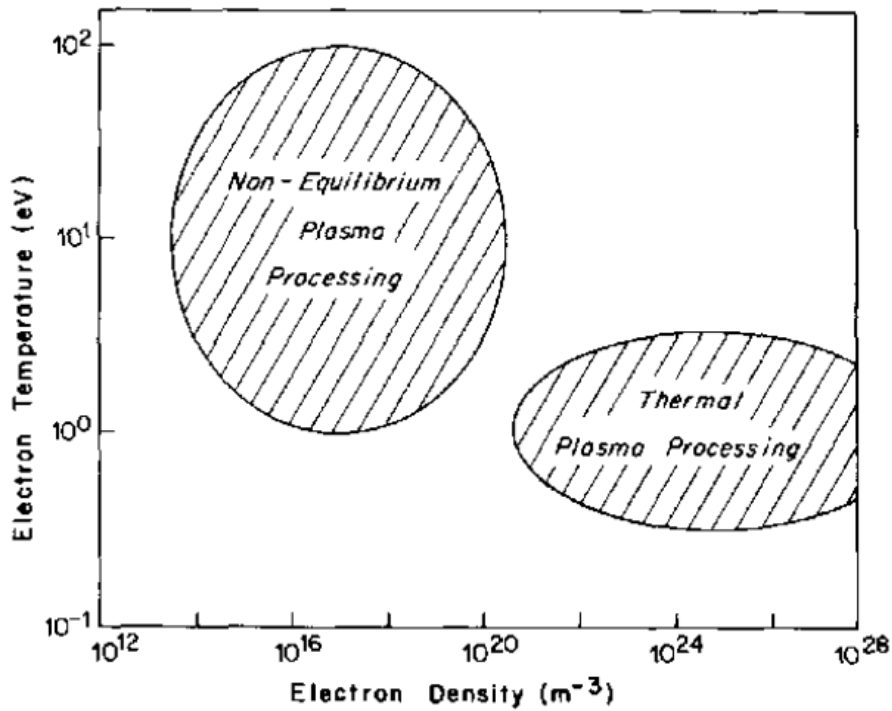
Figure 26. Electron temperature and density ranges for TPs and NTPs (non-equilibrium plasmas) [90].

Another classification for different types of plasmas is based on the value of voltage multiplied by current as illustrated in Figure 27 [36]. It is evident that TP typically exhibits high amperes and low voltages. The key distinctions between TP and NTP are outlined in Table 3 [89].
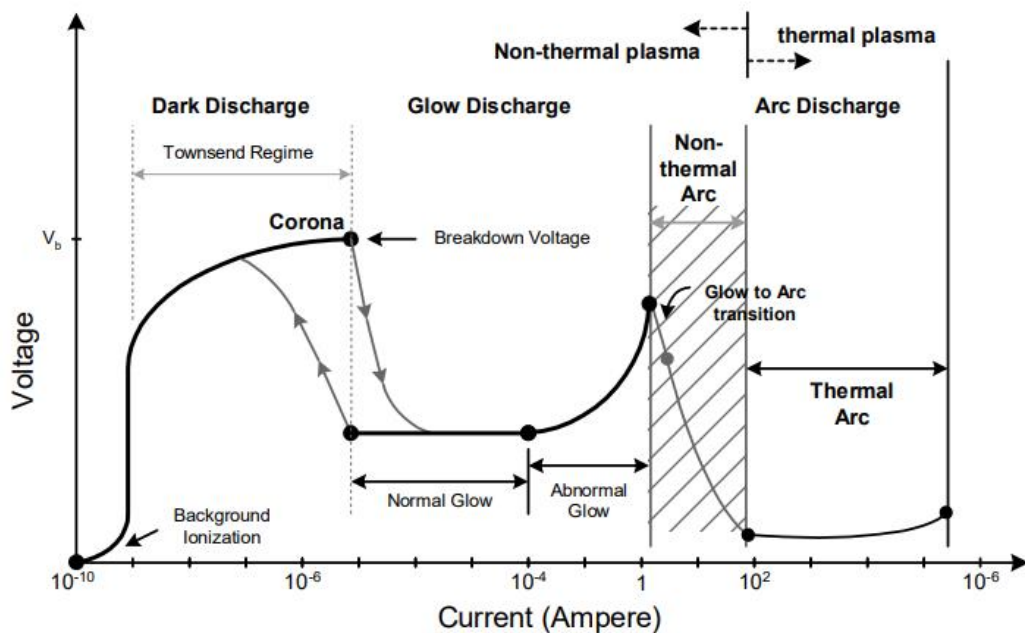
Figure 27. Plasma types shown using voltages versus amperage [89].

Table 3. TP vs NTP [89].

Characteristics	Thermal plasma (TP)	Non-thermal plasma (NTP)
Temperature [°C]	> 10,000	5,000 – 10,000
Discharged volume	High	Low
Reaction conversion	High	Low
Input flow rate	High	Low
Difficulty to handle	Difficult	Easy
Safety	Relatively dangerous	Relatively safe
Installation cost	Expensive	Cheap

As explained before, depending on multiple factors beyond operating temperature, different types of plasmas can be generated. These include DC and AC plasmas, glow discharges (GD), RF, MW, DBD, GAD, plasma jets and plasma torches [91]. A classification of these plasma types based on their temperature ranges is depicted in Figure 28 [91].
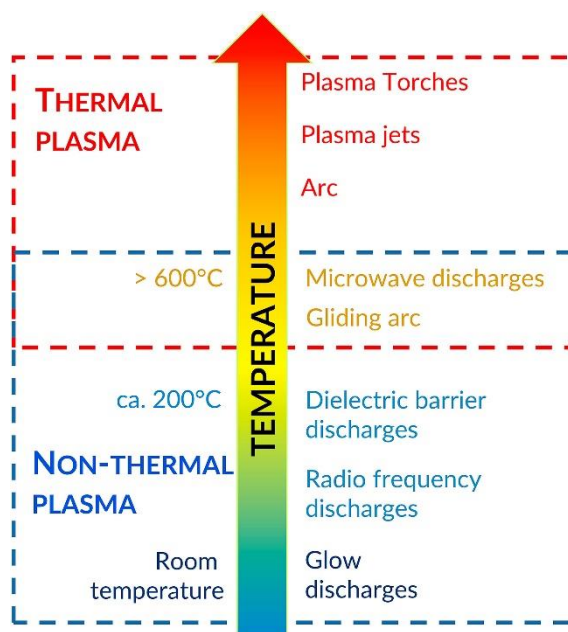
Figure 28. Temperature classification of some plasma types [91].

3.3 Various methods for plasma pyrolysis of methane

Plasma technology offers numerous advantages for the pyrolysis of methane. Certain phases of plasma exhibit significantly higher temperatures and energy densities compared to traditional catalytic methods. Moreover, plasma assists in producing concentrated quantities of energetic and chemically active particles, thereby enhancing reaction rates. Additionally, plasma systems can operate effectively outside of thermodynamic equilibrium, allowing chemical reactions to progress without dependence on catalytic effects. However, attaining suitable states and optimal discharge parameters within these complex systems, which are far from equilibrium, poses a challenge [87,91]. Furthermore, various applications of plasma in methane pyrolysis are described individually.

3.3.1 Dielectric barrier discharge (DBD)

A typical DBD reactor consists of two electrodes separated by an insulating material, often composed of materials like glass, quartz, ceramics, or polymers with low dielectric loss and high breakdown strength. The insulating medium serves to restrict current flow and prevent sparks and arcs. An AC high-voltage power supply drives the DBD, gradually transitioning the reactive gas from an insulating to a discharge state as voltage increases. Initially, insufficient voltage leads to an insulating gas state. However, as the voltage increases, the electron density rises, leading to electron collisions with gas molecules and eventually causing gas breakdown and discharge. Plasma generation in the DBD reactor yields a NTP characterized by electron temperatures ranging from 1 to 30 eV and gas temperatures between 30 and 300 °C. Gas molecule dissociation primarily occurs through electron collisions, resulting in the production of free radicals, ions, and excited species. DBD technology enables homogeneous plasma distribution and offers scalability, low energy consumption, and mild operating conditions. Despite its advantages, improving DBD plasma efficiency for methane pyrolysis remains a significant challenge [87].

Two categories of DBD reactors can be identified according to their electrode arrangement: parallel plate and coaxial. In parallel plate reactors, electrodes are aligned in parallel, separated by the dielectric barrier material. On the other hand, coaxial DBD reactors consist of one electrode placed within another, with the dielectric barrier separating them. Refer to Figure 29 for visual representation [87].
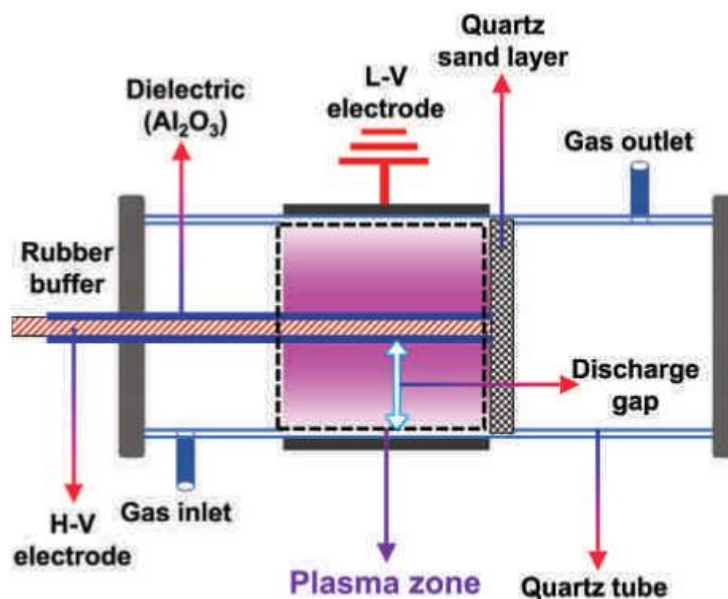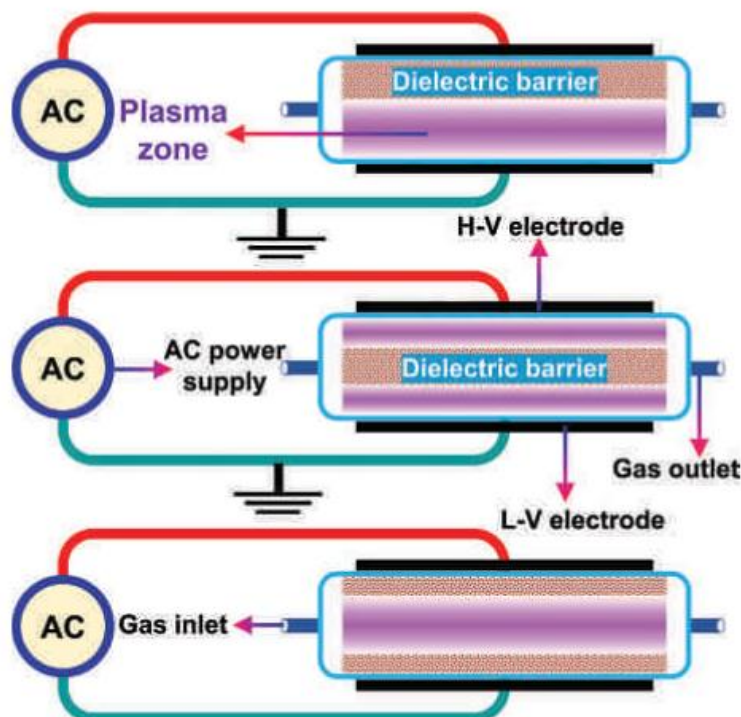
Figure 29. DBD reactor types, categorized by their electrode configurations [87].

3.3.2 Microwave (MW) discharge

MW encompass wavelengths ranging from 1 to 1000 mm and frequencies from 0.3 to 300 GHz, with common frequencies being 900 MHz and 2.45 GHz, used for instance in household microwave ovens. Since its introduction in chemical research in 1967, microwave technology has found diverse applications in fields such as chemistry, materials science, medicine, biochemistry, and catalysis. In recent years, there has been a renewed interest in MW for

methane pyrolysis due to its high conversion rates and energy efficiency. Operating conditions can vary significantly, with MW plasma ranging from non-thermal to nearly thermal states. Key advantages include reduced reaction times, automated operation for improved safety, and environmental friendliness. MW technology's capability to prevent carbon deposition on catalysts enhances stability, albeit requiring high input power to maintain stable plasma conditions. Despite challenges, integrating catalysts with MW plasma facilitates the development of lightweight methane pyrolysis reactors suitable for medium-sized plants, although research in this area is still limited [87]. An example of a microwave plasma is outlined in Figure 30 [87].
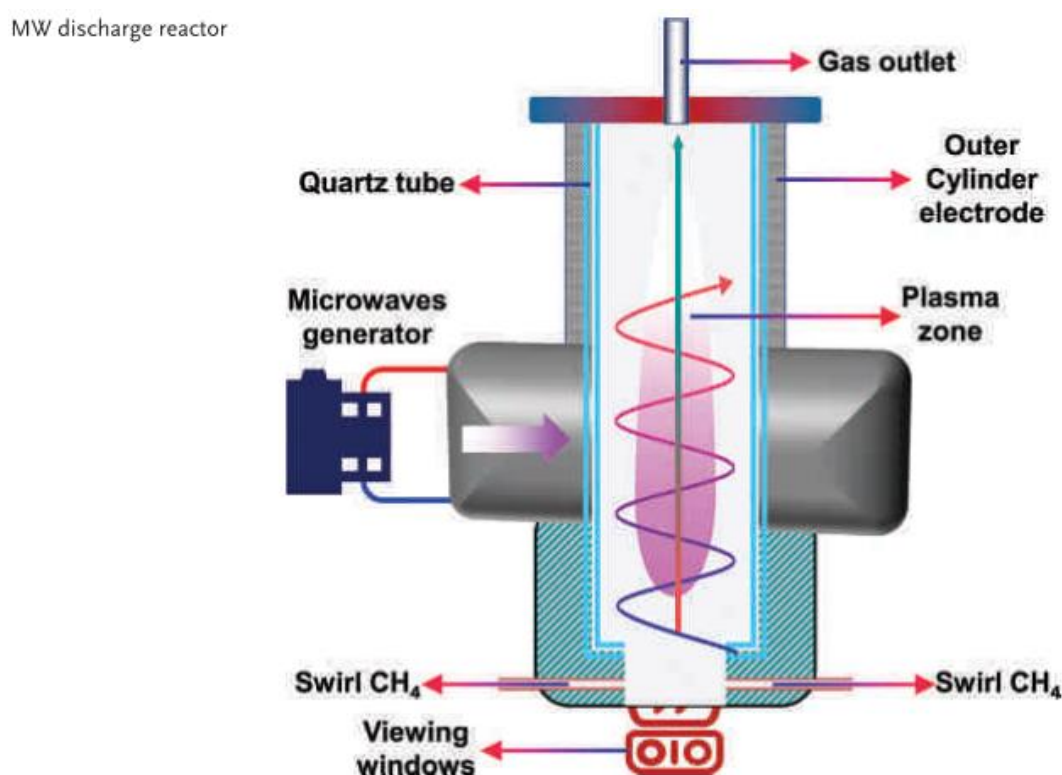
Figure 30. An example of a microwave plasma for methane pyrolysis [87].

3.3.3 Gliding arc discharge (GAD)

The thermal process in GAD reactors is initiated by an electric discharge between two electrodes. GAD reactors are preferred due to their compact design, high conversion rates, and energy efficiency. However, traditional arc reactors encounter challenges such as the inhomogeneous distribution of plasma and active species. Despite their advantages, GAD reactors also face issues related to the uneven distribution of plasma. A solution comes in the form of rotating sliding arc (RSA) discharge, a TP source that enhances performance by periodically rotating the arc, resulting in higher electron density and moderate gas temperatures.

The RSA reactor system is relatively straightforward and exhibits potential for commercialization in methane reforming applications [87]. Figure 31 demonstrates an example of such a reactor type.
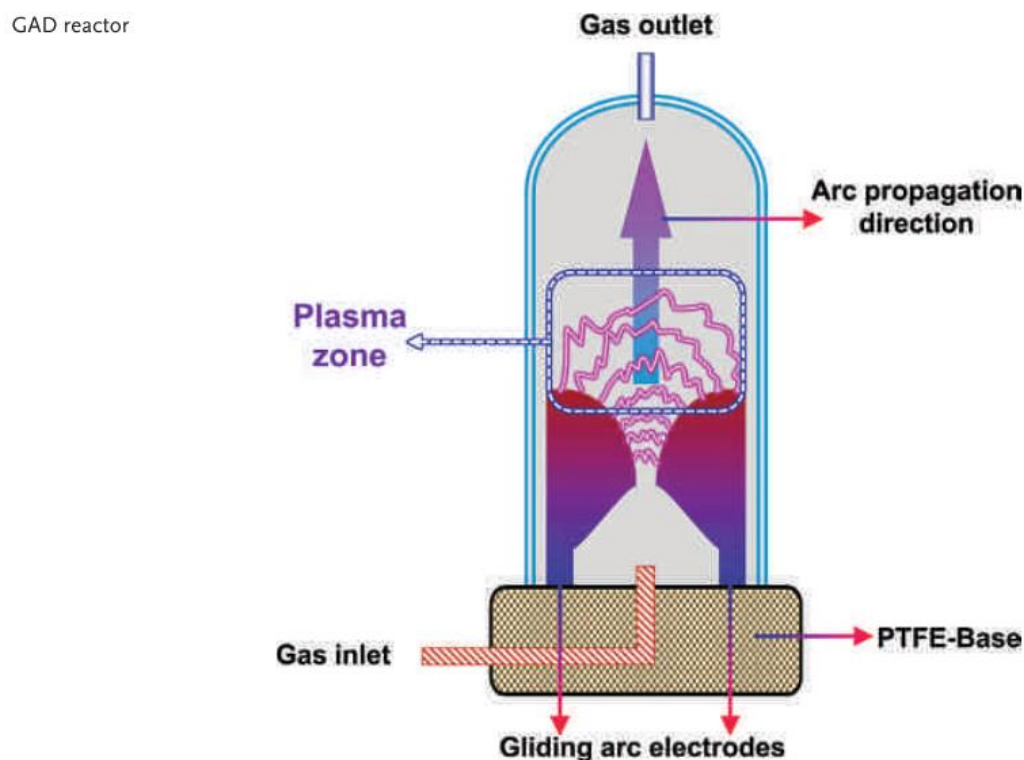
Figure 31. GAD reactor type for methane pyrolysis [87].

3.3.4 Radio frequency (RF) discharge

In a system producing RF plasma, electromagnetic energy from an RF power source induces the formation of RF thermal plasma. A precisely tuned RF plasma torch is achieved by employing an internally water-cooled quartz tube. The RF plasma torch, operating within the low-frequency range (1–100 MHz), ensures uniform distribution of plasma throughout the volume of the reactor. RF reactors offer advantages for CH_4 reforming, as they enable the generation of NTP at low pressures (1–103 Pa). RF reactors are gaining attention in industry due to their improved scalability. Energy efficiency is enhanced by utilizing an impedance-matching network. The electrode responsible for generating the RF plasma torch is situated outside the reactor, avoiding its involvement in the pyrolysis process. However, the abundance of product species in RF reactors heavily depends on discharge parameters [87].
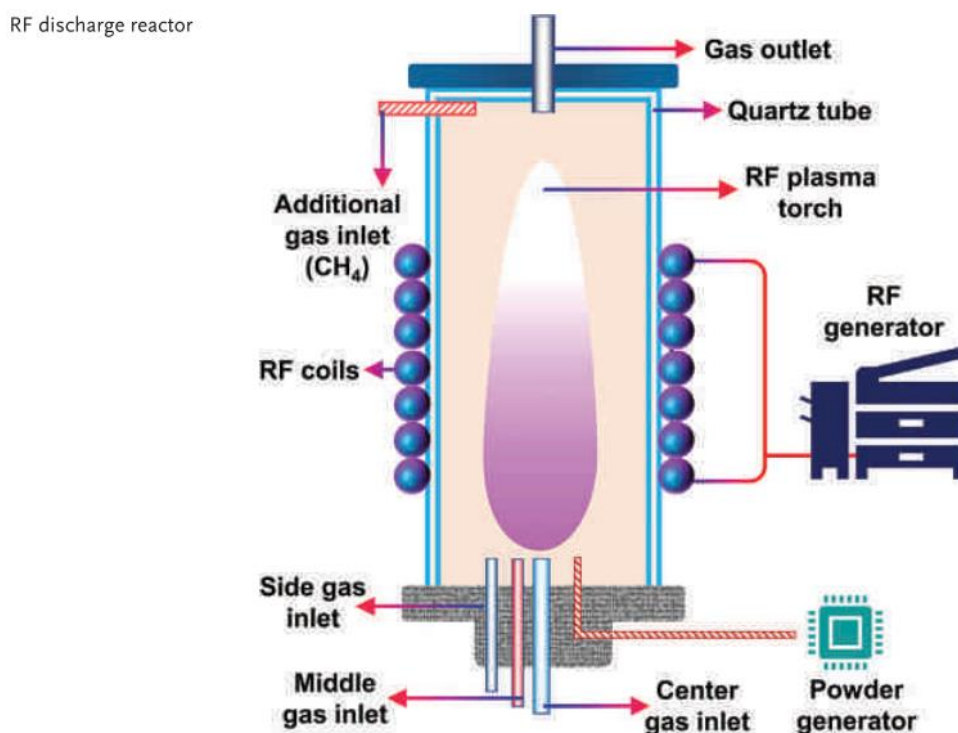
Figure 32. RF reactor layout for methane pyrolysis [87].

3.3.5 Thermal plasma (TP)

TPs can be artificially generated by supplying high-voltage electric energy, either through DC or AC power sources. This initiates an electric discharge or arc between two electrodes, which is guided by a gas flow. TP encompasses various configurations such as arcs, plasma jets, and plasma torches. The TP itself can be further categorized into non-transfer or transfer types, depending on whether the cathode and anode are connected. In the transfer type, the plasma temperature increases noticeably due to the flow of electrical current between the electrodes. These electrodes are positioned at a relatively greater distance, ranging from a few centimetres to nearly 1 m, compared to non-transferred systems [87,91]. This arrangement allows for higher operating voltage and consequently greater plasma power for the same arc current. The arc current is a critical parameter that strongly influences the energy efficiency of the arc and the lifespan of the electrodes [87,91]. Another type involves the combination of multiple electrodes, known as multi-electrode arcs, as depicted schematically in Figure 33.
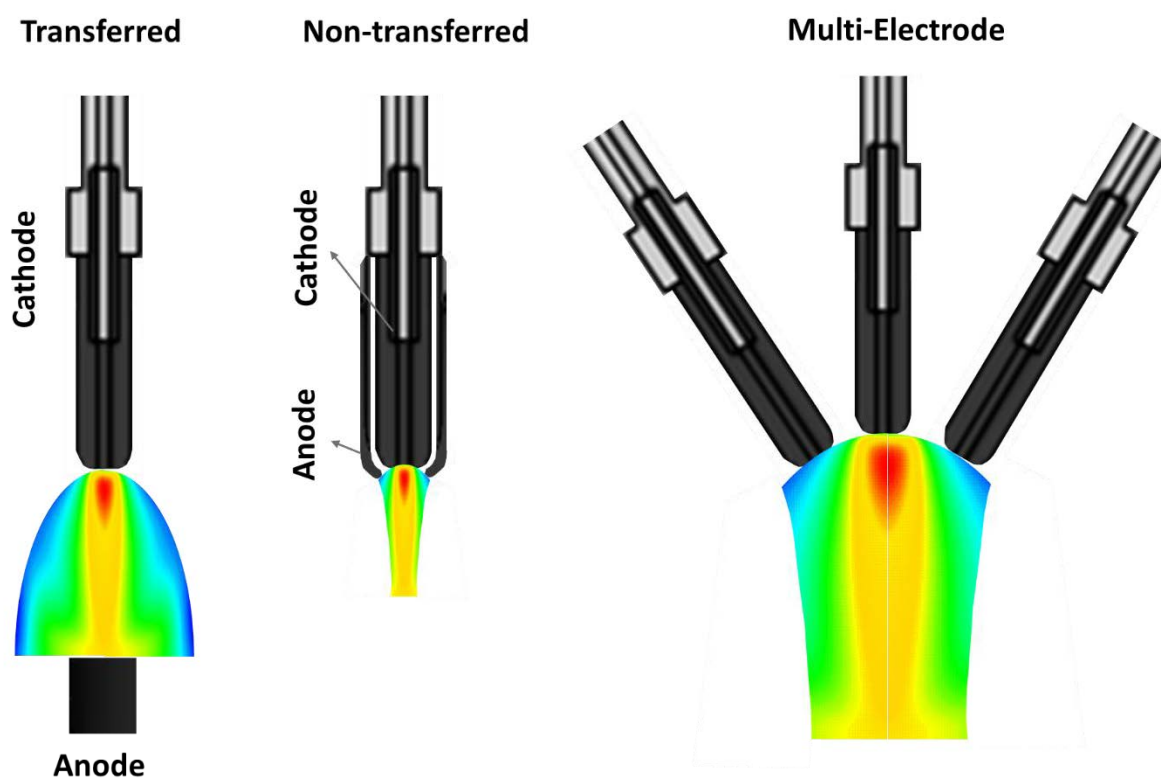
Figure 33. Various types of plasma arcs.

In TPs, the flow of plasma gas is accountable for the narrowing of the arc column in this area, leading to an increase in current density and, consequently, the maximum plasma temperature. Monoatomic inert gases like argon (Ar) require less energy to attain ionized states, which assists in stabilizing the plasma. Conversely, gases with more complex molecules such as CH_4, where carbon forms four bonds with hydrogen atoms, necessitate higher energy for plasma arc stabilization. Apart from the gas type, flow rate, and pressure, the plasma arc is also influenced by the surrounding magnetic field [92].

Usually, the addition of inert gases to methane plasma serves two main purposes: first, to improve the conversion rate by lowering the excitation energy, and second, to act as a third-body molecule capable of absorbing surplus energy from molecular collisions. When comparing the inert gases like Ar and helium (He), they display almost identical traits in methane plasma reactions, with no noticeable differences observed in the resulting products [36].

TP technology encompasses a broad spectrum of applications and ongoing developments, which can be classified as follows:

(1) TP coating techniques, which include plasma spraying, wire arc spraying, and plasma CVD;

(2) TP synthesis of fine powders, particularly those in the nanometer size range;

(3) TP waste destruction, specifically targeting toxic waste materials;

(4) TP densification of powders;

(5) TP metallurgy, covering melting and re-melting applications in large furnaces;

(6) TP extractive metallurgy; and

(7) TPPM to produce H_2 and C [27].

3.4 Thermal plasma pyrolysis of methane (TPPM)

The pyrolysis of methane process, leading to the production of turquoise hydrogen, directly competes with blue hydrogen. As mentioned before, in pyrolysis of methane, all the carbon content in methane is captured in solid form rather than being emitted as CO_2 [93].

Different methods for TPPM are currently being studied and developed, as it offers a significant competitive advantage in producing high-quality carbon materials. These methods involve modifying various parameters such as electrode geometry and materials, flow rate, the characteristics of applied current, and different plasma gases [3].

To provide an up-to-date understanding of TPPM, it is crucial to consider not only scientific publications but also industrial research and development activities. In the subsequent sections, after presenting a brief history of TPPM, we describe the current status and patented processes. Subsequently, we provide an overview of various experimental works on TPPM.

3.4.1 History and current status: Players of commercial processes

As mentioned before, TPP was initially developed to dispose of hazardous waste such as medical residues. The well-known Hüls method, originating from Germany in the 1940s, utilizes TPP to decompose hydrocarbons, resulting in the production of C_2H_2. This method involves reactors with dimensions of 100 mm in diameter and 1.5 m in length, operating at a power level of 8 MW. The carbon produced by the Hüls process was considered waste primarily because of the presence of hydrocarbon impurities [94,95].

In the 1990s, with the growing demand for CB, the Norwegian company Kvaerner endeavored to produce high-quality and pure CB. However, the process was halted in 2003 because the quality of the carbon did not meet expectations [36]. Despite these challenges, recent

advancements in plasma technology and the increasing demand for environmentally sustainable energy solutions have revived interest in TPP for generating carbon-free hydrogen and high-quality CB byproducts [36,59,79]. Further details regarding the development roadmap of TPP for methane by various key participants are outlined below.

3.4.1.1 Kvaerner

The name Kvaerner is derived from its developer, Aker Kværner Solutions, a Norwegian company that holds several patents, including those with inventors Lynum et al. Some of these patents include a patent, registered in 1996 with the title "Plasma Torch Device for Chemical Processes," and a patent, registered in 2000 for "Decomposition of Hydrocarbon to Carbon Black" [36,96,97].

"The CB & H Process", the Kvaerner process, utilizes a DC plasma torch reactor with coaxial graphite electrodes, a design initially introduced in the 1980s (Figure 34) [36]. During arc generation, there is a possibility of spatial focusing, which is mitigated by the use of a magnet coil. This coil induces rotation of the arc, ensuring uniform heating and pyrolysis of the feedstock. Additionally, the rotation of the arc helps minimize electrode erosion. The reported rate of electrode erosion is approximately 0.1 g/kWh [36].
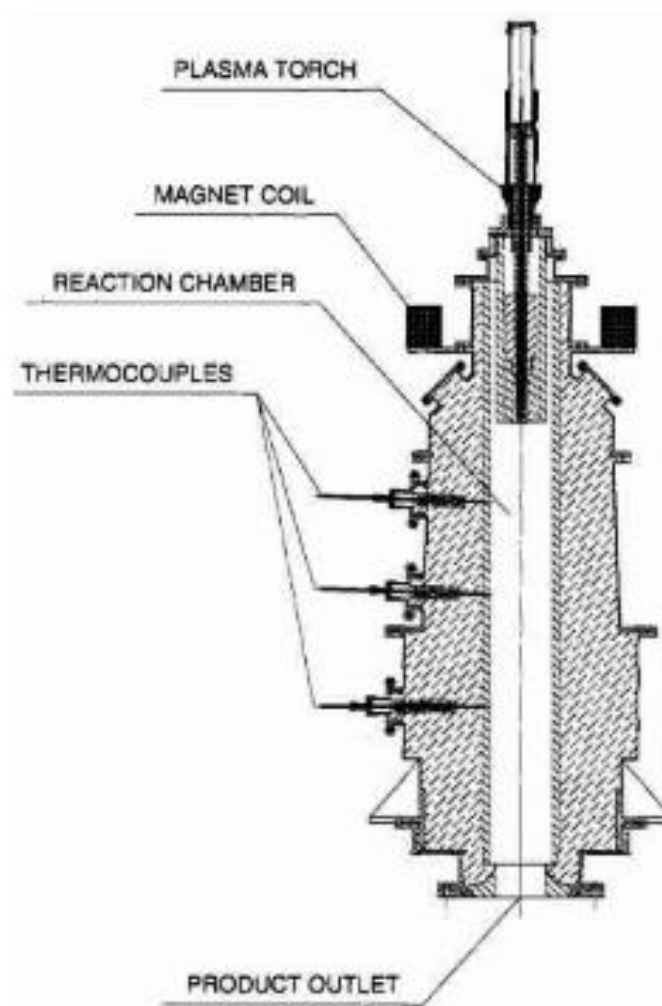
Figure 34. The plasma reactor from the Kvaerner process [36].

The key parameters of the process include the flow rate and temperature of the feedstock, as well as the method of feedstock feeding (such as the location and number of ports). Since the electrode is graphite, other by-products not present in the feedstock are not generated [36].

A flow chart of the process is illustrated in Figure 35.
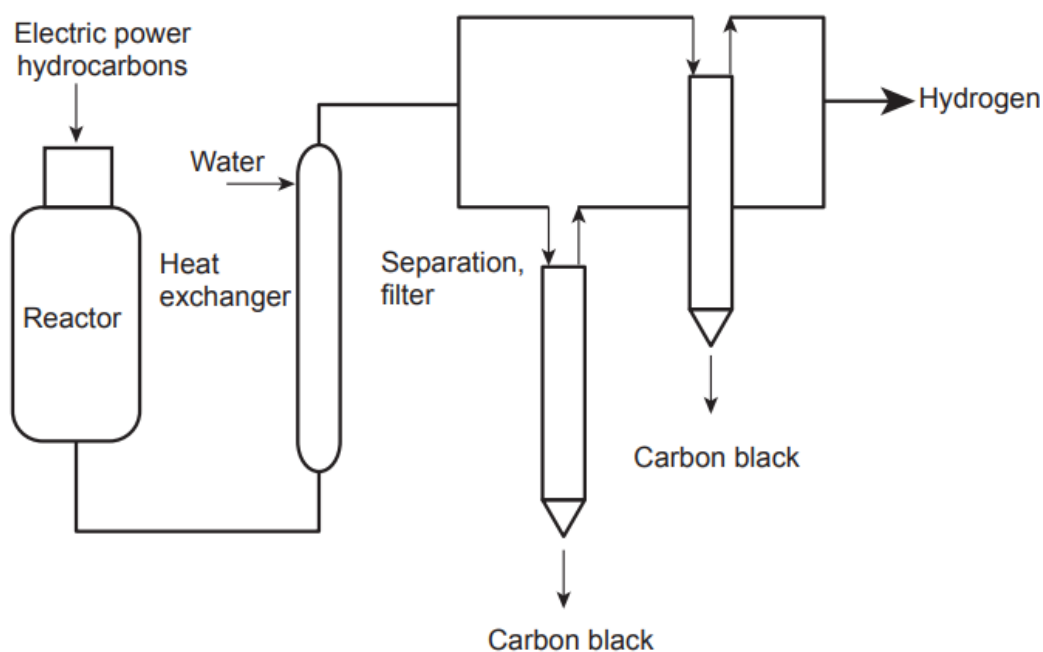
Figure 35. Flow chart of Kvaerner process for H and CB production [36].

H_2 is employed as the plasma gas, and a portion of the hydrogen generated is recirculated into the plasma torch. Prior to entering the reactor, both NG and plasma gas are preheated [72].

Following the successful operation of a pilot plant with a plasma output of 3 MW, Kvaerner initiated the construction of a commercial-scale "Karbomont" plant near Montreal, Canada, in 1997. The Karbomont plant was completed in 1998 with a production capacity of 20,000 tons of CB [36,79]. However, achieving the expected quality of CB proved challenging, resulting in the carbon being sold at a significantly lower price than anticipated. Meanwhile, the nearby refinery purchased the hydrogen produced. Due to the insufficient quality of the CB product, the plant was shut down in 2002 and subsequently demolished in 2003 [36,79].

3.4.1.2 Monolith

Established in 2012 in California by two Stanford engineering alumni, Monolith Materials draws upon Kvaerner technology licensed from Aker Solutions in 2013, as well as research conducted by Laurent Fulcheri's team at the Centre for Processes, Renewable Energies, and Energy Systems at Mines Paris Tech PSL Research University. By combining these various technologies through further engineering endeavors, Monolith developed the innovative Monolith process [72].

Monolith collaborates closely with the Center for Processes, Renewable Energies, and Energy Systems at MINES ParisTech PSL Research University in Paris, conducting pilot-scale

reactor testing since 2018. Furthermore, the company collaborates with Aker Solutions to capitalize on the insights gained from the Karbomont commercial-scale plant [72].

The pilot-scale setup, which stands at a height of two meters, is located in the laboratory of the Center PERSEE – MINES ParisTech – PSL, in Sophia-Antipolis, as depicted in Figure 36. The setup operates with a three-phase AC power supply with a capacity of 100 kW. Graphite electrodes positioned on the upper part of the reactor create a heated zone for the reaction. Carbon is separated from the gas using a filtration unit [98].
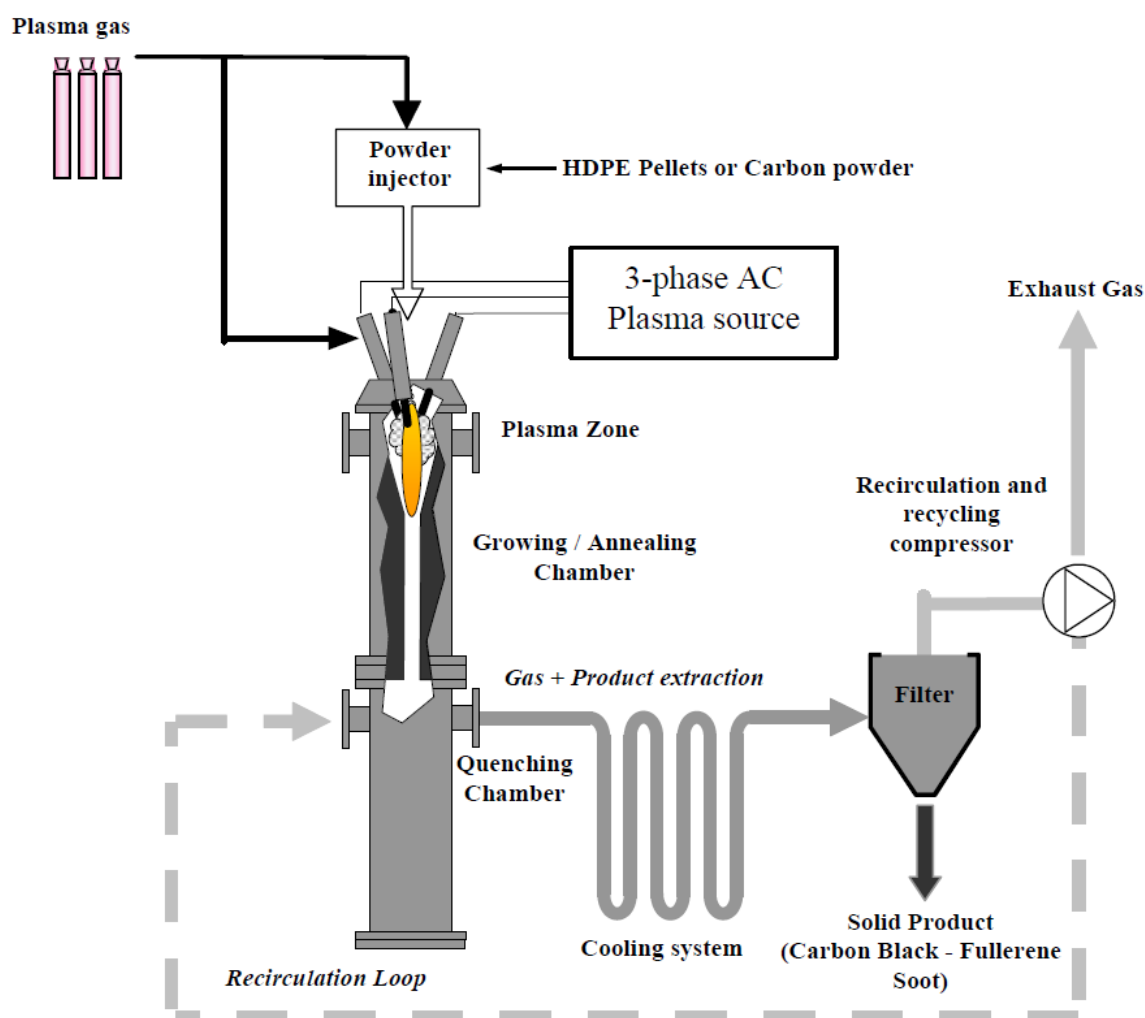
Figure 36. The pilot scale thermal plasma reactor from MINES ParisTech [98].

Monolith utilizes its thermal plasma process to produce CB as its main product, along with valuable hydrogen tail-gas as a secondary output. NG, in combination with process gas, is introduced into the upper portion of a plasma reactor, where it undergoes heating to temperatures ranging from 1,500 to 2,000 °C through electric plasma [79,88].

In September 2014, the Seaport I demonstration pilot plant reached completion in Redwood City, California, with CB production beginning in April 2015. The facility had an annual production capacity of 700 tonnes of CB and 200 tonnes of H_2. After the successful demonstration of the technology, the pilot plant was shut down in the autumn of 2018 [72,79,88,99,100].

Construction of the commercial-scale Olive Creek I (OC1) facility near Hallam, Nebraska, began in October 2016, and by 2020, the plant was operational, producing its first batch of CB. OC1 has an annual production capacity of 14,000 tonnes of CB and 4,500 tonnes of H_2, with a capital cost of approximately USD 100 million [72,99].

The second phase of expansion, Olive Creek II (OC2), is planned to have around 12 times the capacity of OC1. It is projected to produce approximately 194,000 tonnes of CB annually (comprising 180,000 tonnes/year from OC2 plus 14,000 tonnes/year from OC1) and 275,000 tonnes of clean ammonia per year. The estimated cost for OC2 is approximately USD 1 billion. Notably, the technology does not require scaling, as Monolith intends to adopt a modular approach by replicating the reactor 12 times. The expansion facility will require approximately 1.2 to 1.5 million cubic meters of water annually for cooling purposes. Construction of the OC2 facility began in the second quarter of 2023, with completion expected by 2025 [79,99,101]. The development of Monolith process is summarized in Figure 37 [88].
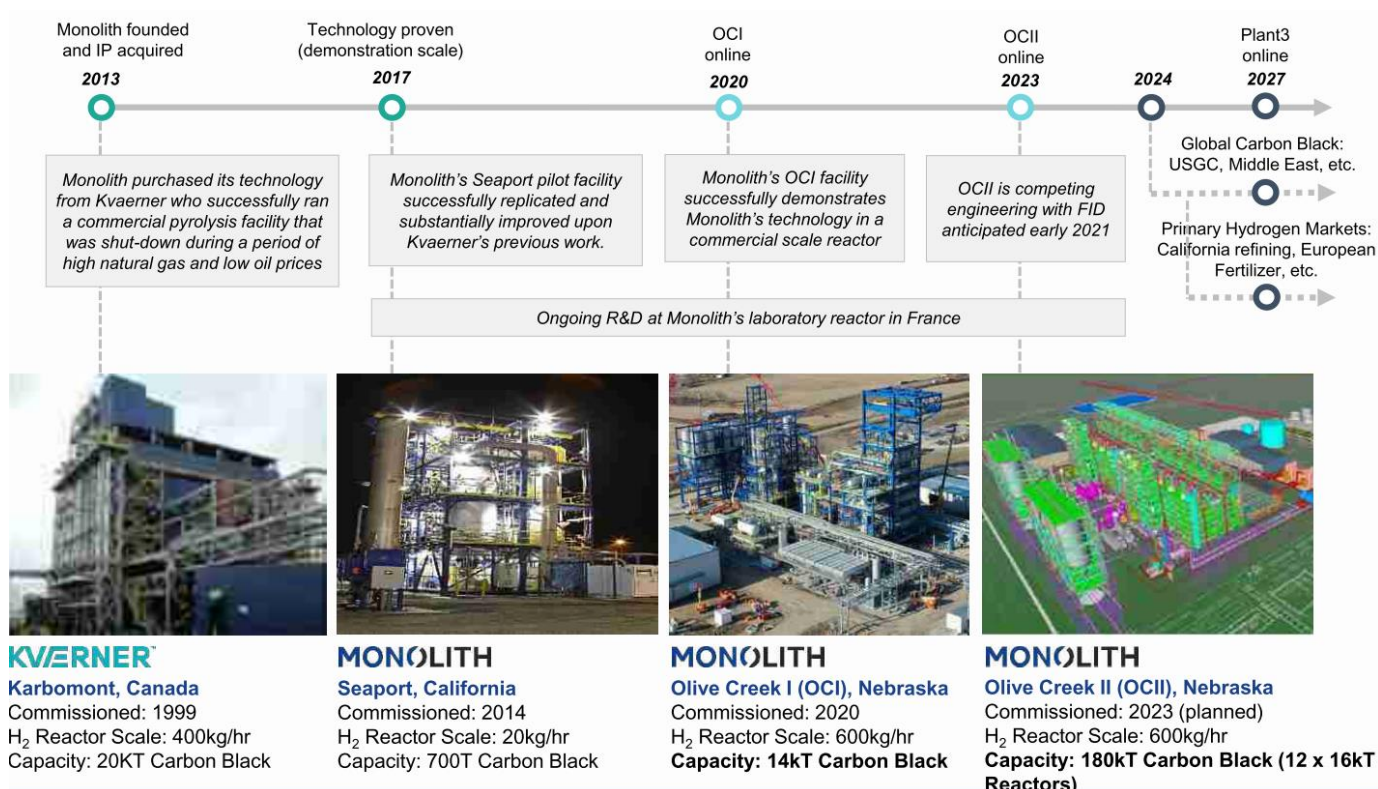
Figure 37. Development pathway of the Monolith process [88].

3.4.1.3 Plenesys

Sabri Takali, a former doctoral candidate under Laurent Fulcheri, has established his own venture named Plenesys. This small startup company was founded in 2018 and is situated in Valbonne, southeastern France [102,103].

Plenesys is presently developing the HyPlasma® Process, which utilizes a TP technique employing its patented AC plasma torch with a power supply ranging from 150 to 250 kVA. This method entails generating TP through an electric arc discharge between three graphite electrodes. Figure 38 provides a visual representation of how the process operates [72,102,103].
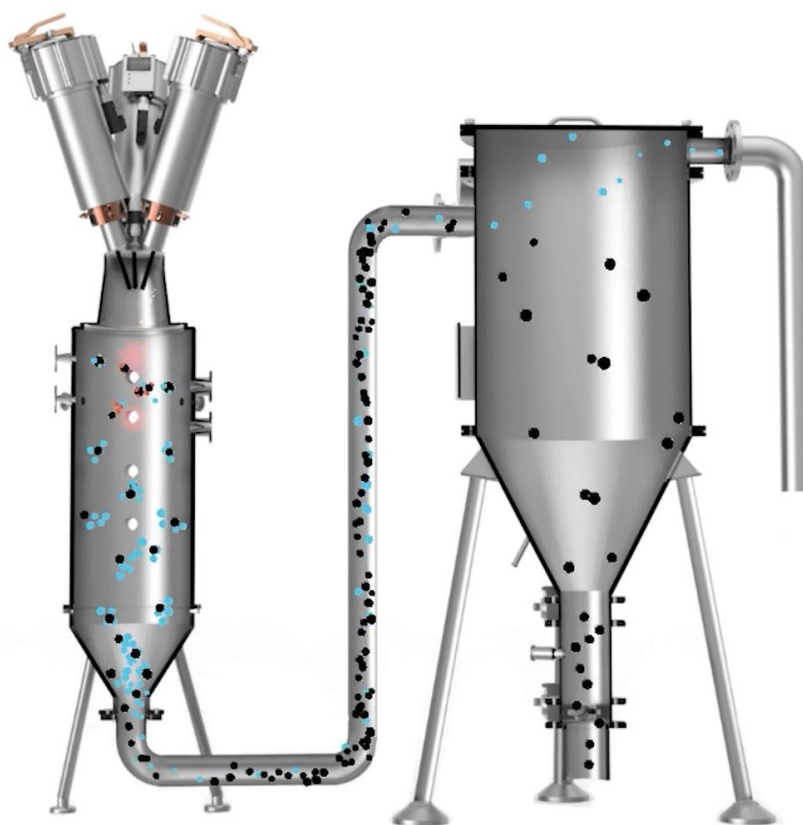
Figure 38. 3D demonstration of the HyPlasma® reactor [103].

3.4.1.4 Graforce

Graforce, a German company has pioneered a TP technology driven by DC plasma system, where the plasma arc is ignited using high frequency high voltage current and stabilized by implanted magnets. The facility is still in demonstration scale level with capacities scaling up to 6,500 Nm^3/h [79].

3.4.1.5 Atlantic Hydrogen

The Canadian company Atlantic Hydrogen Inc. has developed CarbonSaver™ technology, which comprises a series of proprietary pulsed plasma torches and additional equipment. Initially, the aim was to produce hydrogen-enriched NG, containing up to 20 vol% H_2. The CarbonSaver™ process can be implemented at various points along a pipeline close to end users [72]. Boutot et al. filed a patent, 'Decomposition of Natural Gas or Methane Using Cold Arc Discharge" [104], for a cold arc discharge plasma enabling reactor operation at temperatures below 200 °C, while also mentioning a TP torch reactor operating at temperatures between 1,500 and 2,500 °C [20]. In 2009, a three-year pilot project was launched, producing approximately 25 m^3/h of NG (> 85% CH_4) or CH_4. Subsequently, the company shifted its focus to producing hydrogen suitable for fuel cells using a 100 kW microwave plasma to reach temperatures of 700–900 °C [105]. A field demonstration plant was under construction in New Brunswick and was stated to be operational in 2015. However, the company filed for bankruptcy that same year, and the technology was not further developed [72,79].
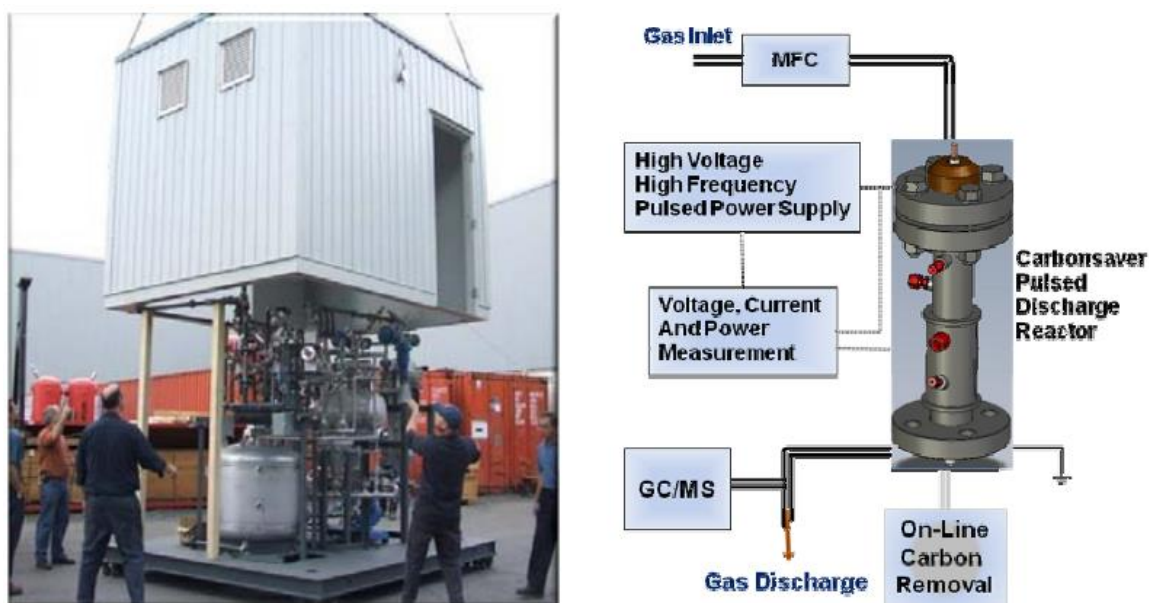
Figure 39. Pilot scale of CarbonSaver™ process; MFC: mass flow controller; GC/MS; gas chromatograph with mass spectrometer [105].

3.4.1.6 HiiROC

HiiROC is a newly established startup founded in 2019 and based in Hull, UK. Collaborating with the University of Hull. HiiROC is focusing on a unique thermal plasma torch technology to produce H_2 from biomethane, flare gas, or NG. Although precise technical specifications are not publicly disclosed, these units are engineered to be flexible, scalable, portable, and deployable

directly at the required locations. This approach leverages existing infrastructure and eliminates the need for storage and transportation expenses [106]. An illustration depicting the concept of the process has been provided by the developer, as shown in Figure 40 [106].
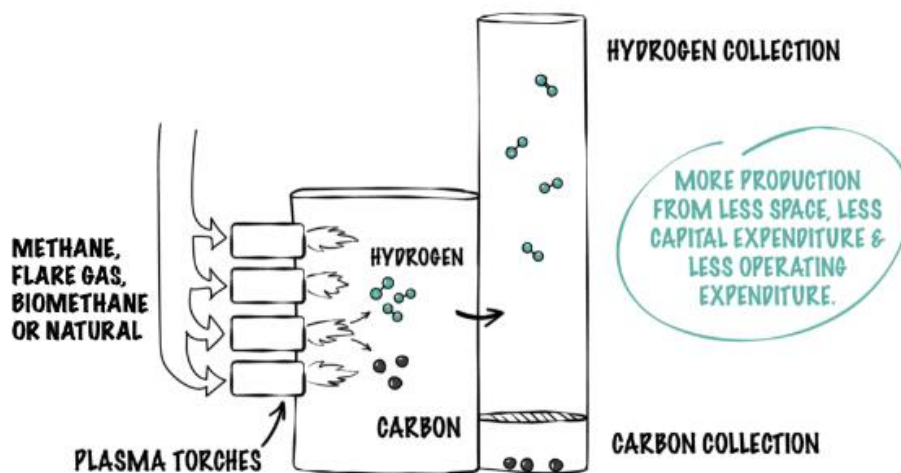
Figure 40. HiiROC process concept [106].

Several other processes have been developed, which operate on NTP principles. These include the TOMSK-GAZPROM method [72], GasPlas [79], Spark Cleantech [107], Levidian-LOOP [108], Sakowin Green Energy [109], and Hycamite [110]. However, as they are not the primary focus of the current work, further details on these processes are not provided.

3.4.2 Review on the experimental laboratory studies

Fincke et al. [35] examined TPPM employing a DC plasma reactor. Their investigation focused on the carbon yield concerning gas residence time, proposing a model for carbon growth. Additionally, they explored potential reaction byproducts like C_2H_2 and C_6H_6. Two methods were suggested to enhance carbon yield: Raising process pressure to elevate reactant concentration and increasing nucleation rate through the introduction of nucleation sites, such as graphite electrodes [94].

Lee et al. [111] utilized a DC TP system featuring three torches. Their investigation centred on the CH_4 conversion rate and resultant products, such as H_2 and C_2H_2, by manipulating the CH_4 flow rate and quenching conditions. H_2 concentration in the product gas increased when CH_4 flow rate was increased, and the quenching rate was reduced. At the same time, a higher CH_4 flow rate reduced the CH_4 conversion rate. The carbon produced exhibited characteristics akin to CB, with a more graphitized structure. But they could not find a relation between the process parameters and the carbon characterization [111].

Similarly, Li et al. [20] employed a DC plasma setup following the same principle. They examined the impact of different gas injection methods on plasma stability and CH_4 conversion rates to H_2 and C_2H_2. They noted that the conversion rate was higher when Ar and CH_4 were pre-mixed and introduced through the plasma torch, albeit with more severe graphite electrode erosion. Furthermore, they confirmed that increasing CH_4 in the gas mixture affected plasma stability and constrained testing time. Conversely, introducing CH_4 after the torch outlet did not influence the plasma state [20].

Boutot et al. [105] have used a commercial plasma reactor to partially convert NG to H_2 and solid carbon. They demonstrated that increased pressure necessitates higher voltages for operation, and pressure levels exceeding 2 bar would demand additional power supply, thereby increasing the cost of the process. They also investigated the produced carbon and reported it as a structured mixture of amorphous and nanostructured carbons. They also addressed the issue of process stability and its limitations: the deposition of carbon on the surface of the electrodes leads to bridging and short circuits, resulting in immediate interruptions of the plasma arc [105].

Maslani et al. [112] employed a DC plasma reactor with a distinct methodology. They used water vapour and Ar as plasma gas stabilizers, with CH_4 introduced separately into the reactor. Their investigation centred on the CH_4 conversion rate and the system's energy balance, which were explored by varying the CH_4 flow rate. They noted that higher CH_4 flow rates correlated with lower conversion rates. Furthermore, their examination of the formed carbon revealed well-defined spherical particles measuring 1 µm in size. However, they also detected carbon oxides in the product gas due to operation in a slightly oxidizing atmosphere [112].

Kim et al. [113] utilized a combination of a DC plasma torch and a RF torch for H_2 production and examined the characterization of the resulting carbon through microstructure investigation techniques. They observed slight variations in the structural properties of the carbon depending on its position within the reactor. Carbon collected from the inner wall of the chamber exhibited a more crystalline structure compared to the finer carbon collected in the product gas filter, attributed to prolonged exposure to high temperatures. In another investigation [114], they identified the produced carbon as nanostructured sheet-like carbon and conducted comprehensive studies on it. They concluded that the size of the carbon product is influenced by plasma temperature, regulated by power input. Lower power and temperature levels inhibited product formation, leading to the retention of small structures resembling CB. Higher temperatures facilitated carbon growth, resulting in the formation of 2-D sheet-like synthetic carbon. This thermal environment promoted crystal growth, yielding sheet-like carbon structures

characterized by high specific surface area and significant crystallization. These properties make the material appealing for various applications, including energy storage and fuel cells.

Fulcheri et al. [59] utilized a three-phase AC plasma system, each connected to three graphite electrodes, with H_2-N_2 serving as the plasma gas. CH_4 was introduced separately into the plasma zone. Their investigation focused on the CH_4 conversion rate, carbon product, and determining the system's energy balance. Their calculations revealed an energy intensity of 25 kWh/kg of H_2, which is 42% less than that of electrolysis, that is around 60 kWh/kg of H_2. They also noted that the carbon particles exhibited an aggregate morphology resembling CB, albeit without the typical spherical or turbostratic characteristics of CB's primary nuclei. This deviation in characterization was attributed to the highertemperature compared to conventional furnaces used in CB production. These findings suggest promising prospects for their product potentially capturing a significant portion of the CB market [59].

Li et al. [20] from Tsinghua University in Beijing conducted an experimental study focusing on C_2H_2 production, albeit on a smaller scale. They observed the presence of H_2 in the product gas, which can be stabilized at room temperature through gas quenching, similar to the Hüls process. Using a 2 kW DC plasma arc device, they explored various process conditions and conducted two testing scenarios. They compared the effects of pre-mixing CH_4 in the plasma gas with direct CH_4 injection without pre-mixing. Quenching of the product gas was achieved using 10 Nl/min Ar. Gas chromatographs were used for product gas analysis to determine conversion rates and C_2H_2 selectivity. The study concluded that pre-mixing had a beneficial impact on methane conversion, ranging between 90-99%, and resulted in lower electrode erosion. Conversely, direct CH_4 injection into the arc resulted in much lower conversion rates, ranging from 60 to 80%, depending on power input and CH_4 flow rate. It was suggested that methane, when not pre-mixed, struggles to fully interact with the jet zone. Increasing power input improved the conversion rate, but higher flow rates reached a point where further increases decreased arc efficiency, testing duration, and consequently, CH_4 conversion rate. Endothermic decomposition reactions inducing local cooling were identified as another reason for arc instability, causing non-uniform properties within the plasma gas phase. This dynamic led to arc movement, ensuring it remained within high-temperature zones in space, resulting in voltage fluctuations. Observations revealed that a higher Ar flow rate enhanced arc stability but reduced the average enthalpy of the jet flow. The study identified an optimized Ar flow rate of 10 Nl/min, yielding the best results. It was demonstrated that a higher quench gas flow rate increased selectivity to C_2H_2, reducing C production. To counter this effect and promote H_2 and solid carbon production, sufficient time for C_2H_2 decomposition is crucial [20].

Table 4. Summary of literature on TPPM.

Authors	Experimental setup	Focus of study	Reference
Fincke et al.	DC plasma reactor	• carbon yield concerning gas residence time • potential byproducts like C_2H_2 and C_6H_6	[35]
Lee et al.	DC TP system featuring three torches	• product gas analysis • CH_4 flow and gas quenching rates • characterization of the carbon microstructure	[111]
Li et al.	DC plasma setup	• impact of different gas injection methods on plasma stability • CH_4 conversion rates to H_2 and C_2H_2	[20]
Boutot et al.	pulsed discharge plasma reactor	• effect of the operating pressure on the required electric power • examination of the produced carbon • process stability	[105]
Maslani et al.	DC plasma reactor	• CH_4 conversion rate • system's energy balance • effect of CH_4 flow rates • morphological examination of the formed carbon	[112]
Kim et al.	DC-RF plasma torch	• morphological characterization of the resulting carbon	[113,114]
Fulcheri et al.	a three-phase AC plasma system	• CH_4 conversion rate • morphological characterization of the carbon product • determining the system's energy balance	[60
Li et al.	DC plasma arc device	• effect of plasma gas mixture on the resulting product gas • C_2H_2 production yield • quenching rates of the product gas and C_2H_2 selectivity	[20]

In light of the recent advancements in plasma technology, it is essential to develop a structured framework for understanding how different process variables impact the results of pyrolysis of methane. This framework should encompass factors influencing methane conversion rates and the quality of carbon generated. Such an endeavor is pivotal in bridging

existing knowledge deficiencies and enhancing our comprehension of plasma pyrolysis' potential as an eco-friendly approach for generating both H_2 and carbon. However, before delving into this, it is essential to determine the technical feasibility of the process using the available setups.

4 Testing the feasibility of a plasma furnace for pyrolysis of methane

The present chapter outlines the findings of a technical feasibility investigation into TPPM. It provides an overview of the concept and methodology employed, followed by a demonstration of the plasma reactor layout and a detailed description of the test protocol to ensure the reproducibility of the process. The study pursues three distinct approaches and study areas by specifying key variables in the process parameters. Ultimately, the chapter concludes with a comprehensive discussion of the results.

The fundamental concept revolves around exposing CH_4 to a plasma arc, causing its breakdown into H_2 and solid carbon. Following this, the H_2 is to be collected and enriched, while the residual carbon undergoes additional processing for its utilization as a valuable second product. Figure 41 provides a visual representation of the demonstrated concept. It is imperative to thoroughly investigate and optimize both H_2 production and carbon quality in this process [115].
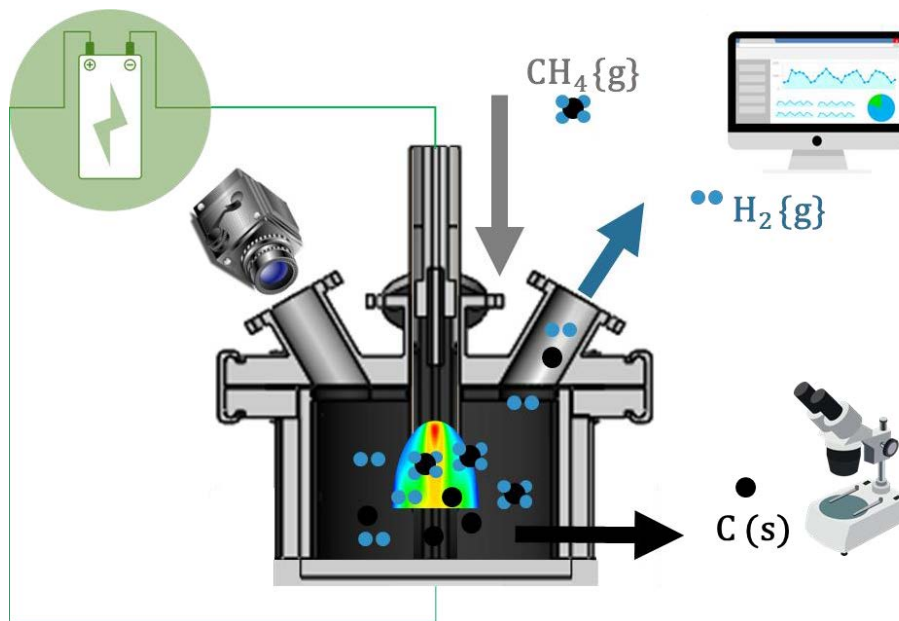
Figure 41. Illustration of the study concept for hydrogen and carbon production using green electricity [115].

A set of experiments were undertaken to evaluate the pyrolysis process under various parameters. The objective was to ascertain the viability of the process concept and identify the key parameters or conditions that have a substantial impact on its outcomes. It is crucial to achieve optimal H_2 production and attain the utmost process stability while maximizing the CH_4 conversion rate.

4.1 Plasma reactor layout

For the production of H_2 and solid carbon, a plasma furnace in the laboratory of the Chair of Ferrous Metallurgy located at the Montanuniversität Leoben (MUL) was used. The configuration of the facility is depicted in Figure 42. Numerous research papers have utilized this facility for studying steelmaking [116–119]. However, for the purposes of this study, slight modifications were made to the facility, which will be elaborated upon later.
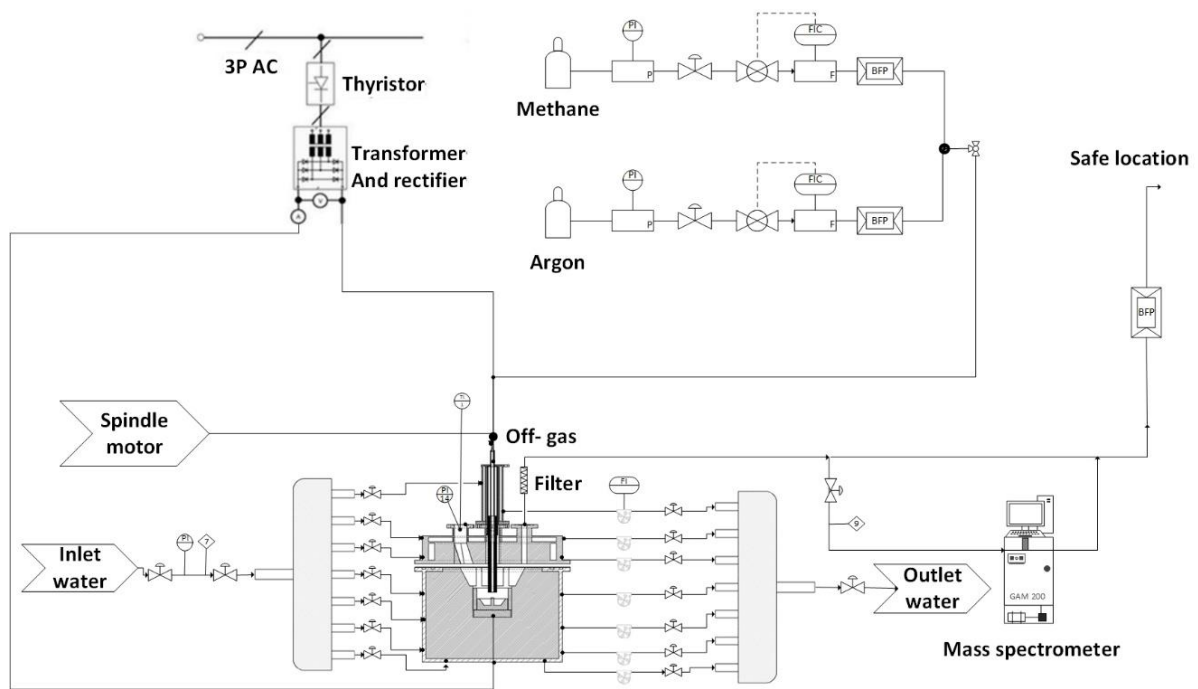
Figure 42. Layout of the thermal plasma facility, used in this study [92].

The furnace comprises two distinct sections: the upper lid and the main body. Both sections are lined with refractory materials and are equipped with a water cooling system. These are shown in Figure 43 [92].
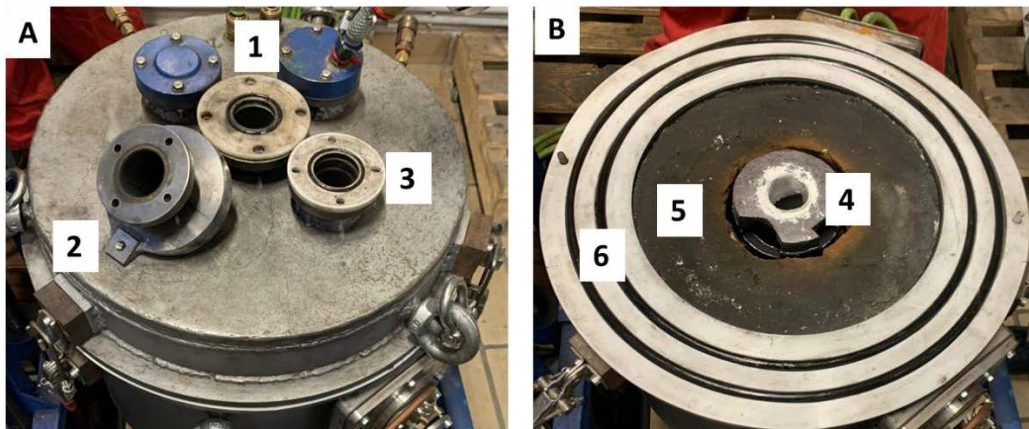
Figure 43. Reactor installation: A: the lid with three openings (1. cathode inlet, 2. camera window, 3. product gas outlet), B: the reactor (4. graphite reaction chamber, 5. lining, 6. sealings) [92].

A graphite ignition pin is positioned atop a graphite crucible to initiate and maintain a concentrated arc discharge. The arc is vertically initiated between the anode pin and a graphite hollow cathode. A DC power supply, manufactured by Messer Grießheim GmbH, with an average input of 5 kVA is employed. Subsequently, the arc length will be manually increased using the spindle drive engine. The current flow is controllable through an implanted thyristor

(silicon-controlled rectifier or SCR) connected to a three-phase transformer, supplying a power range of 1 to 16 kVA in two adjustable levels. The thyristor trigger can be manually adjusted within a range of up to 100%. Current and voltage are recorded during operation [92].

The gas is injected into the furnace through a hollow cathode. Both the cathode and anode pin are shown in Figure 44. The hollow cathode features an inner diameter of 5 – 7 mm (d_{in}), an outer diameter of 24–27 mm (d_{out}), and a length of 120–150 mm (L_c). The anode pin, on the other hand, has a diameter of 28 mm (d) and a length of 40 mm (L_a). The reaction chamber, also crafted from graphite, is specifically designed to optimize solid carbon trapping within the reaction zone and prevent impurities in the deposited carbon [92].
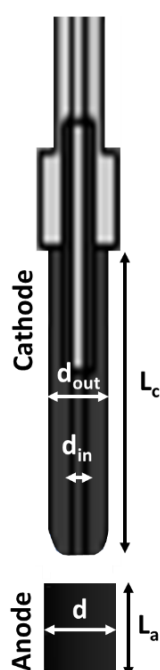
Figure 44. Drawing of the hollow graphite cathode and the graphite anode pin [92].

The gas input consisting of Ar and CH_4 is controlled by two EL-Flow PRESTIGE F-210C mass flow controllers produced by Bronkhorst High-Tech BV. The CH_4 used in the test is supplied by Methane 2.5 cylinder with a purity higher than 99.5. Moreover, Ar had a purity of over 99.99% [92].

The resulting gas will leave the reaction chamber through the designated opening in the top lid, as illustrated in Figure 43(A-3) and be forwarded for dust removal to a ceramic hot gas filter, type FE2 from ABB Ltd, and a fine filter. Thereafter the product gas will be analysed by a gas mass spectrometer, type GAM 200, produced by InProcess Instruments Gesellschaft für Prozessanalytik mbH. Camera system AXIS-Q1775 provided a live stream of the arc from Axis Communications AB integrated on the top lid of the furnace [92].

Observation of the arc, facilitated through the opening indicated in Figure 2(A-2), is conducted using a camera system (Axis-Q1775) from Pieper GmbH, Schwerte, Germany. Details of the camera setup are illustrated in Figure 45 [92].

Figure 45. The camera system and instalment to the top lid of the plasma furnace [92].

The pyrolysis test procedure demonstrated in Figure 46 consists of the following steps [92]:

(1) Purging the entire reactor with Ar to provide an inert atmosphere and ensure safe operation.

(2) Moving the cathode to the arc ignition position, where it comes into contact with the anode, causing a brief short circuit.

(3) Igniting the arc using Ar as the plasma gas and promptly returning the cathode to a pre-defined stable arc length position. Adjusting to a 5 kW power input as an example.

(4) Monitoring the plasma arc through the camera installed on the top window of the lid. This stage is active until halting the power supply, hence the plasma arc.

(5) Introducing CH_4 to the transferred arc by transitioning the gas from pure Ar to a mixture of Ar and CH_4, taking 60% Ar and 40% CH_4 as an example.

(6) Monitoring the reaction using the data from the gas mass spectrometer device installed on the product gas pipeline. The product gas analysis is watched during the entire test.

(7) Halting the CH_4 flow upon completion of the intended test and transitioning to 100% Ar. Powering off and discontinuing the plasma gas flow simultaneously.

(8) Purging the entire reactor with Ar before dismantling it.
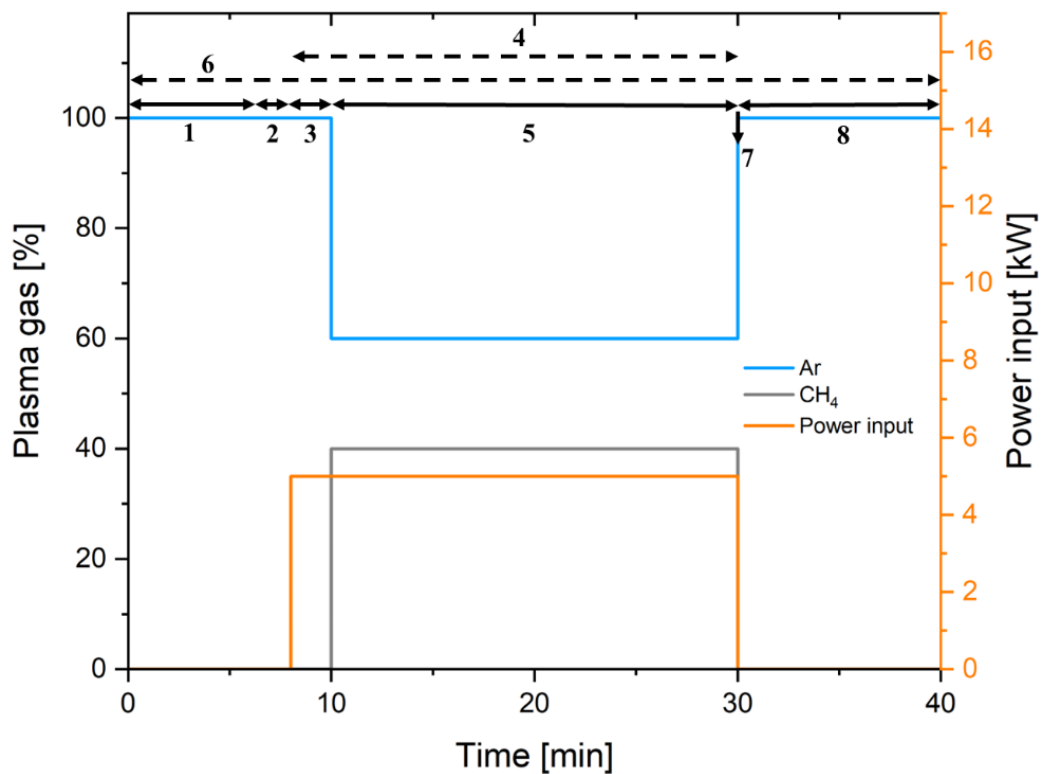
Figure 46. Example of a pyrolysis test procedure [92].

This systematic approach allows for precise control and observation throughout the pyrolysis test, facilitating a comprehensive understanding of the process dynamics.

4.2 Experimental design

Multiple pre-tests and six tests were carried out to evaluate the feasibility of the process under varying parameters. In one test using identical setups, testing conditions were altered in different stages to examine the factors affecting the outcomes and their correlation with resultant changes. The experiments with adjustable variables are divided into three categories, each focusing on specific influences, as elaborated in Table 5. The results corresponding to the distinct study areas, as detailed in Table 5, are further elaborated in Subsection 5.4. The testing parameters were chosen based on their significant impact on the process observed during pretesting [92].

Table 5.The testing conditions of different phases with listed variables [92].

Pretest	Target	Influencing Parameter	Phase No.	Gas Total [Nl/min]	Methane Content [%]	Arc Length [mm]	Thyristor Level [%]
Area 1	Plasma arc stability	Gas composition	1-1	5	0	20	75, 80, 85, 90, 95, 100
		Arc length Power input	1-2	5	0, 20, 40	20, 25, 30, 35, 40, 45	
Area 2	H$_2$ yield	Gas composition	2-1	3	33	20	85
			2-2	5	40	20	85
		Gas volume	2-3	3.5	43	20	85
Area 3	H$_2$ yield	Power input	3-1	5	40	20	75, 80, 85, 90

4.3 Evaluation

The mass spectrometer measures the volume fraction of specified gas components, namely Ar and H$_2$, recorded in cycles lasting 5 to 6 seconds each. product gas analysis was utilized for thermodynamic computations of Ar and H$_2$ volumes in the product gas. To compute the absolute volume of each gas in the cycles, the initial step involves determining the constant volume of Ar. This is achieved by multiplying the Ar flow rate per second by the cycle time in seconds, as detailed in Equation (4-1). Subsequently, employing Equation (4-2), the absolute volume of produced H$_2$ in each cycle can be ascertained. The calculation takes into account the percentage ratio to Ar for H$_2$, acknowledging Ar as an inert gas with a consistent volume [92].

$$V_{Ar} = t_{cyc} \cdot \dot{V}_{Ar} \qquad \text{4-1}$$

$$V_{H_{2-produced}} = C_{V,H_2} \cdot \frac{V_{Ar}}{C_{V,Ar}} \qquad \text{4-2}$$

$V_{H_{2-produced}}$ and V_{Ar} represent the gas volume for the corresponding gas in each measuring cycle, [Nl]; C_{V,H_2} and $C_{V,Ar}$ stand for the gas concentration in the product gas in each cycle, [vol. %]. $\dot{V}_{Ar}$ is the volume flow rate of the input gas, [Nl/min]; t_{cyc} is the time of a measuring cycle, [min] [92].

Maintaining a steady CH_4 flow rate into the reactor gas, the absolute volume of the CH_4 inlet can be calculated similarly to that of Ar, according to Equation (4-3) [92].

$$V_{CH_{4-in}} = t_{cyc} \cdot \dot{V}_{CH_{4-in}}$$
4-3

$\dot{V}_{CH_{4-in}}$ stands for the volume flow gas of CH_4 input, [Nl/min]; $V_{CH_{4-in}}$ refers to the gas volume in the measuring cycle, [Nl].

Consequently, the H_2 yield can be determined by establishing the ratio of H_2 in the product gas to the CH_4 inlet. The division by two is essential because each CH_4 molecule can split stoichiometrically into two H_2 molecules, according to Equation 4-4 [92].

$$H_2 \; yield = \frac{V_{H_{2-produced}}}{2 \cdot V_{CH_{4-in}}} \cdot 100$$
4-4

4.4 Results and discussion

As previously mentioned, the main objective of this chapter is to gain a comprehensive understanding of how specific process parameters impact the overall efficiency of methane plasma pyrolysis [92].

Table 5 outlines the effects of the chosen testing parameters, which are thoroughly examined in the following subsections. In Area 1, different gas compositions are tested to identify various stability zones, compared to pure Ar. Areas 2 and 3 focus on analyzing the hydrogen yield rate during pyrolysis tests, with attention given to the influences of plasma gas and power input, respectively. The successful detection of hydrogen gas in the product gas analysis, along with the production of high-purity solid carbon, represents a significant achievement [92].

Upon disassembling the facility, solid carbon presence was noted in the reaction chamber, as illustrated in Figure 47. Initially, solid particles deposited on the inner surface of the graphite chamber, which then formed aggregates and agglomerates. While the hot gas filter effectively captured fine carbon carried by the product gas, solid carbon left in the reaction zone disrupted the electric discharge focused on the designated spot: the anode pin. Consequently, tests could only be sustained for short durations, with the most favorable results occurring within the initial 10 to 15 minutes. Subsequently, there were gradual declines in process stability and efficiency. Despite the encountered challenges, it was essential to proceed to achieve the study's objectives and evaluate the influencing process parameters. Therefore, despite a decrease in H_2 yield, specific process parameters were intentionally varied to investigate their

correlation with H_2 yield. Another significant challenge was the outworn of both the graphite cathode and anode throughout the test. Moreover, carbon deposition on the cathode tip during testing led to a narrower gas inlet gap. Concurrently, the outworning of the anode affected the plasma arc, resulting in changes in arc length [92].

Figure 47. The reaction chamber following the test, showing carbon deposited on its inner surface [92].

4.4.1 Influence of gas composition, the arc length, and the power input on the arc stability — Area 1

In light of a prior investigation into the stability of the plasma arc, it was established that arc stability depends on factors such as power supply, gas composition, cathode geometry, and the magnetic field generated by the circuit [92]. Normally, the arc is not perfectly centered, leading to an uneven distribution of temperature across the field. Comprehending arc stability is essential for guaranteeing a consistent operation and enhancing effectiveness [92].

A series of methodical experiments were conducted to elucidate the connections among gas composition, power input (including current and voltage ranges), and arc length. These investigations involved testing different proportions of CH_4 in the plasma gas, varying arc lengths, and adjusting electrical current, thereby affecting power input [92].

In one set of trials, while maintaining a constant arc length and gas composition, the current was gradually reduced using the thyristor until the arc disconnected. The data points were recorded in descending order of current values. These results are depicted in Figure 48, showing voltage plotted against current values, highlighting trends observed in stable arcs with varying gas compositions and arc lengths. The horizontally shaded area represents 100% Ar in the plasma gas with a 20 mm arc length, while the vertically shaded area represents a gas

mixture comprising 60% Ar and 40% CH_4, with arc lengths ranging from 20 to 35 mm in 5 mm increments [92].

When reducing the current for 100% Ar, the voltage remains relatively consistent, indicating a stable arc requiring lower power input. However, transitioning to the gas mixture containing 40% CH_4 reduces the stability range and does not permit low amperage values. Essentially, lowering the amperage for 100% Ar results in nearly unchanged voltage, necessitating less power input for plasma generation. Conversely, introducing 40% CH_4 in the gas mixture leads to increased voltage fluctuations, requiring higher power input. For instance, maintaining a consistent arc length of 20 mm for both gas types reveals that the same amperage demands voltages approximately 20 V higher for the gas with 40% CH_4 content. However, due to limitations in the experimental setup, higher voltage ranges were not achievable, restricting the use of higher CH_4 content [92].

As a result, the inclusion of a gas mixture containing 40% CH_4 significantly undermined arc stability, resulting in process interruptions. This can be attributed to the greater atomization and ionization energy necessary for the five atomic constituents of CH_4 compared to the single-atomic Ar. The 40% CH_4 content served as the upper threshold for conducting the experiment, as any further increase promptly led to the arc being disrupted [92].
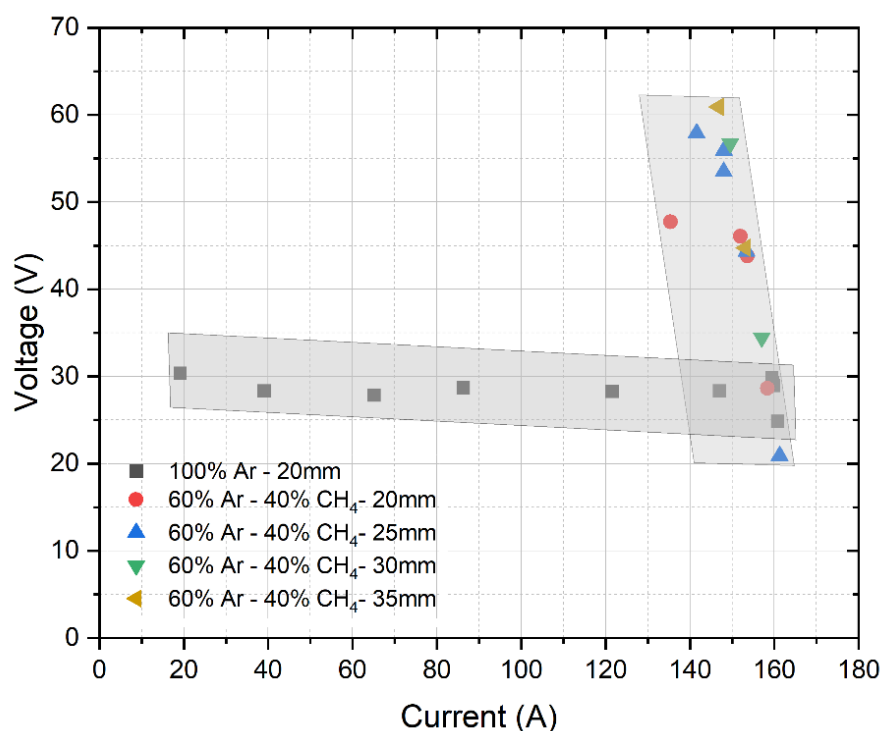
Figure 48. Arc stability range depicted as a function of voltage and current for gas mixtures of 0% CH_4 and 40% CH_4 [92].

The impact of introducing 20% CH_4 into the plasma gas is depicted in Figure 49, illustrating the transitional range between the critical states observed with 0% and 40% CH_4. Here, the arc length is gradually extended from 20 mm to 45 mm in 5 mm increments. A lower CH_4 content extends the stability range, allowing for longer arc lengths and highlighting the confirmed influence of CH_4. However, even with lower amperage values, the stability range remains shorter, requiring increased voltages. Arc lengths beyond 45 mm resulted in unstable arcs and were deemed impractical for processing. Longer arc lengths exhibit more pronounced trends for the gas containing 20% CH_4. It is noteworthy that longer arc lengths correspond to a broader heat source and an expanded reaction zone, leading to higher H_2 yield rates. This aspect is further explored in the subsequent subsection. In essence, the addition of CH_4 introduces voltage fluctuations and necessitates a higher power supply compared to pure Ar [92].
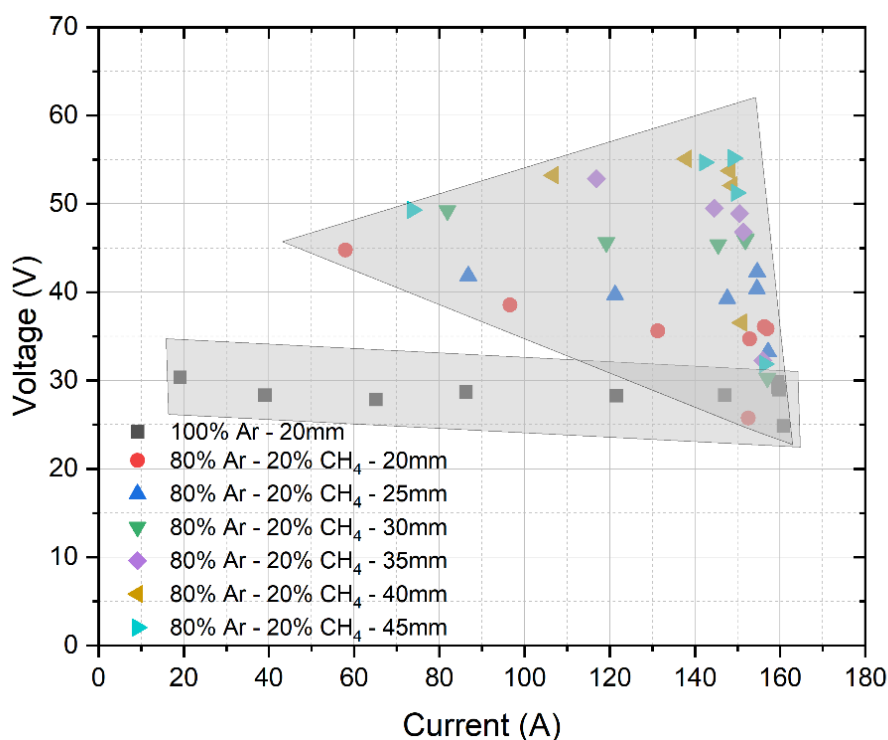
Figure 49. Arc stability range depicted as a function of voltage and current for gas mixtures of 0% CH_4 and 20% CH_4 [92]

4.4.2 Influence of gas composition and volume on H_2 yield rate — Area 2

As previously mentioned, in the overall decomposition reaction, each mole of CH_4 gas produces two moles of H_2, leading to an increase in pressure within the reactor. To ensure safety and prevent gas leakage, a maximum gas flow rate of 5 Nl/min was tested. Gas flows below 3 Nl/min also adversely affect plasma arc stability, rendering the test unreliable at such

low flow rates. Thus, two different operational gas flow rates were examined: Phase 1, with a total gas flow of 3 Nl/min, and Phase 2, where the total gas flow increased to 5 Nl/min. The results, displayed as H_2 yield vs. time in Figure 50, reveal that it takes approximately 4 minutes for the gas concentration to stabilize, as detected by the gas mass spectrometer device. Therefore, the initial substantial increase in H_2 yield primarily reflects the response delay in the gas mass spectrometer analysis and should not be interpreted kinetically. This delayed response is also evident after terminating the test in the later phase, attributed to the response time of the equipment [92].

Examining the calculated curves of the H_2 yield for both phases, it is apparent that a higher total gas flow rate with a slight increase in CH_4 content does not result in a higher H_2 yield; instead, it decreases it. In essence, the majority of the CH_4 introduced into the furnace exits without being decomposed to H_2. This observation is attributed to the fact that a higher flow rate reduces the residence time of gas in the reaction zone, while a higher CH_4 content diminishes arc stability, as discussed earlier [92].
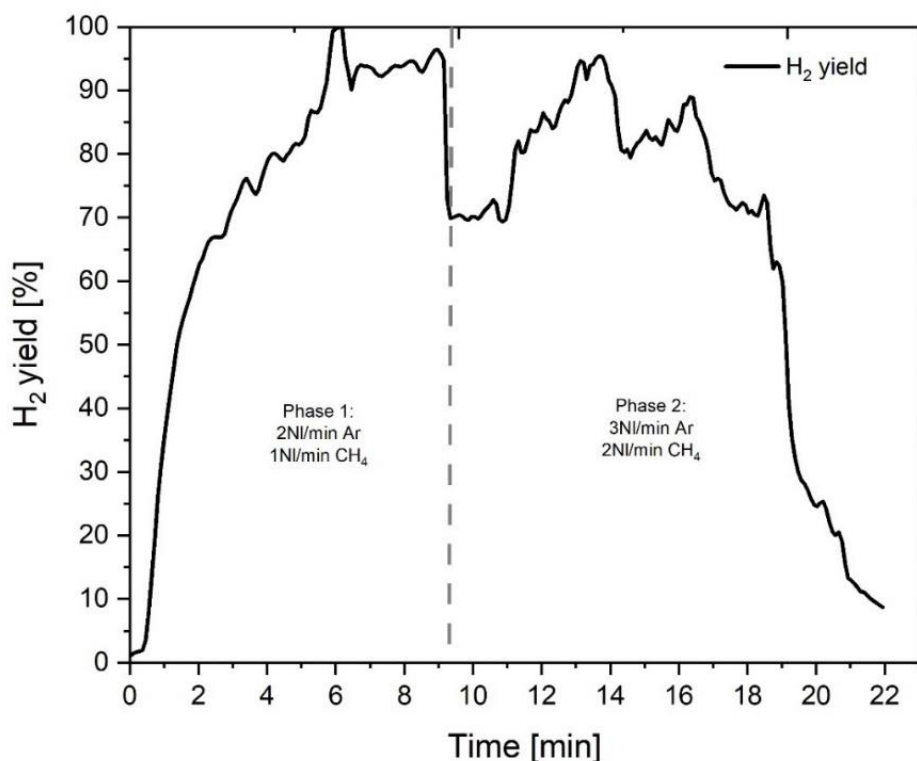
Figure 50. H_2 yield rate for total inlet gas flows of 3 and 5 Nl/min during the pyrolysis test [92].

The fluctuations observed in the curve are attributed to the dynamic nature of the arc zone, where the position of the arc shifts, creating dynamic hotspots within the reaction zone. Consequently, the stability of the arc significantly influences process efficiency, as discussed earlier [92].

In another test conducted in two phases, Phase 1 involved introducing 2 Nl/min of Ar and 1 Nl/min of CH_4, followed by a transition to 1.5 Nl/min of CH_4 while maintaining the Ar flow, resulting in an increased CH_4 content from 33 to 43%. As illustrated in Figure 51, it is apparent that higher CH_4 content in the gas leads to a 20 to 30% reduction in H_2 yield [92].
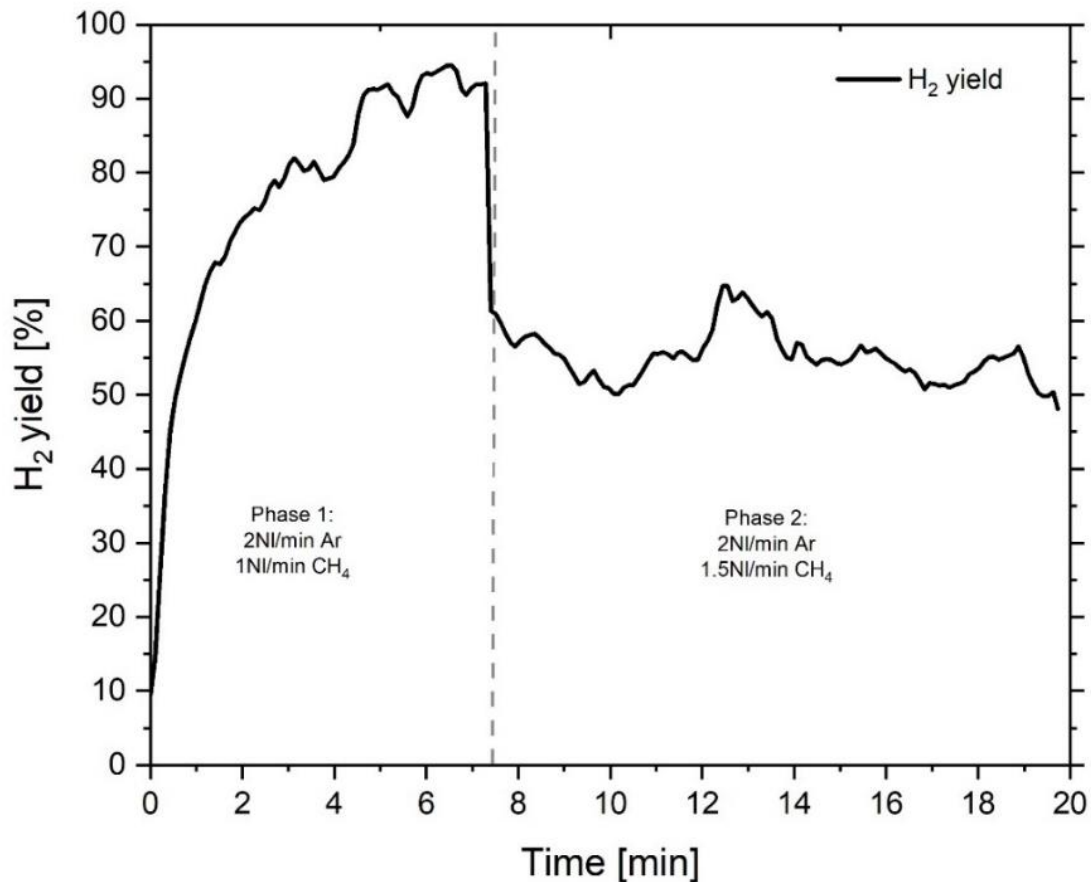
Figure 51. H_2 yield for various CH_4 content levels in the inlet gas flows during the pyrolysis test [92].

4.4.3 Influence of power input on H₂ yield rate — Area 3

In another experiment involving varied power input, the investigation focused on the H_2 yield, as depicted in the corresponding H_2 yield rate shown in Figure 52. It is essential to highlight that the low H_2 yield rate is primarily due to the contaminated chamber and the presence of pre-existing solid carbon, both of which affect the quality of the arc and restrict the reaction. Current and voltage are recorded every second, while gas analysis is conducted in a cycle of approximately 5 seconds. To synchronize the data on power input with the H_2 yield, average power values over 5 seconds are utilized, corresponding to that cycle [92].

Clearly, increasing the power input from 4 to 7 kW results in an approximately 10% increase in the H_2 yield.
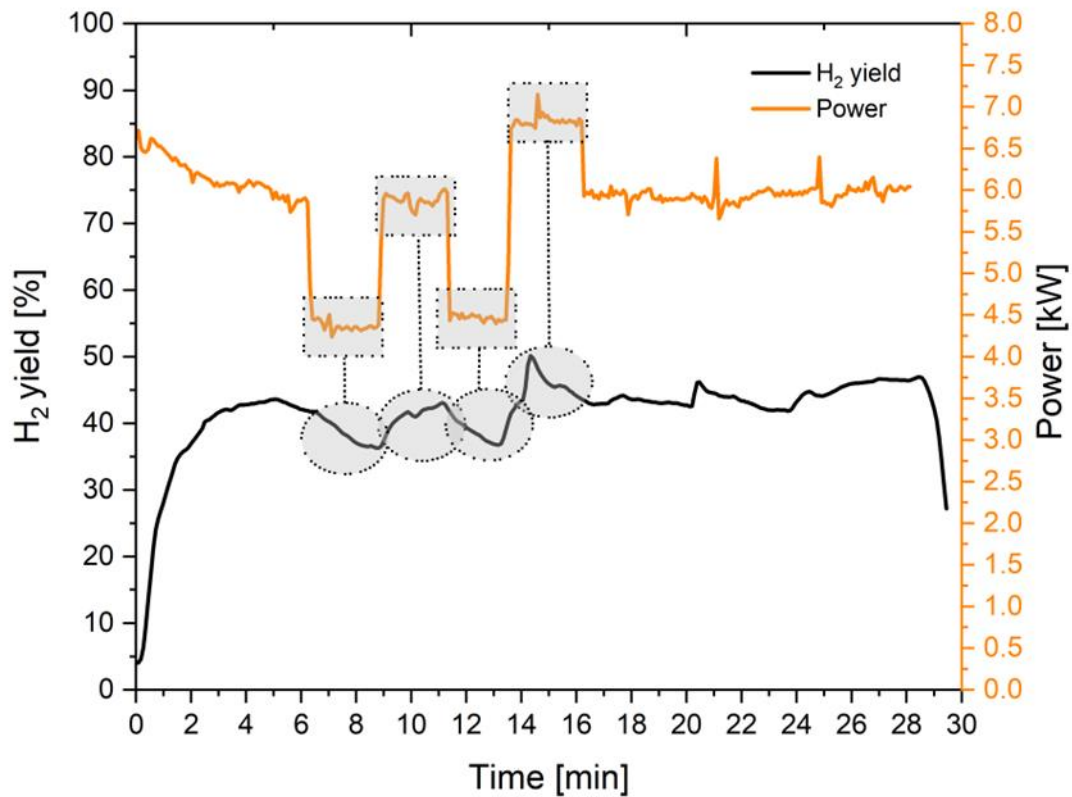
Figure 52. H_2 yield rate with varied power input during the pyrolysis test [92].

4.4.4 The plasma arc behavior

Figure 53 documents the progression of the plasma arc and the formation of solid carbon. The plasma arc is represented by an oval, and a comparison between Figure 53(a) and (b) illustrates the simultaneous deposition of carbon, indicated by the straight arrows. Moreover, Figure 53(c) displays carbon deposited on the edges of the anode, marked by a rectangle, with additional growth evident in Figure 53(d) [92].
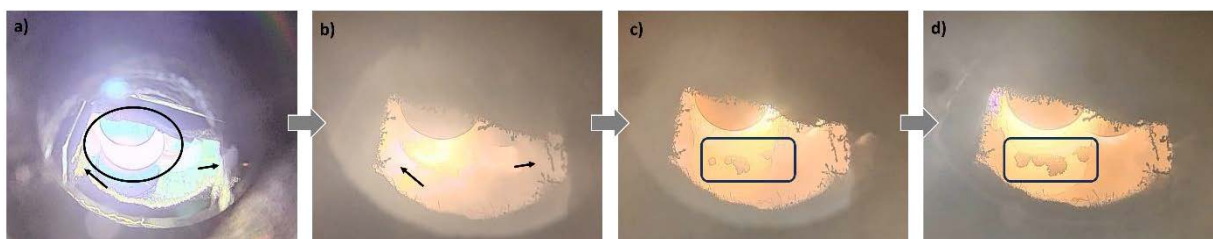
Figure 53. The development of the plasma arc and the formation of solid carbon during the test are illustrated from (a) to (d) [92]

Figure 54 depicts an additional test involving an arc jump and interruption. The initial phase is halted in Figure 54(d), and the second phase resumes in Figure 54(e). The challenge arises as the deposited carbon interferes with the arc plasma, creating new surfaces that divert the discharge from the anode, as previously discussed. The jump in the arc can be observed by comparing its position, represented by an oval in Figure 54(b), with that in Figure 54(c). This comparison also holds true for Figure 54(e) and (f). The curved arrows in Figure 54(b) and e illustrate the movement of the arc, while the straight arrows in the remaining images indicate the deposition of carbon [92].
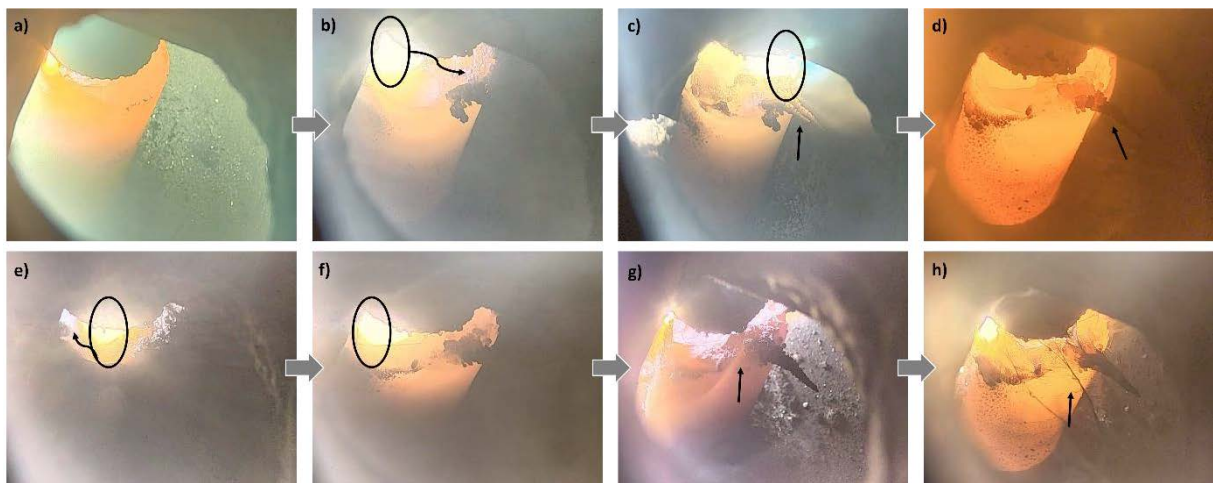
Figure 54. The plasma arc jump during the test is illustrated progressively from (a) to (h) [92].

The dendritic growth of carbon is more prominently depicted in Figure 55. It begins with a coral-shaped carbon structure hanging from the cathode edge, as seen in Figure 55(a). Figure 55(b–d) show the advancement of this growth, as it extends and contaminates the reaction zone, ultimately leading to the interruption of the arc, as seen in Figure 55(d) [92].
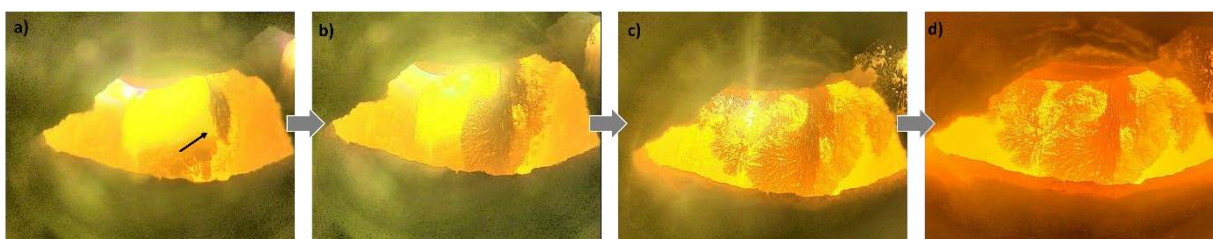
Figure 55. The progressive development of the dendritic growth of the deposited carbon is depicted from (a) to (d) [92].

4.5 Summary and conclusions

The investigation has determined that TP represents a technically viable and effective method for producing H_2, alongside generating valuable solid carbon by-products. Through systematic experimentation using a laboratory-scale plasma furnace, several crucial influencing factors were examined. The key findings of this study are outlined as follows [92]:

- The experimental analysis showcases the technical feasibility of methane plasma pyrolysis, yielding H_2 ranging from 60 to 100%, contingent upon process variables. Enhanced setups and optimized conditions hold promise for boosting process efficiency, ensuring consistently superior and increased H_2 yields.

- Gas composition, particularly the presence of CH_4, imposes constraints on power input, with pure Ar demonstrating optimal arc stability. Beyond the parameters explored here, the nuanced characteristics of arc stability are intricately shaped by factors such as geometry, magnetic fields, and facility configuration.

- A mere 10 % increase in CH_4 concentration, from 33 to 43%, within the plasma gas resulted in a notable 20 to 30% decrease in H_2 yield (from 90 to around 60%). It is important to acknowledge the challenge of establishing a direct correlation and quantifying results, given the complexity of the plasma process influenced by numerous factors.

- Introducing CH_4 presents challenges, leading to difficulties in sustaining arc discharge and occasional interruptions. Initial trials suggest that for the conditions of this work, a mixture comprising 60% Ar and 40% CH_4 strikes a balance between process stability and productivity. With a power supply capable of delivering higher voltage levels, the CH_4 content could potentially be increased further while maintaining stable operation.

- Higher gas flow rates reduce gas residence time, leading to more unreacted CH_4 and consequently lower H_2 yields. Increasing plasma gas flow from 3 to 5 Nl/min resulted in a 10 to 20% decrease in H_2 yield (from 95 to around 75%).

- Solid carbon rapidly accumulated on the inner surface of the reaction chamber during pyrolysis. Initially deposited carbon evolved into aggregates, agglomerates, and eventually larger particles. Carbon deposition complicates plasma arc discharge in the reaction zone, acting as a conductive material that reduces plasma arc stability and H_2 yield over time.

- Increasing power input by 3 kW, achieved by enhancing amperage, promoted the pyrolysis reaction, resulting in a 10% higher H_2 yield (from 40 to 50%).

- The degradation of both cathode and anode alters plasma arc conditions, affecting arc length and destabilizing plasma arc discharge.

5 Optimization of thermal plasma pyrolysis of methane

In this chapter, additional experimental investigations were undertaken to refine the process, aiming for improved outcomes. The objective was to develop a broad qualitative model regarding the correlation between the results and certain process parameters.

5.1 Approach

An experimental investigation was conducted, designing a series of experiments using MODDE® 13 Pro from Sartorius AG software to determine optimal conditions. The selected influential parameters were CH_4 content in the plasma gas, electric current, and arc length, with corresponding responses being H_2 yield, stability time, and power input, listed in Table 6. Each of these responses is explained and discussed in corresponding subsections [115].

Thirteen tests (P1-P13) were performed, including three for experimental reproducibility confirmation. Section 5.3 details the statistical parameter analysis. In addition to process parameters, comprehensive characterization of the produced carbon was performed, involving analyses to elucidate morphological, microstructural, chemical composition, and surface area properties. The results of the carbon characterization are reported in the next chapter [115].

Notably, the reaction chamber was entirely constructed from graphite to prevent impurities, given the unit's primary design for steelmaking tests. The function is explained in detail in a previous chapter, therefore, here, it is only briefly explained [115].

Both H_2 yield and power input were calculated from the raw data, while the stability time, a steady process time without disruption, was recorded and documented during the test. Evaluation of the results will be undertaken in the subsequent section [115].

Table 6. The variable factors for the design of experiments and the resulting responses [115].

	Factors			Responses		
	(pre-defined inputs)			(the resulting changes)		
Test Name	CH₄ [%]	Electric current [A]	Arc Length [mm]	H₂ yield [%]	Power input [kW]	Stability time [s]
P1	20	90	15	79	4.4	6
P2	20	120	15	90	5.2	20
P3	20	105	15	76	4.3	30
P4	40	90	15	79	5.0	5
P5	40	120	15	99	6.5	6
P6	20	90	25	100	5.2	13
P7	20	120	25	94	4.0	15
P8	40	90	25	68	5.5	2
P9	40	120	25	70	7.8	1
P10	30	105	20	90	6.0	5
P11	30	105	20	83	5.9	3
P12	30	105	20	96	5.1	6
P13	30	105	20	96	5.2	3

5.2 Evaluation

The H_2 yield is calculated as explained in the previous chapter. The power input cannot be directly adjusted; however, the amperage is controlled through the thyristor. The power input is calculated based on data obtained from the transformer [115].

$$Power\ input\ [kW] = \frac{I.V}{1000}$$

5-1

where I represents the current in amperes [A], and V represents the voltage in volts [V].

5.3 Example for test interpretation

To facilitate the understanding of the data analysis from the pyrolysis test, it is helpful to provide an example of the data observed during the test and its subsequent interpretation. For instance, Figure 56 illustrates three distinct stages encountered during a pyrolysis test. The initial stage involves purging, where only Ar gas is introduced to eliminate other gases and air from the reactor [115]. The actual pyrolysis experiment begins when the arc is ignited by contacting and short-circuiting the electrodes, as shown in Figure 56 [115]. The arc length is then immediately extended to 10 mm to prevent overheating of the electric supply unit and to establish a stable plasma arc. The thyristor level is pre-set between 95-100% for the initial plasma arc, which is supported solely by Ar. Subsequently, the gas is switched to the intended Ar and CH_4 mixture, and the thyristor level is adjusted to achieve the desired amperage. Consequently, a brief peak in power can be observed in the initial seconds, labeled as 1 and 3 for phases 1 and 2, respectively. Peak 2 represents a failed attempt to initiate the arc [115].

Notably, immediately after the onset of the pyrolysis phases, there is a gradual increase in H_2 in the product gas. However, based on experiments, there is a delay before H_2 is detected by the gas mass spectrometer. This delay, termed the H_2 response time, is consistently defined as 4 minutes for subsequent evaluations, as shown later in Figure 57 [115].

The observed drop in power is attributed to a momentary deviation of the plasma arc, denoted as 4 and 5, which almost disrupts the arc. The worst-case scenario is a total arc disruption, indicated by label 6 [115].
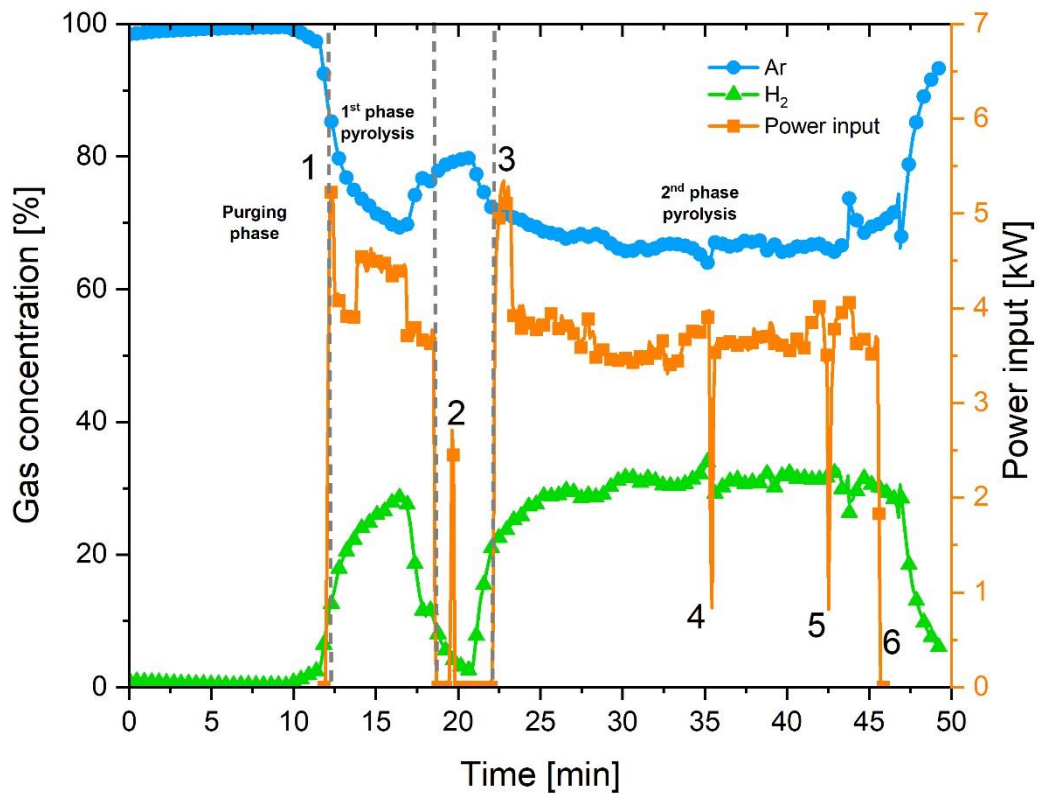
Figure 56. Examples of product gas and power input analysis during a pyrolysis test [115]. The different phases and the numbered peaks are explained in the above text.

The H_2 yield rates during pyrolysis were calculated and illustrated in Figure 57. The H_2 response time indicated on the H_2 yield curve served as the reference point for data extraction in the experimental design. Consequently, the H_2 yield value after the 4-minute response time is considered the response value. This 4-minute H_2 response time was chosen because it represents the point at which the curves stabilize and reach a steady state [115].
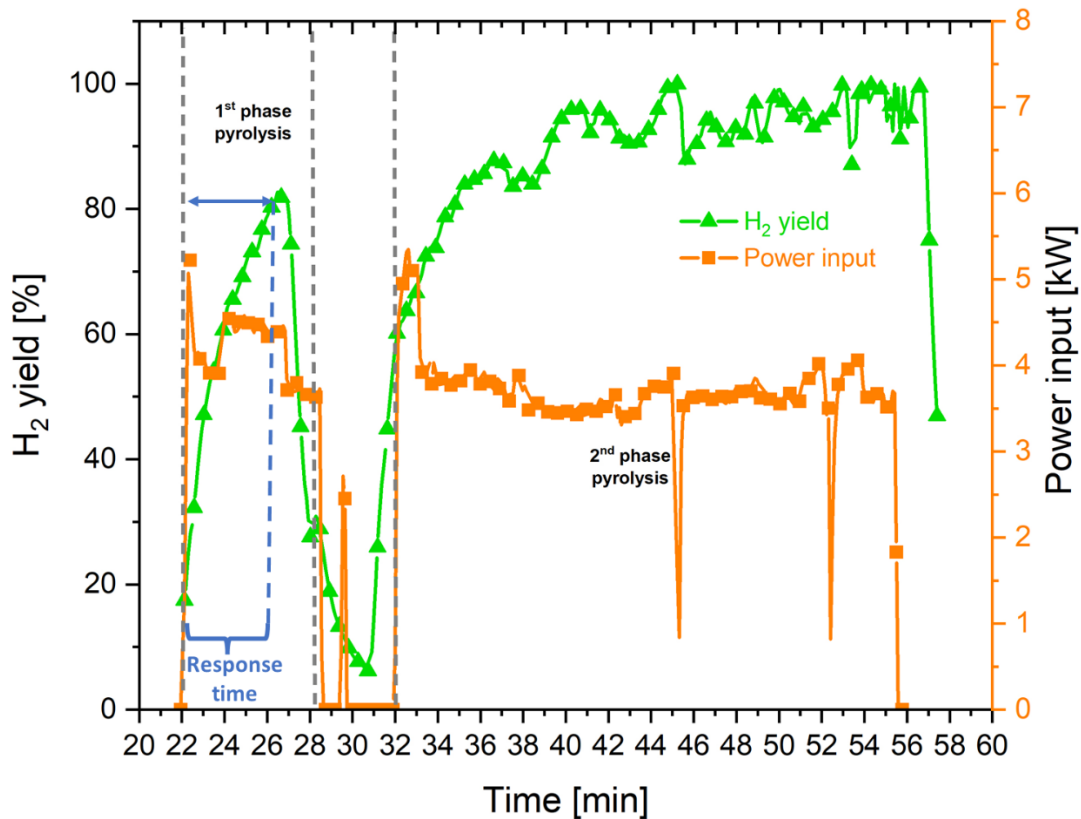
Figure 57. An example for H_2 yield and power input rate of the pyrolysis test [115].

5.4 Results and discussion

The calculated data was used to analyze a model for the influencing factors, which are presented individually in the following sections. When two factors are examined in relation to the respective response, the third factor is kept constant.

5.4.1 H_2 yield

An increase in the H_2 content within the product gas, and consequently a higher H_2 yield, indicates improved process output. Therefore, the dependence of this efficiency on various process parameters has been thoroughly investigated. The graphical representations in Figure 58 show that an increased CH_4 content in the plasma gas tends to reduce the H_2 yield, while higher current and arc lengths enhance it [115]. CH_4 is identified as a gas component that affects the plasma arc, reducing its stability and preventing it from achieving optimal conditions to provide the necessary energy for the reaction. In contrast, higher electric current levels contribute to increased power input, supplying more energy for the process. Additionally,

longer arc lengths create a larger environment for the reaction, leading to a higher H_2 yield. These trends are further illustrated in Figure 59. Besides, longer arc lengths require higher power input [115].
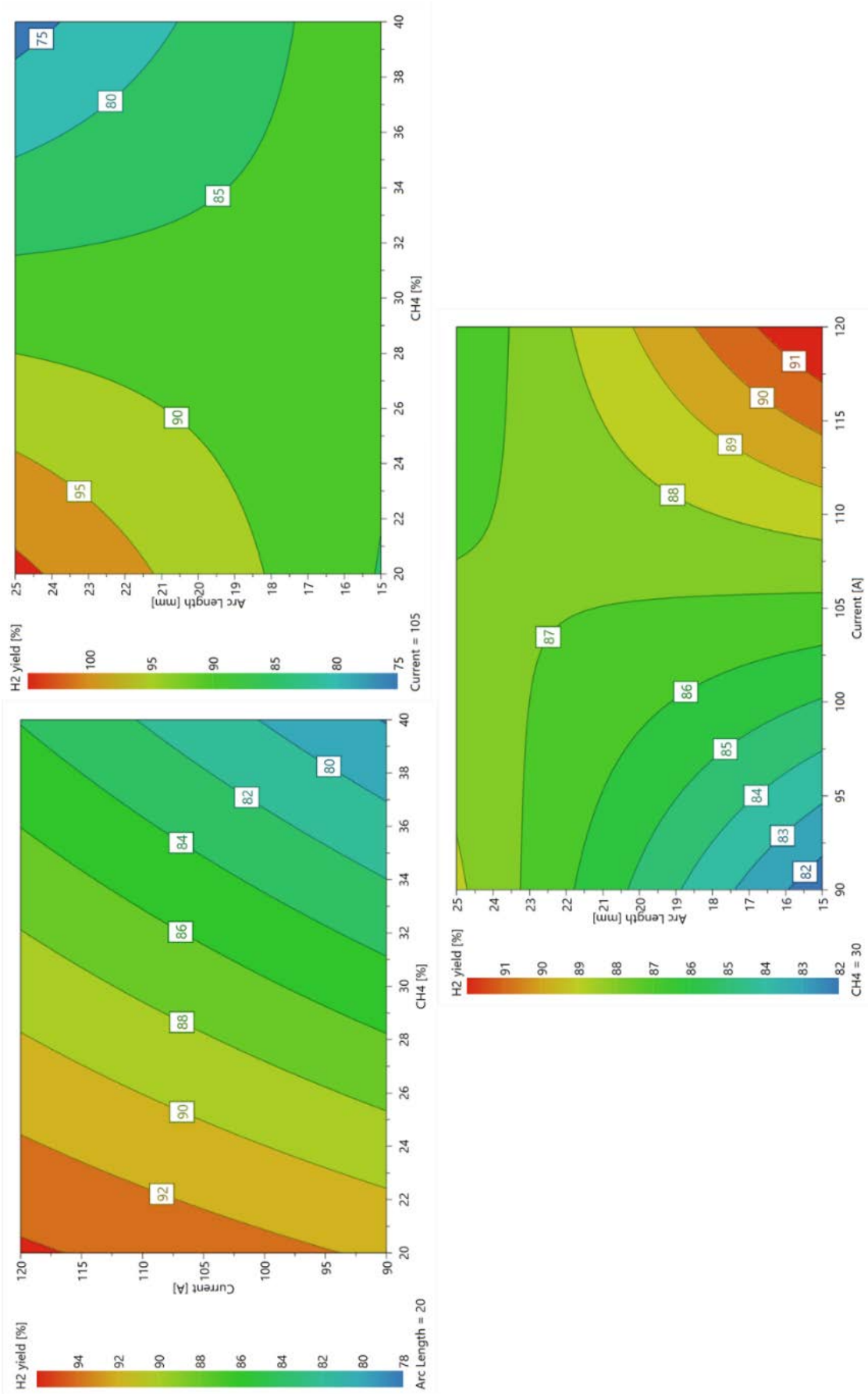
Figure 58. The H₂ yield in relation to the interacting process parameters [115].
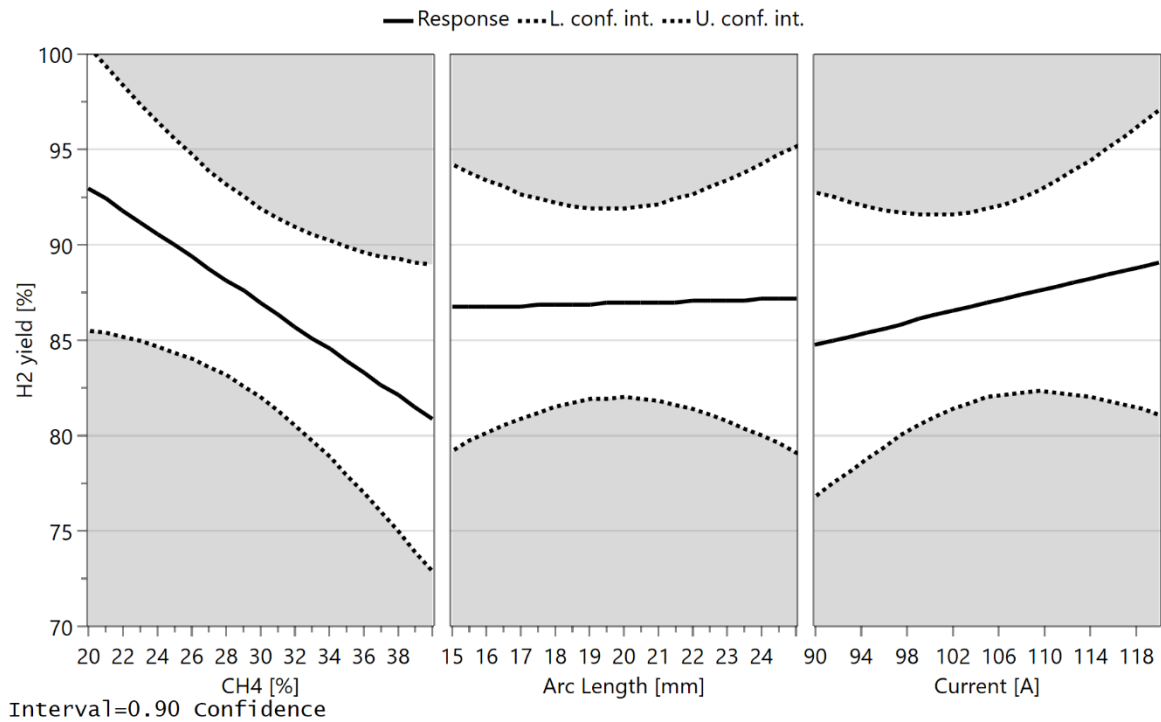
Figure 59. H$_2$ yield dependence on the process parameters [115].

5.4.2 Power input

The power input cannot be directly manipulated, but it can be controlled indirectly by adjusting the electric current and the arc length. Increasing the current results in higher power, providing more energy for the pyrolysis reaction. Through adjustments to the electric current using the thyristor level, the current can vary between 90 and 120 A, leading to power changes within the range of 5 to 7 kW. Additionally, both a high CH$_4$ content and an extended arc length increase power input, as shown in Figure 60 [115]. This is because CH$_4$ requires more energy for excitation and ionization, and a longer arc length increases the voltage, thus necessitating higher power input. Figure 61 illustrates the power input variations with these variables [115].
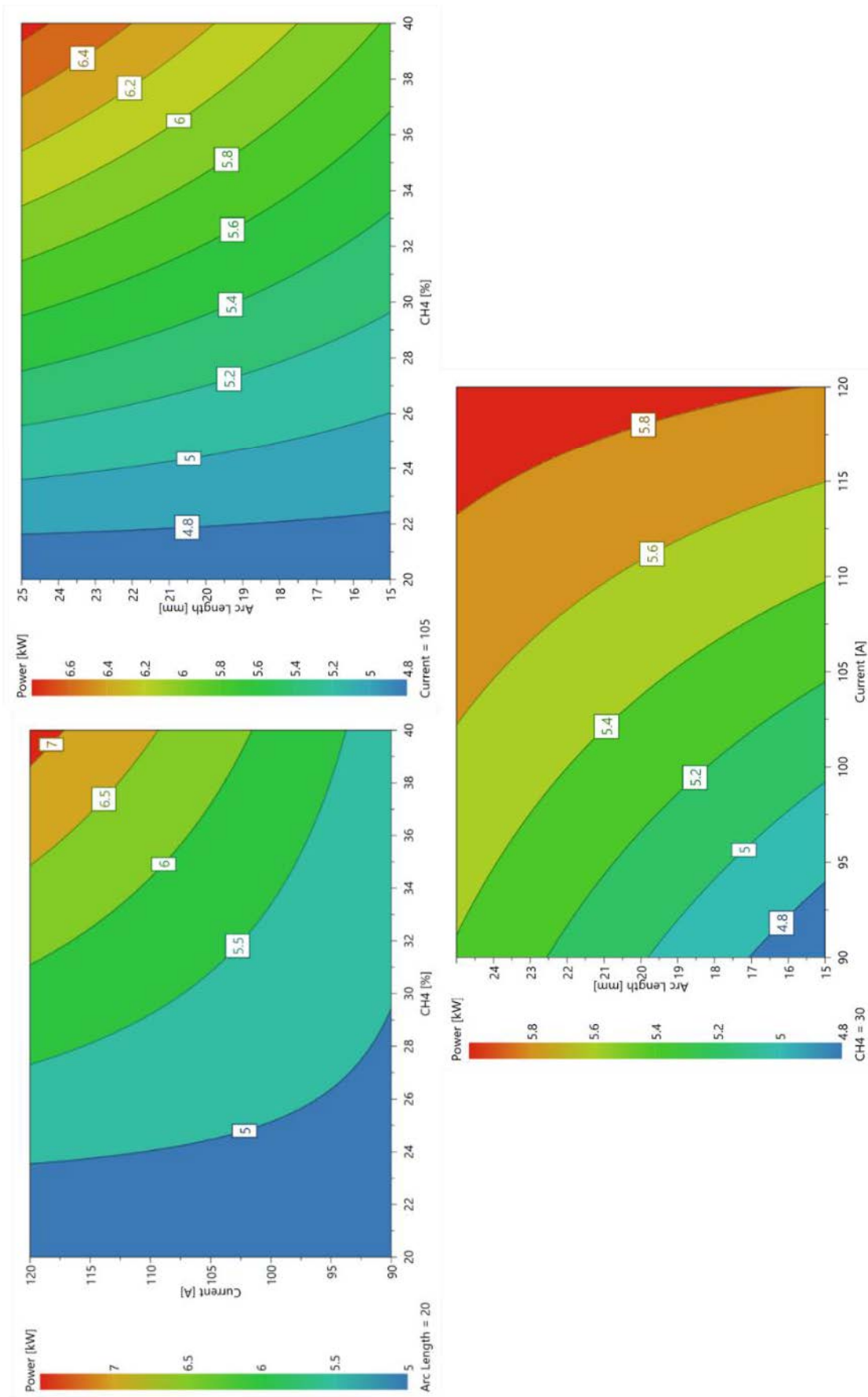
Figure 60. Power input in relation to the process parameters [115].
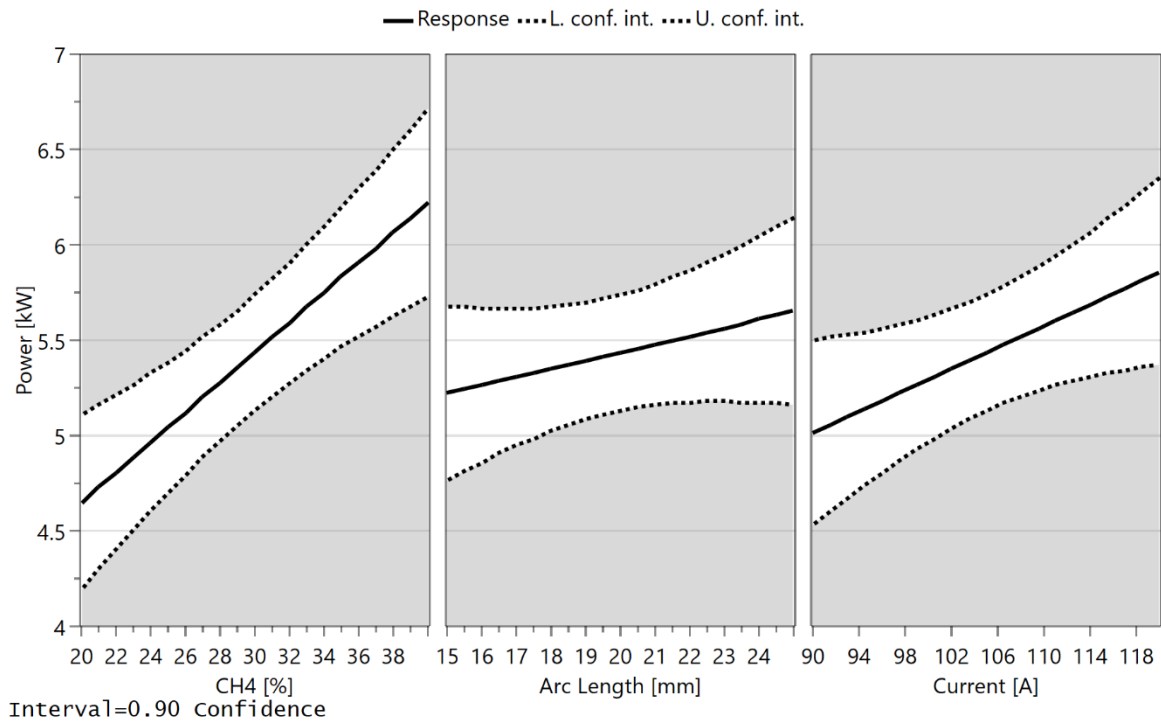
Figure 61. Power input dependence on the process parameters [115].

5.4.3 Stability time

The stability time is defined as the duration of the process before the first occurrence of arc disruption, serving as a crucial metric for evaluating process stability. During the tests, a maximum stability time of approximately 30 minutes was used, indicating that a test with a stability time of 30 minutes or slightly longer did not experience any arc disruptions [115].

It is important to note that stability time is influenced by various parameters. As previously mentioned, the plasma furnace used is not specifically designed for the methane pyrolysis process. Even under optimal conditions, arc disruptions can occur due to constraints such as the electrical unit's limits or the reactor's geometry. Figure 62 clearly shows that higher CH_4 content and extended arc length significantly affect arc stability, leading to disruptions and reducing stability time. The amperage and, consequently, the power input are limited by the electric unit's capacity. Overloading the AC transformer by pushing the electric current to its maximum limit results in overheating of the electric unit due to core losses and insufficient cooling. This necessitates an immediate shutdown to prevent damage, thereby reducing stability time. The relationships between stability time and process parameters are summarized in Figure 62 and Figure 63 [115].
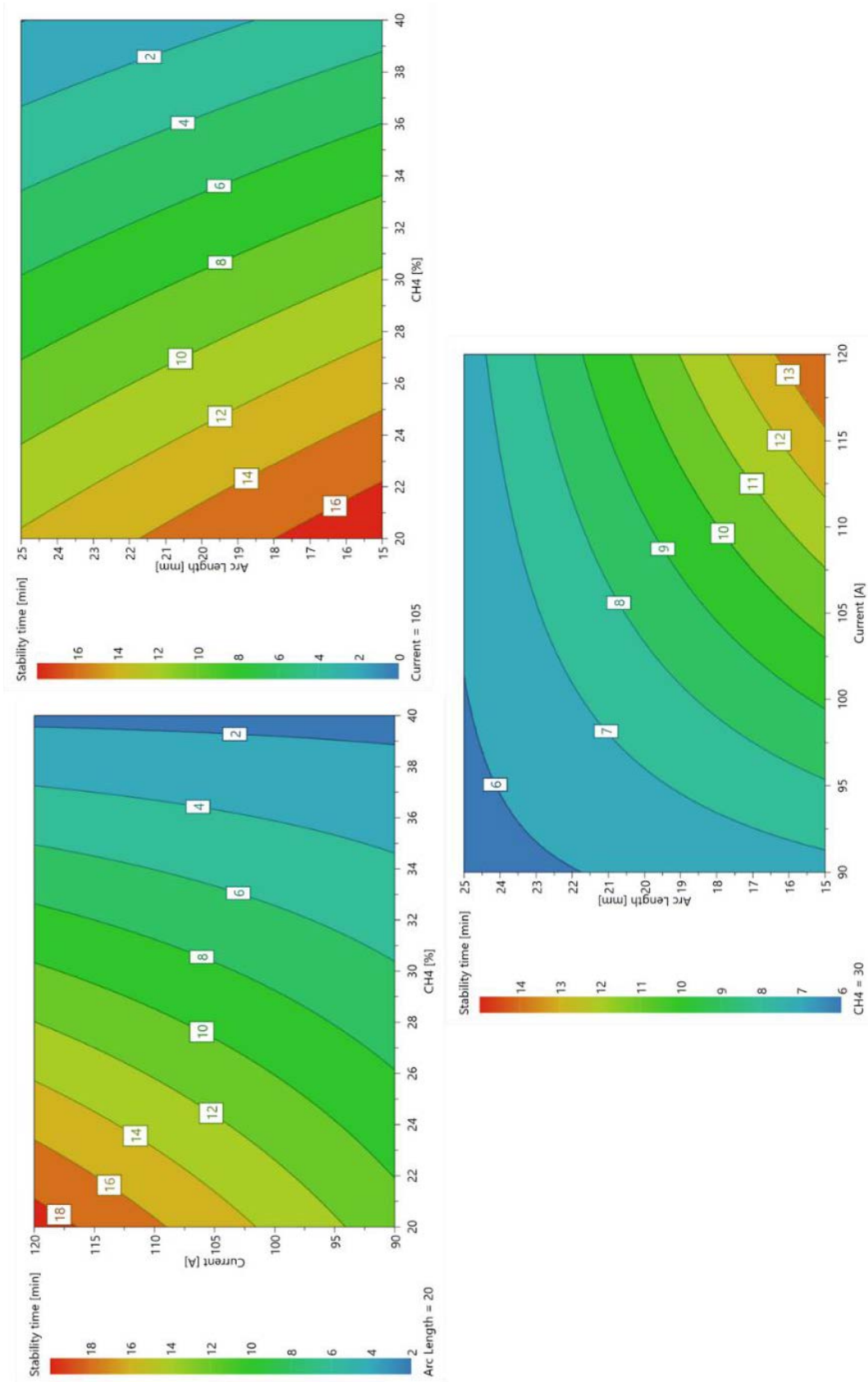
Figure 62. Interaction of stability time with the process parameters [115].
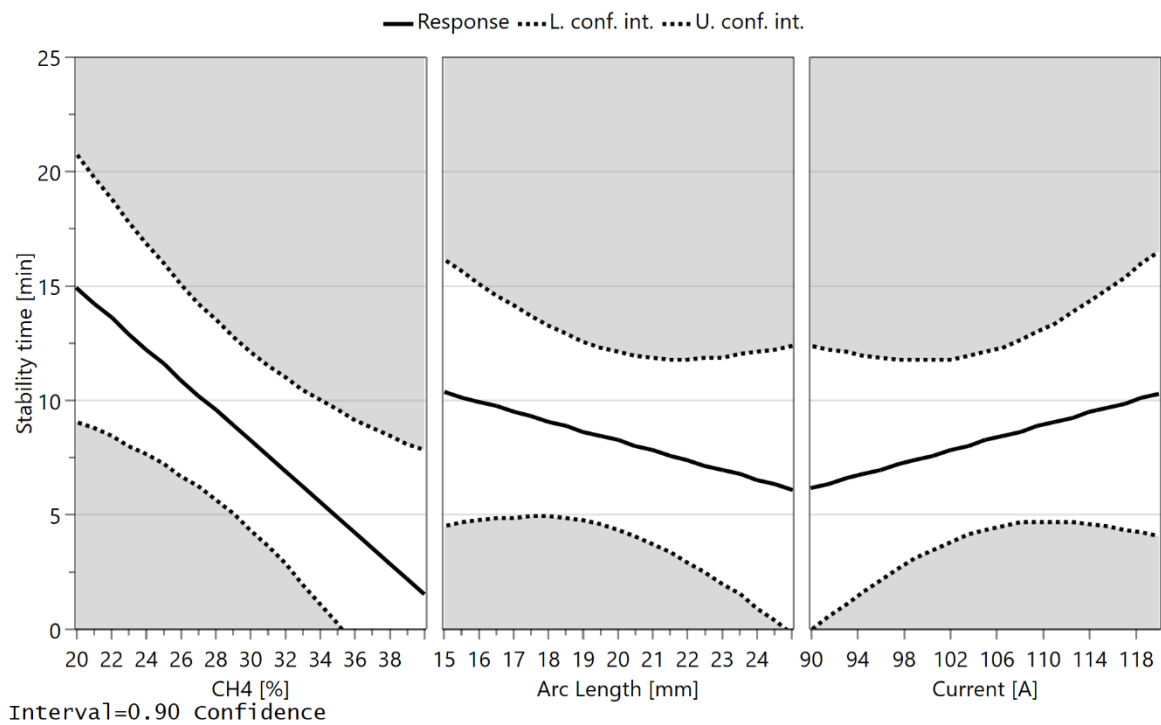
Figure 63. Stability time dependence on the process parameters [115].

Another factor that significantly impacts process stability is the formation of carbon in the reaction zone. This interferes with the optimal functioning of the plasma arc and causes disturbances [115].

5.5 Summary and conclusion

Thirteen pyrolysis experiments were conducted following an experimental plan developed using a specialized experimental design tool. The research focused on three primary variables: the CH_4 content in the plasma gas, the electric current, and the arc length, all of which varied within a specific range. The results showed a high H_2 yield, ranging from 67 to 100%. However, the process demonstrated instability, which was attributed to the reactor's design and constraints previously discussed in another study [92]. A comprehensive analysis of the H_2 yield, stability time, and power input provided valuable insights into the interaction of these parameters [115].

Increasing the CH_4 content in the plasma gas was found to reduce plasma arc stability, leading to process interruptions. This problem could be addressed by increasing the power input, though this would result in higher operational costs. Longer arc lengths also posed a

greater risk of arc disruption, but this risk could be managed by boosting the power input. Although longer arcs created a larger hot reaction zone and improved H_2 yield while extending stable processing time, they required more power. This approach could also lead to higher thermal stress and faster erosion of the graphite electrodes [115].

5.6 Outlook

Significant enhancements are required for the testing device in response to the challenges observed during the trial. Increasing the power input and expanding the voltage range can help stabilize the plasma arc when using CH_4, enabling a more continuous process. Implementing a vertical reactor design and enlarging the reaction zone are crucial steps to improve process stability, ensuring a consistent discharge of solid carbon and creating a larger, cleaner area for reactions and the plasma arc. A refined design should be developed to streamline the process.

Efforts to create a new design for a demonstration plant are currently underway and progressing actively at Montanuniversität Leoben (MUL). This will enable a systematic examination for process optimization and advancement of the technology readiness level (TRL), ultimately leading to commercial scalability. Concurrently, a deeper and more thorough understanding of the influencing factors is crucial.

The design is described in details in chapter 7.

6 Investigation on the produced carbon

6.1 Methodology and material

The solid carbon produced from methane pyrolysis can exhibit various morphologies, ranging from amorphous CB to structured graphitic materials and even nanostructures like CNTs and carbon nanofibers. The market value and quality of this solid carbon are crucial factors influencing its price. Therefore, producing high-quality carbon can significantly boost revenue and shorten the return on investment for large-scale pyrolysis facilities [73].

Existing research underscores the impact of several key parameters, such as reactor geometry, operating temperature, and plasma gas flow rate, on the properties of the resulting carbon [24,105]. In the study from Boutot et al. [105], it was determined that carbon reproducibility varied considerably, making it difficult to establish a direct correlation between different conditions and the properties of the produced carbon [24,105]. However, it was observed that the characteristics of the samples were influenced by their source, whether collected from the gas filter or directly from the reactor [105].

In this chapter, the produced carbon underwent detailed characterization using various analytical techniques to elucidate its nature and quality.

6.1.1 Scanning electron microscopy (SEM) and Energy Dispersive Spectroscopy (EDS)

SEM is a technique that creates magnified images that reveal microscopic and even nanoscopic-scale information on a specimen's size, shape, composition, and other properties. Characterization of the samples was performed using a JEOL 7200 F field emission SEM (JEOL Germany GmbH, Freising, Germany) equipped with a 100 mm^2 silicon drift detector for EDS (Oxford Instruments Ultim Max 100; Oxford Instruments GmbH NanoAnalysis, Wiesbaden, Germany). EDS is an analytical technique for elemental analysis of a specimen. To analyze the morphologies and chemical compositions, the Oxford Instruments Nanoanalysis AZtec 6.0 software was employed. The chemical composition was detected using an area scanning for 1 s at a beam energy of 15 keV [115].

6.1.2 Inductively coupled plasma mass spectroscopy (ICP-MS)

Approximately 50–200 mg of each carbon sample underwent microwave digestion in a reagent mixture of 6 ml of concentrated HNO_3 and 2 ml of H_2O_2 within an Anton Paar Multiwave PRO closed-vessel digestion system. This system was equipped with a 24HVT50 rotor (Anton Paar, Graz, Austria) and 30 ml PTFE vessels. The microwave program was configured to attain a maximum temperature of 200 °C, which was reached within a ramp time of 10 minutes and then maintained for 15 minutes. The maximum microwave power utilized was 1500 W. Following digestion, the contents were filtered and appropriately diluted with 1% HNO_3. The concentrations of elements in the sample solutions were determined using an Agilent 7500ce ICP-QMS (Agilent Technologies, Tokyo, Japan). The analysis employed an external standard calibration with a multi-element standard solution mixture Merck VI (Merck Certipur, Darmstadt, Germany) in 1% HNO_3, utilizing internal standardization to ascertain the concentration of trace elements [115].

6.1.3 Raman spectroscopy

Raman spectroscopy is a spectroscopic method commonly employed for identifying the vibrational patterns of molecules and solid substances. Raman spectra were acquired using a WiTec alpha300R Raman spectrometer equipped with a diode-pumped solid-state laser emitting at a wavelength (λ) of 532 nm. A power of 1 mW was applied along with a 2 s iteration time and 100 accumulations. To facilitate laser focusing and sample observation before

measurement, a confocal microscope was employed using a 50× long-working distance objective lens [115].

6.1.4 X-ray diffraction (XRD)

XRD is a scattering technique utilizing a single wavelength of X-rays as an incident beam. The intensity of the diffracted beam is recorded as a function of the scattering angle 2θ, or more generally, the scattering vector. XRD allows to investigate matter on the nanoscale to determine properties like the crystal structure of a given material as well as extract information for its purity [115].

XRD measurements were performed on a Bruker D8 Advance Eco equipped with Cu Kα radiation (~1.5418 Å wavelength) using a voltage of 40 kV and a current of 25 mA. Diffraction patterns were obtained using the Bragg-Brentano configuration with a continuous scan speed in a diffraction angle 2θ range of 10° to 90° with a step size of 0.02° and 1.2 s exposure time [115].

6.1.5 Gas sorption analysis: Brunauer-Emmett-Teller (BET) method

BET method is applied in gas sorption data (e.g., N_2 at 77 K) for determining the specific surface area (SSA) of a given material. This method relies on the physical adsorption of gas molecules onto the surface of a solid material and takes into consideration the monolayer adsorbate capacity and the cross-sectional area of the adsorbate molecule. N_2 gas adsorption and desorption isotherms were collected at 77 K (−196 °C) using an Anton-Paar QuantaTec Autosorb-iQ3 manometric gas sorption analyzer and by employing ultra-pure (99.999%) N_2 gas as adsorbate, ultra-pure (99.999%) helium (He) gas for void volume calculations and liquid N_2 as cryogen. Prior to the tests, samples of ~150 mg were degassed under vacuum (10^{-6} mbar) at 250 °C for 24 h to remove physisorbed species and make the surface more accessible. The SSA was calculated by applying the multi-point BET method in the adsorption data for relative pressures (P/P_0) between 0.05 and 0.3 [115].

6.2 Characterization of the produced carbon

The detailed findings, discussed in the following subsections, offer valuable insights into the properties of the produced carbon. However, it is crucial to recognize the limitations of the current experimental setup, which may restrict the control over the characteristics of the carbon

product. Consequently, a systematic study of how different influencing parameters affect solid carbon properties requires a more controllable plasma system [115]. After analyzing the samples from all tests, no significant differences in characteristics were observed. The only deviation was found when comparing samples collected from the reactor chamber to those from the gas filter. Therefore, to highlight this difference in characteristics, samples from tests P10-P13, which were produced under the same conditions, were selected for further analysis.

6.2.1 Scanning electron microscopy (SEM) and Energy Dispersive Spectroscopy (EDS)

Figure 64 presents SEM images of the carbon samples produced. The F(1-3) images show samples collected from the filter, which have a fine texture carried away by the gas flow. In contrast, the C(1-3) series displays samples collected from the chamber. These chamber-collected samples are larger and adhere to the inner surface of the reaction chamber, forming significant dendritic particles that remain inside. The C(1-2) images reveal these samples' dendritic and coral-like shapes, with higher magnification showing nanocrystals and primary particles. On the other hand, the filter-collected samples in the F(1-3) images appear fluffier [115].

These observations are consistent with other studies. For example, Boutot et al. [105] described the carbon produced by their plasma pyrolysis process as a blend of amorphous and nanostructured materials. Additionally, as noted in the introduction, literature indicates that the carbon microstructure can vary based on its formation location and growth conditions, including the reactor's temperature and shape [115].
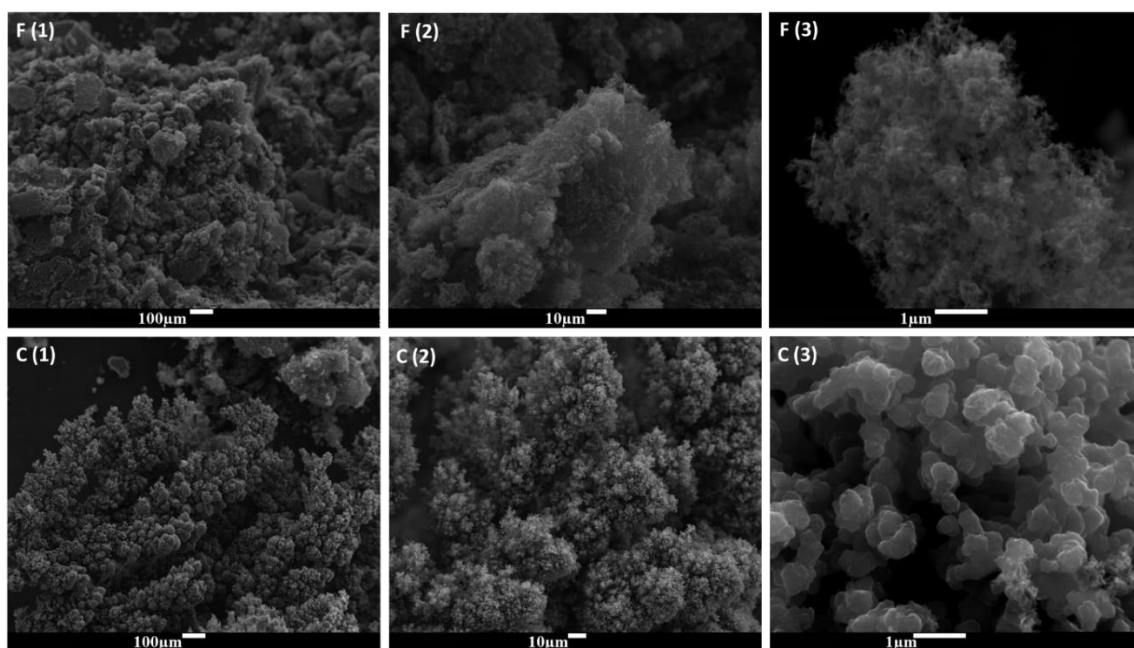
Figure 64. SEM images of the carbon samples, obtained from filter F (1-3), and reaction chamber C (1-3). The magnifications of the images were 70x for (1), 600x for (2), and 1600x for (3) [115].

When considering the use of carbon, especially in fields like agriculture, it is crucial to avoid harmful impurities. However, removing these impurities can be difficult or sometimes impossible, potentially leading to carbon oxidation and CO_2 emissions [115].

EDS analysis provides an initial assessment of potential impurities in the carbon. The results indicate that the carbon is of high purity, with metal elements present at less than 1 wt% in the gas filter. For a more precise evaluation of purity and elemental composition, additional methods with higher accuracy are required. Figure 65 illustrates an example of the chemical analysis for a pure carbon sample collected from the reaction chamber [115].
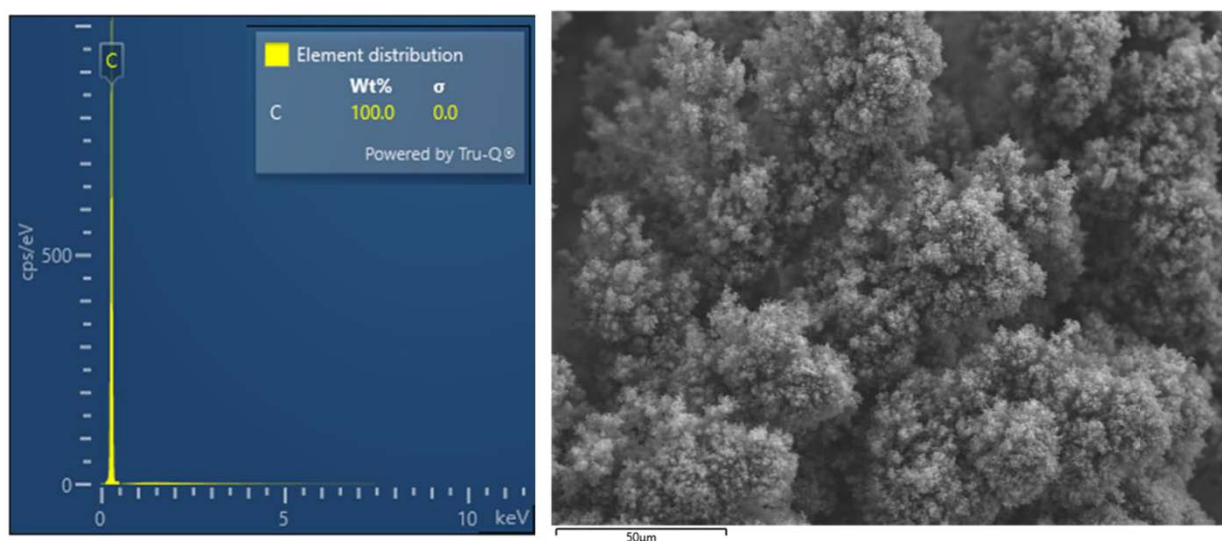
Figure 65. An example of the EDS analysis of a carbon sample from the reaction chamber. The entire image's area (600x) was scanned [115].

6.2.2 Inductively coupled plasma mass spectroscopy (ICP-MS)

The ICP-MS analysis confirmed the high purity of the carbon product, with only minor impurities, corroborating the findings from the EDS analysis. The results indicated that the carbon purity was 99.7% for the chamber-collected samples and 99.4% for the filter-collected samples. The primary impurities detected were metals, which originated from prior contamination of the filter used in steelmaking and alloying tests. These contaminants are negligible and can be disregarded. This conclusion is further supported by comparing the filter-collected samples to the pure samples obtained from the reaction chamber [115].

6.2.3 Raman spectroscopy

The Raman spectra of the carbon samples were compared with those from a high-purity natural graphite powder used as a reference. All carbon samples display three characteristic bands in their Raman spectra (Figure 66): the defect-activated D band at ~1338 cm^{-1}, the graphitic G band at ~1570 cm^{-1}, and the second-order D band, G'(2D) band, at ~2700 cm^{-1}. Unlike the D band, which requires defects for activation, the 2D band can be seen in defect-free graphitic materials. This comparison confirms the presence of graphitic-like structures with a low level of defects, as indicated by similar D/G intensity ratios for the pyrolysis-derived carbons. However, these samples show structural differences from ideal graphite, primarily due to defects and vacancies, as evidenced by the higher intensity of the D band relative to the reference graphite. On the other hand, the G'(2D) band typically signifies some degree of

order within the carbon material. A single, non-split G'(2D) peak suggests the formation of a graphite-like structure on a two-dimensional lattice with an incomplete transition to three-dimensional graphitization. This is supported by the current studies, where the G'(2D) band shows no splitting, indicating that the three-dimensional graphite lattice is not fully developed [120]. Table 7 lists the positions and intensity values of the bands. Notably, the intensity ratio of the D band to the G band (I_D/I_G) increases from the chamber-collected carbon to the filter-collected carbon, suggesting a rise in defects [121]. The reference graphite sample shows the lowest ID/IG ratio, indicating the most ordered and defect-free structure. Among the pyrolysis-derived carbon samples, the filter-collected carbon has a higher defect concentration compared to the chamber-collected carbon. This difference can be attributed to the higher temperature inside the reactor compared to that of the filter [115].
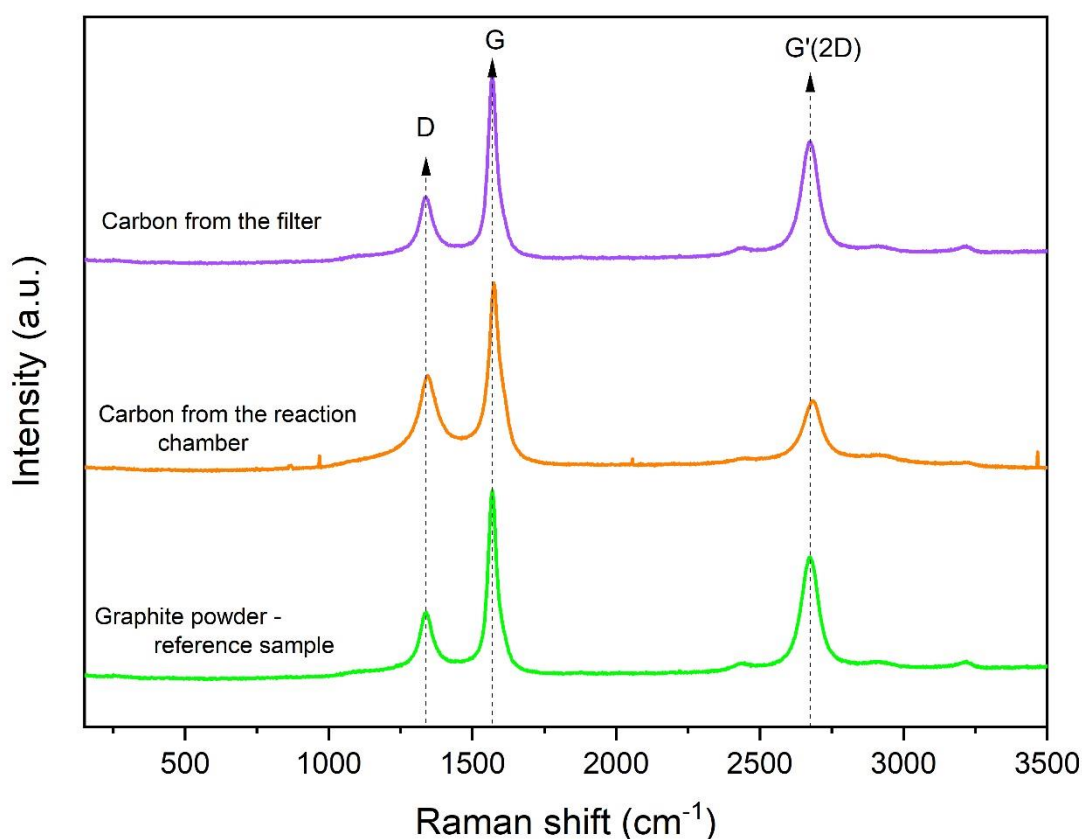
Figure 66. Raman spectra for the carbons collected from the filter and the reaction chamber versus a reference graphite powder of high carbon purity [115].

Table 7. Results of Raman spectroscopy [115].

Samples	D band		G band		G'(2D) band		I_D/I_G
	Position (cm⁻¹)	Intensity (a.u.)	Position (cm⁻¹)	Intensity (a.u.)	Position (cm⁻¹)	Intensity (a.u.)	
Filter carbon	1344.96	0.74	1574.16	1	2679.65	0.41	0.74
Chamber carbon	1344.97	0.51	1574.16	1	2683.61	0.38	0.51
Graphite reference	1340.26	0.27	1565.03	1	2697.69	0.42	0.27

6.2.4 X-ray diffraction (XRD)

X-ray diffractograms for all the studied samples are presented in Figure 67. The XRD analysis revealed crystalline structures similar to graphitic carbon (JCPDS card no. 75-1621), with no crystalline impurities detected in the pyrolysis-derived carbons. All XRD patterns exhibited a prominent peak at 2θ ~26°, corresponding to the (002) graphitic reflection. This peak was followed by less intense peaks at ~43°, ~54°, 77°, and 83°, which represent the (100)/(101), (004), (110), and (112) crystal planes, respectively. Generally, a narrower and more intense (002) peak indicates better orientation of the aromatic layers, while a narrower and more intense (100)/(101) peak suggests larger aromatic layers. Both carbon materials showed relatively narrow (002) peaks, but only the carbon from the chamber exhibited larger aromatic layers compared to the filter-collected carbon. Diffraction peaks corresponding to the (100)/(101), (004), and (110) planes of graphitic carbon typically appear at very high temperatures, such as those in the reactor. These peaks were more pronounced in the chamber-collected carbon, indicating a more ordered structure, and were nearly absent in the filter-collected carbon, suggesting it was less exposed to the high temperatures. The (112) peak, which may indicate a complex crystalline structure or multiple phases, was only slightly visible in the reference graphite sample and was absent in both the filter and chamber carbon samples [115].
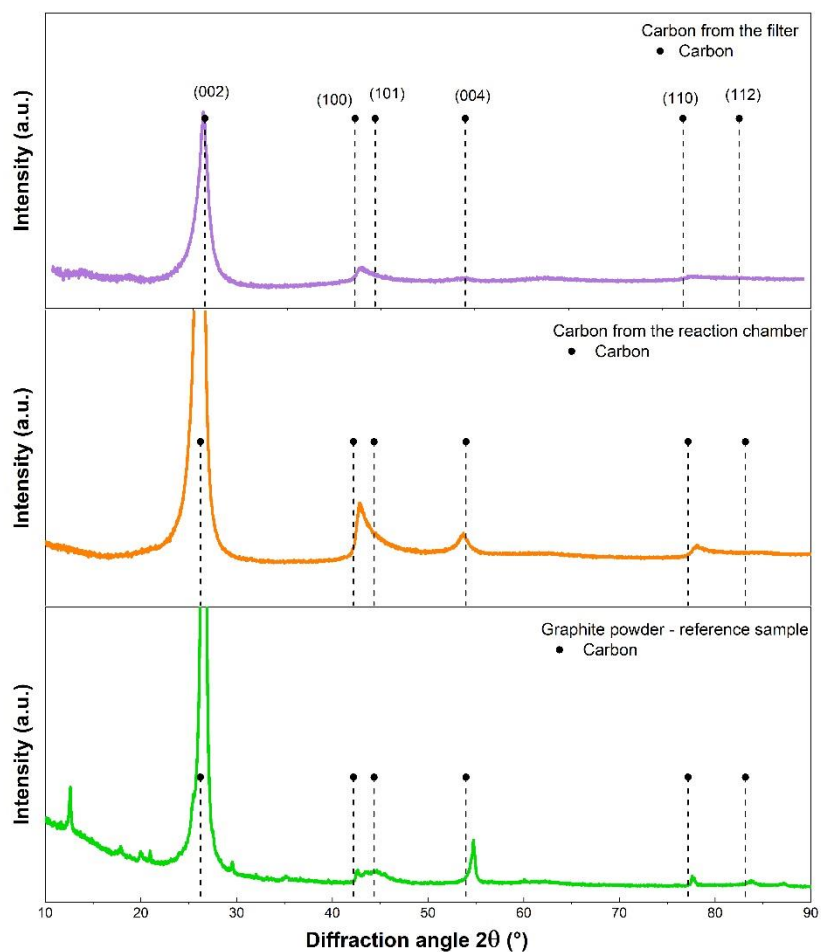
Figure 67. X-ray diffractograms for the carbons collected from the filter and the reaction chamber versus a reference graphite powder of high carbon purity [115].

6.2.5 Brunauer-Emmett-Teller (BET) method and specific surface area (SSA)

Selected carbon samples were analyzed for their BET SSA. It was observed that the fine carbon collected from the filter, with its smaller particle size, exhibited a higher BET SSA compared to the samples collected from the reactor [115].

To evaluate the obtained results, it is useful to review existing literature. Kim et al. [122] reported a BET SSA of 60 m²/g for carbon from the cyclone and 385 m²/g for filter-collected samples. Another study [114] found BET SSA values of 42 to 49 m²/g for nanostructured sheet-like carbon materials, while Fulcheri et al. [59] reported values ranging from 90 to 110 m²/g. In this study, the filter-collected carbon samples had BET SSA values ranging from 40 to 170 m²/g, which is notably higher than the 27 m²/g BET SSA of the reference graphite powder sample. Conversely, the chamber-collected carbon samples had a lower BET SSA, between

approximately 7 and 30 m²/g. As discussed earlier, these differences in SSA are likely due to the finer and smaller particle sizes in the filter-collected samples compared to those from the reaction chamber. Additionally, the increased defect concentration detected through Raman analysis might contribute to the higher SSA observed. Figure 68 presents the N_2 adsorption and desorption isotherms at 77 K for the selected samples, with the corresponding BET SSA values indicated. No significant correlation was found between the process parameters and the BET SSA values [115].
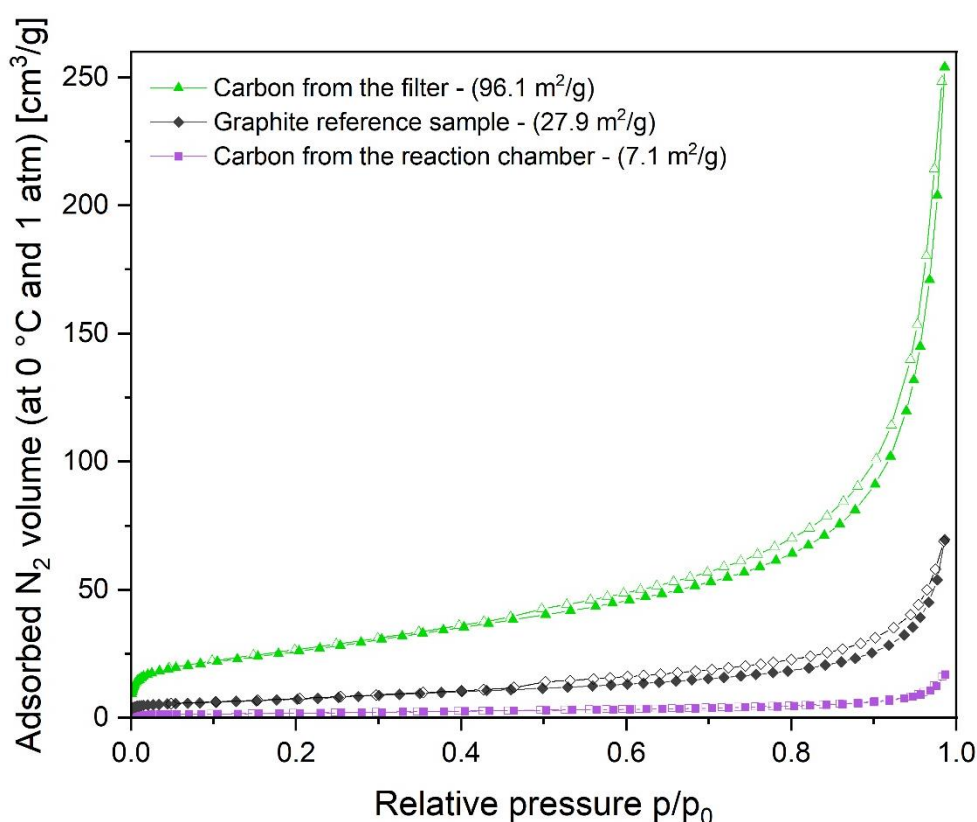
Figure 68. Results of adsorption and desorption experiments using N_2 at 77K. Solid symbols denote the adsorption branch; empty symbols denote the desorption branch of the isotherm [115].

6.3 Summary

The characterization of the produced carbon utilized a range of analytical techniques to assess morphological, microstructural, chemical, and surface area characteristics. SEM analyses revealed distinct microstructural differences between samples collected from the product gas filter and those from the reaction chamber. The filter-collected samples had finer textures, while the chamber-collected samples were larger and featured dendritic particles.

Raman spectroscopy confirmed that all carbon samples had graphite-like crystalline structures with low defect concentrations. XRD results supported this, showing crystalline structures similar to graphitic carbon. EDS and ICP-MS analyses confirmed that the carbon was of high purity, with minor impurities primarily due to initial filter contamination, which are negligible when comparing the filter samples to the purer chamber samples. Gas sorption measurements showed notable differences, with filter-collected samples exhibiting higher BET SSA values ranging from 40 to 170 m²/g, compared to chamber-collected samples with values between 7 and 30 m²/g. These differences are attributed to the smaller particle size and higher defect concentration in the filter-collected samples. This comprehensive characterization underscores the importance of considering both the source and collection method when evaluating carbon samples. The insights gained provide a solid foundation for further research and development, suggesting that advanced experimental setups are necessary to explore the complex relationships between process parameters and carbon properties. Such research will enhance our understanding and help optimize the plasma pyrolysis process for producing carbon materials with targeted properties [115].

7 Thinking bigger: Adapting and scaling up

Drawing from insights gained through experimental work, a novel process concept has been formulated to address existing limitations and propose potential solutions. This chapter thoroughly explores the elucidation of this concept and the design of the reactor. The envisaged laboratory facility is designed to conduct pyrolysis tests in accordance with the stipulated objectives. The plasma plant is conceptualized to possess adaptability, allowing for operation with diverse gas compositions and electrical power levels. Such flexibility is imperative for accommodating the varied parameters requisite for academic research endeavors, enabling comprehensive exploration of process dynamics. Through systematic variation of process parameters, the objective is to enhance understanding of the process intricacies and delineate optimal conditions for subsequent scaling up and industrialization. This iterative process of optimization is pivotal for the eventual realization of the concept into a viable industrial process.

7.1 Concept

The plasma facility operates on the principle of a DC-transferred arc, powered by a minimum supply of 120 kW. The reactor is a straightforward vertical chamber constructed of steel. Any excess heat not involved in the reaction must be dissipated from the vessel's walls via the developed cooling system. To shield the steel from direct radiation, the inner wall will be coated with graphite felt. It is essential for the reactor to remain simple and compact for versatility in integration into different setups.

The plasma arc, forming the hot core, is initiated between two symmetric and dynamic electrodes. This arrangement ensures continuous production of H_2 and carbon, unlike the horizontal design where solid carbon filling led to process interruptions. The primary plasma gas considered is Ar, although there's a possibility of mixing H_2 and CH_4 with the plasma gas introduced through the electrodes. The main process gas mainly pure CH_4 enters from an external lance positioned at the top, with alternative additional synthetic pre-mixed gases such as biogas. As carbon forms, it descends due to both its weight and the downward gas flow within the reactor.

Product gas exit the reactor with the extremely fine particles for filtration and analysis, while N_2 is utilized as a purging gas. Maintaining a gas-tight system is crucial for handling process gas (CH_4) and product gas (H_2), especially considering operation under high pressures of up to 10 bar (gauge). Another critical safety consideration is electrical isolation, particularly concerning the high-voltage electrical unit connected to the electrodes. Proper isolation ensures that the discharge occurs only between the cathode and the anode, mitigating potential risks.

During the following section, the general specifications and definitions of the reactor and the process are provided to facilitate the understanding and implementation of the concept.
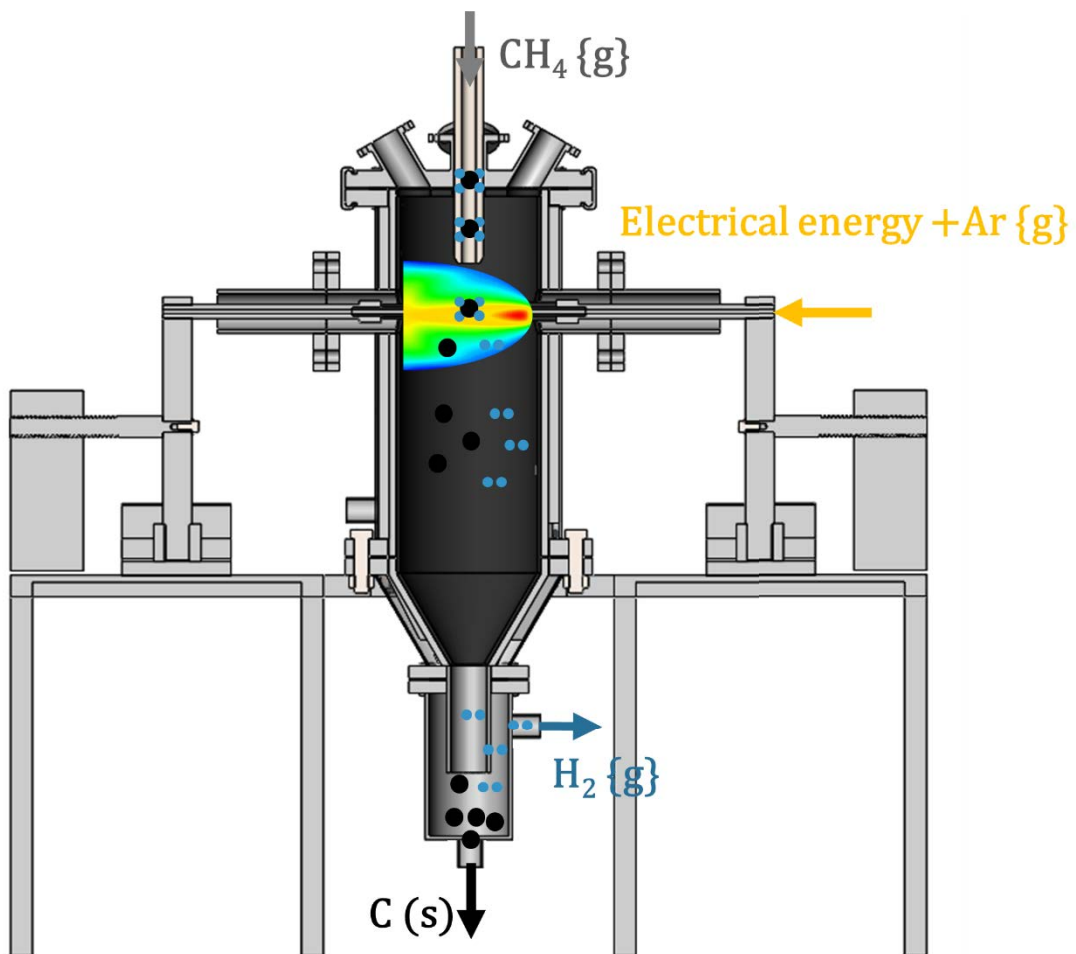
Figure 69. Visualization of a new concept for TPPM.

7.2 Rough specification of the design

7.2.1 Mass balance

The filter and gas membrane unit have a capacity of 25 Nm^3/h. This serves as a crucial reference point for estimating the gas input capacity and conducting calculations for different gas mixtures, considering various scenarios for the system.

Table 8. Three different considerations regarding the gas composition of the process and the mass balance.

Scenario	Extreme case maximum		Extreme case minimum		Common case	
Gas compounds	[Nl/min]	%	[Nl/min]	%	[Nl/min]	%
Input gas	297.62	100	50	100	120	100
Plasma gas						
Ar	119.05	40	25.00	50	48.00	40
H_2	14.88	5	5.00	10	6.00	5
sum	133.93	45	30.00	60	54.00	45
Process gas						
CH_4	119.05	40	10.00	20	48.00	40
Purge and support gas						
Ar	29.76	10	5.00	10	12.00	10
N_2	14.88	5	5.00	10	6.00	5
sum	44.64	15	10.00	20	18.00	15
Output (product) gas						
H_2	252.98	60.71	25.00	41.67	92.40	56.62
CH_4	0.00	0	0.00	0	4.80	2.94
Ar	148.81	35.71	30.00	50	60.00	36.76
N_2	14.88	3.57	5.00	8.33	6.00	3.68
sum	416.67	100	60.00	100	163.20	100
Carbon product	[g/min]	[g/h]	[g/min]	[g/h]	[g/min]	[g/h]
	63.79	3,827.34	5.36	321.50	23.15	1,388.86

7.2.2 Energy balance

Initially, the energy needed to elevate the gas mixture temperature from 25 to 3000 °C in 1 bar for 1 mol of CH_4, Ar, and H_2 in the maximum case scenario was computed using FactSage 8.2 software with the FactPS database. Subsequently, an isothermal calculation was conducted to estimate the energy necessary for the reaction at this temperature, taking into account the potential products of H_2, C, C_2H_2, C_2H_4, and C_2H_6.

According to the FactSage 8.2 software calculations, ΔH for the studied system equals 218,269 kJ, equivalent to approximately 60 kWh. Assuming a 50% efficiency of the electric unit and power supply system, a power supply of 120 kW is determined to be necessary.

Table 9. Estimation of the energy requirement for the design.

25 to 3000 °C	CH_4	Ar	H_2	N_2
mol/h	321	402	40	40
Required energy		60 kW/h		

7.2.3 Reactor shape and geometry

For clarity in describing the reaction vessel, it is segmented into four zones, as illustrated in Figure 70 and explained individually further.
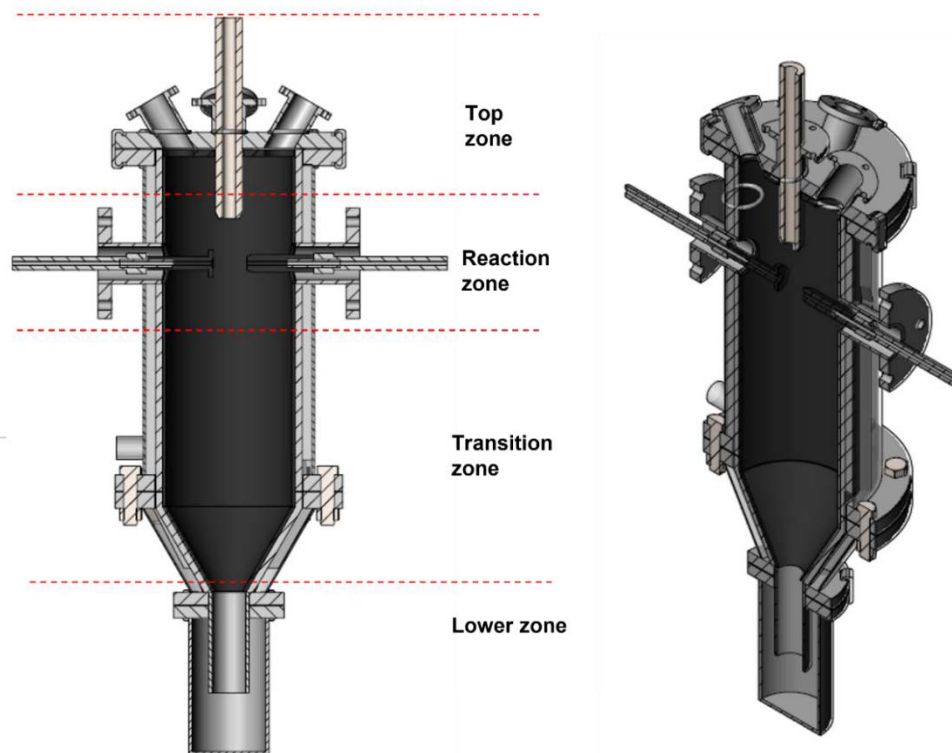
Figure 70. Different zones of the reaction vessel's design.

Top Zone: The reaction vessel is capped by a top lid affixed with clamp screws for easy assembly, a prerequisite before and after each test. This lid features five openings: one centrally located for the CH_4 nozzle, another designed as a window for arc monitoring, and a third connected to Ar and N_2 for continuous purging during testing. A pressure indicator will be attached to the fourth opening, while the fifth remains reserved for potential future developments.

Reaction Zone: Two electrodes penetrate the reaction vessel through symmetric openings. Positioned facing each other, one serves as the cathode while the other functions as the anode. It is important to electrically isolate the electrodes from the vessel using appropriate insulating materials to facilitate the intended electrical discharge. Optionally, an external magnetic field could be installed to enhance arc stability and precisely target the point of electrical discharge. This setup could help prevent unwanted side arcing to the surrounding inner wall of the reactor.

Given the presence of potentially explosive gas components within the reactor, ensuring a gas-tight seal from the surrounding atmosphere is critical. While designing the electrode

openings presents a challenge due to sealing considerations, a concept addressing this challenge is briefly introduced, with further development reliant on contractor support.

The electrodes are adjustable and can be symmetrically shifted from both sides within a guiding tube with the assistance of an electric motor. The arc length must be adjustable in a range of 0 to 300 mm. Each electrode comprises two hollow pipes: one made of stable steel (a threaded rod) connected to the power supply, and the other made of graphite, which can be screwed onto the steel pipe. While the graphite head enters the reaction vessel, the steel pipe remains within the electrode's guiding tube.

Alongside the electrical power port, the gas inlet is also connected to the guiding tube, entering the hollow steel pipe. N_2 gas should be connected and supplied to this area to prevent gas leakage into the environment and avoid oxygen intake. Sealing rings and insulating sheets are employed to prevent gas leakage and isolate the guiding tube from the vessel, respectively.

Solid carbon formation may occur on the surfaces of the vessel, electrodes, or within the gas flow. However, it must be purged with a high gas flow from both the top and the sides.

Transition Zone: The reaction products will descend through the transition zones. These transition zones comprise the lower section of the cylinder and the cyclone.

Lower Zone: The gas continues to flow through a neck pipe positioned near the bottom of the container. This neck pipe is situated close to the bottom to minimize gas turbulence within the container. The objective is to retain the carbon within the container while allowing the gas to flow from the vicinity of the neck pipe and exit the reactor through the product gas pipeline. In the event that a significant portion of the produced carbon disperses with the gas instead of remaining in the container, the inclusion of a second cyclone within the product gas pipeline may be required as an alternative solution.

The three-dimensional design of the reactor is depicted in Figure 71.
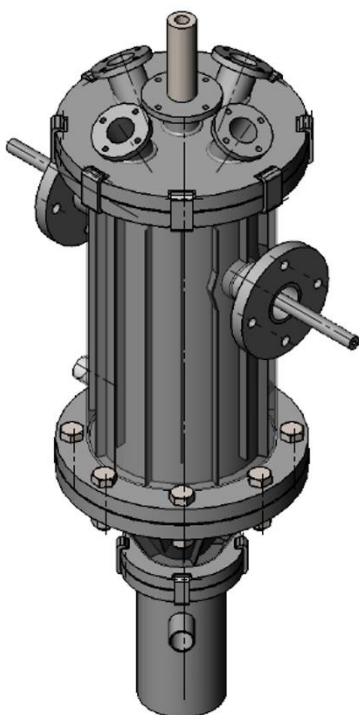
Figure 71. The three-dimensional rendering of the plasma reactor.

7.2.4 The gas supply unit

Pressure reducers upstream of the reaction vessel gradually decrease the pressure in three stages from 200 barg to a range of 10 barg. Thermodynamically, higher pressures are not optimal for the process; however, to prevent gas suction from the environment and to maintain safety, the pressure within the reaction vessel must remain slightly higher than atmospheric pressure. Additionally, this setup allows for testing across a broad pressure range.

Gas components are mixed and introduced into the reaction vessel from four directions:

1. **Cathode side - Plasma gas inlet:** Ar and H_2 are introduced into the reaction vessel through the hollow cathode after thorough mixing.
2. **Anode side - Alternative plasma gas inlet:** The plasma gas can be directed also through the anode side for varying testing conditions.
3. **CH_4 nozzle:** CH_4 or biogas, optionally mixed with H_2, is introduced into the reaction vessel through the nozzle from above, directed towards the plasma arc. N_2 serves as a purge gas before and after testing and in emergency situations, also entering through this inlet.

4. **Top lid - N₂ and Ar gas inlet:** N_2 and Ar are connected to the top via an inlet integrated into the lid. These gases are utilized during testing to augment gas flow within the reactor. While Ar can enhance arc stability, its higher cost makes N_2 the preferred choice.

All piping carrying explosive gas components must be interconnected with N_2 purging gas. In the event of an emergency, the facility must be promptly shut down, and immediate purging of the entire system with N_2 must be initiated. These safety measures must be integrated into the automation design. Additionally, the system must undergo purging before and after each test, with sufficient purging time to ensure the removal of all gases. The gas flow and purging time should be determined based on the reactor's volume and the capacities of the filtration system.

As such, the control of N_2 can be managed both manually and automatically by the program. It is critical to verify that N_2 flows through all connected pipes and does not bypass any intended pipelines. To achieve this, the orifices on the N_2 pipes must be adjusted to distribute the gas uniformly through all pipelines.

Furthermore, safety relief measures are implemented on the plasma gas inlet to maintain the process pressure at 10 barg.

7.2.5 The reaction vessel and graphite lining

The graphite lining inside serves to shield the vessel from the effects of arc discharge and allows for adjustment of the inner diameter to accommodate various gas flow ranges. Moreover, it prevents any detrimental effects on the quality of the produced carbon that might occur with alternative refractory materials. Additionally, the graphite lining can prolong the residence time of heat in the reaction zone through a reflection effect.

7.2.6 The cooling system

The reaction vessel and the electrode chamber are double-walled steel chambers with cooling water flowing through to prevent overheating of the reactor. Additionally, to cool the electrodes, a heat exchanger will cool the returned water.

7.2.7 The product gas filtration unit

The product gas will undergo filtration and separation into two main products: H_2 and solid carbon. A mass spectrometer will analyze the composition of the product gas. A manual valve is positioned after the reaction vessel to allow bypassing of the filter and direct the product gas to the combustion vessel. Subsequently, the product gas will be combusted and released into the atmosphere above the facility.

7.2.8 Summary of the process

The procedure for a pyrolysis test is outlined as follows:

1. Purging the entire reactor with N_2.
2. Shifting the electrodes to the arc ignition position to establish a short circuit.
3. Initiating the arc using Ar as the plasma gas and immediately shifting the electrodes back to a stable arc distance position.
4. Monitoring the stable arc through the camera installed on the top window of the lid.
5. Introducing CH_4 to the transferred arc.
6. Monitoring the reaction using the gas analysis device installed on the product gas pipeline.
7. Ceasing the flow of CH_4 when the intended test is completed.
8. Turning off the power and halting the plasma gas flow.
9. Purging the system with N_2.
10. Dismantling the reactor and removing the deposited carbon from the inside of the reactor (graphite inlet).

8 Summary

H_2 presents a promising alternative to fossil fuels, yet its eco-friendly production faces several challenges in production, storage, and transport. However, there is a growing imperative to reduce GHGs, evidenced by shifts toward hydrogen in industries like steelmaking. Current infrastructure limitations necessitate mid-term solutions like methane pyrolysis, converting CH_4 into clean H_2 and valuable carbon without CO_2 emissions.

An overview of pyrolysis methods, mostly involving catalysts, highlights challenges such as carbonization, deactivation, and difficult carbon separation, potentially leading to CO_2 emissions. Recent advancements in plasma technology, particularly TPP, show significant promise, producing pure carbon and high H_2 yield without catalysts.

Plasma, as the fourth state of matter, is created by infusing gas with energy, forming a mixture of electrons, ions, atoms, and other particles. TP, generated through electric discharge or arc, offers various configurations like plasma jets and torches, each suitable for different applications. Plasma pyrolysis technology offers higher reaction rates, enhanced stability, and operates outside thermodynamic equilibrium. However, optimizing these complex systems and improving efficiency remain challenges, indicating avenues for further research and development.

Various studies explore TPPM using different plasma setups and process parameters, analyzing carbon yield, CH_4 conversion rates, product analysis, and energy balance. Investigations highlight the impact of plasma stability, gas injection methods, quenching rates, and electrode erosion on TPPM efficiency. Some studies have been extended to pilot and commercial scales. Key players in TPPM include:

- **Kvaerner:** Developed a plasma torch reactor for CB production, faced challenges in quality.
- **Monolith:** Focuses on CB production and hydrogen gas with innovative processes.
- **Plenesys:** Developing the HyPlasma® Process with AC plasma torches for methane pyrolysis.
- **Graforce:** Utilizes DC plasma system for methane decomposition.
- **Atlantic Hydrogen:** Developed CarbonSaver™ technology for hydrogen-enriched natural gas.
- **HiiROC:** Focuses on thermal plasma torch technology for hydrogen production from methane.

This work centers on methane pyrolysis and includes experimental work. The study focuses on the concept of TPPM, aiming to refine and enhance a process concept for high efficiency and scalability. Key factors for improving process efficiency include maintaining a stable and continuous operation with maximum hydrogen yield and productivity. Another critical aspect is the quality of the produced solid carbon. Experiments cover technical feasibility and parameter optimization, utilizing a thermal plasma reactor with a variable gas mixture of Ar and CH_4 to create a DC-transferred plasma arc. The product gas undergoes analysis, while the plasma arc is captured using a camera mounted on the top lid. A feasibility study and a systematic statistical experimental analysis are conducted using a design of experiments software. The results are outlined below:

- **H_2 yield**:

The H_2 yields varied from 60 to 100%, depending on conditions. Optimizing setups and conditions could significantly enhance efficiency and yield. Elevated CH_4 content reduces H_2 yield, while higher current and arc lengths promote it.

- **Plasma gas composition:**

CH_4 presence affects power input. Pure Ar provides optimal arc stability, but increasing CH_4 concentration decreases H_2 yield notably. Higher gas flow rates reduce H_2 yield due to decreased gas residence time and increased unreacted CH_4.

- **Power input enhancement:**

Power input is indirectly controlled through adjustments in electric current and arc length. Increasing amperage increases power input, provides more energy for the reaction, promotes the pyrolysis reaction, and boosts H_2 yield. Amperage adjustment (90-120 A) varied power within the range of 5 to 7 kW. High CH_4 content and longer arc length increase power input due to energy requirements for excitation and ionization.

- **Plasma arc conditions:**

Changes in cathode and anode affect arc conditions, influencing arc length and plasma arc stability. Introducing CH_4 poses stability challenges, but a mixture of 60% Ar and 40%

CH_4 enhances stability and productivity. Stability time is the duration before the first arc disruption, a crucial parameter for process evaluation, and is influenced by various parameters and reactor constraints, including electrical unit limits and reactor geometry. Greater arc lengths create a larger reaction environment, leading to higher H_2 yield. Solid carbon accumulation during pyrolysis reduces plasma arc stability and H_2 yield over time, complicating the process. Higher CH_4 content and longer arc length significantly impact stability, leading to disruptions. Overloading the AC transformer due to maximum amperage limits results in reduced stability time.

Characterization of the produced carbon reveals the following results:

- **SEM analyses:**

Filter-collected samples had finer textures. Reactor-collected samples had larger sizes and dendritic particles.

- **Raman spectroscopy and XRD:**

Confirmed the presence of crystalline graphite-like structures. Low defect concentrations in all examined carbon samples.

- **EDS and ICP-MS analyses:**

Confirmed high-purity carbon with slight impurities from the filter. Initial filter contaminations are negligible when comparing samples.

- **Gas sorption BET measurements:**

Filter-collected samples had higher BET SSA values (40-170 m^2/g). Reactor-collected samples had lower values (7-30 m^2/g).

Finally, a new concept is introduced to address challenges and provide a platform for commercializing the process. The plasma facility should operate on a DC-transferred arc principle, requiring a minimum of 120 kW power. The vertical steel chamber dissipates excess heat through a cooling system, with inner wall graphite felt coating for radiation shielding. Continuous H_2 and carbon production are ensured through a dynamic electrode arrangement, with Ar as the primary plasma gas and the possibility of mixing in H_2 and CH_4. Gas-tightness maintenance is crucial under high pressure, along with proper electrical isolation for safety.

9 References

[1] Sambo, C., Dudun, A., Samuel, S. A., Esenenjor, P., Muhammed, N. S., Haq, B. *A review on worldwide underground hydrogen storage operating and potential fields*, International Journal of Hydrogen Energy, 2022, *47*, 22840–22880.

[2] Da Silva Veras, T., Mozer, T. S., Da Costa Rubim Messeder dos Santos, D., Da Silva César, A. *Hydrogen: Trends, production and characterization of the main process worldwide*, International Journal of Hydrogen Energy, 2017, *42*, 2018–2033.

[3] Da Costa Labanca, A. R. *Carbon black and hydrogen production process analysis*, International Journal of Hydrogen Energy, 2020, *45*, 25698–25707.

[4] The European Commission. *The European Green Deal 2050: Boosting the economy, improving people's health and quality of life, caring for nature, and leaving no one behind*, 2019, https://ec.europa.eu/commission/presscorner/detail/en/ip_19_6691, accessed: 2024.

[5] The European Commission. *Committing to climate neutrality by 2050*, 2020, https://ec.europa.eu/commission/presscorner/detail/en/ip_20_335, accessed: 2024.

[6] International Energy Agency. *Net Zero by 2050: A Roadmap for the Global Energy Sector*, 2021, https://www.iea.org/reports/net-zero-by-2050, accessed: 2024.

[7] Federal Ministry Republic of Austria. *Hydrogen strategy for Austria*, 2022, https://www.bmk.gv.at/dam/jcr:7788d724-3aed-4a88-a452-37f9df5e1357/bmk_wasserstoff_executive-summary_EN_UA.pdf, accessed: 2024.

[8] Bespalko, S., Mizeraczyk, J. *Overview of the hydrogen production by plasma-driven solution electrolysis*, Energies, 2022, *15*, 7508.

[9] El-Shafie, M., Kambara, S., Hayakawa, Y. *Hydrogen production technologies overview*, Journal of Power and Energy Engineering, 2019, *07*, 107–154.

[10] Hefner, R. *Toward sustainable economic growth: the age of energy gases*, International Journal of Hydrogen Energy, 1995, *20*, 945 - 948.

[11] Magazova, A., Agar, D. W. *Improvement of plasma reactor design for methane pyrolysis by simulation*, Chemie Ingenieur Technik, 2023, *95*, 780–784.

[12] Kim, J., Sovacool, B. K., Bazilian, M., Griffiths, S., Lee, J., Yang, M., Lee, J. *Decarbonizing the iron and steel industry: A systematic review of sociotechnical systems, technological innovations, and policy options*, Energy Research & Social Science, 2022, *89*, 102565.

[13] Primetals Technologies. *Hyfor pilot plant under operation – the next step for carbon free, hydrogen-based direct reduction is done*, 2021, https://www.primetals.com/press-

media/news/hyfor-pilot-plant-under-operation-the-next-step-for-carbon-free-hydrogen-based-direct-reduction-is-done, accessed: 2024.

[14] Spreitzer, D., Wurm, J., Hiebl, B., Rein, N., Wolfinger, T., Sterrer, W., Fleischanderl, A. *Hyfor - Hydrogen-based fine-ore reduction*, *Mitsubishi Heavy Industries*, 2022, *59*.

[15] Posco. *Breakthrough hydrogen reduction ironmaking technology with near-zero emission*, https://www.posco.co.kr/homepage/docs/eng7/jsp/hyrex/, accessed: 2024.

[16] K1-met gmbh. *Sustainable steel production utilising hydrogen*, https://www.k1-met.com/en/non_comet/susteel, accessed: 2024.

[17] Fulcheri, L. *Plasma assisted conversion of hydrocarbons for green and environmental friendly energy*, https://www.researchgate.net/publication/281946596_Plasma_assisted_conversion_of_hydrocarbons_for_a_green_and_envirionmental_friendly_energy_transition, accessed: 2024.

[18] Fulcheri, L., Fabry, F., Takali, S., Rohani, V. *Three-Phase AC Arc Plasma Systems: A Review*, *Plasma Chem Plasma Process*, 2015, *35*, 565–585.

[19] Gautier, M., Rohani, V., Fulcheri, L. *Direct decarbonization of methane by thermal plasma for the production of hydrogen and high value-added carbon black*, *International Journal of Hydrogen Energy*, 2017, *42*, 28140–28156.

[20] Li, T., Rehmet, C., Cheng, Y., Jin, Y., Cheng, Y. *Experimental Comparison of Methane Pyrolysis in Thermal Plasma*, *Plasma Chem Plasma Process*, 2017, *37*, 1033–1049.

[21] Dagle, R., Dagle, V., Bearden, M., Holladay, J., Krause, T., Ahmed, S. *An overview of natural gas conversion technologies for co-production of hydrogen and value-added solid carbon products*, 2017, https://doi.org/10.2172/1411934, accessed: 2023.

[22] Li, T., Rehmet, C., Cheng, Y., Jin, Y., Cheng, Y. *Experimental Comparison of Methane Pyrolysis in Thermal Plasma*, *Plasma Chem Plasma Process*, 2017, *37*, 1033–1049.

[23] Mašláni, A., Hrabovský, M., Křenek, P., Hlína, M., Raman, S., Sikarwar, V. S., Jeremiáš, M. *Pyrolysis of Methane via Thermal Steam Plasma for the Production of Hydrogen and Carbon Black*, *International Journal of Hydrogen Energy*, 2021, *46*, 1605–1614.

[24] Pristavita, R., Mendoza-Gonzalez, N.-Y., Meunier, J.-L., Berk, D. *Carbon Blacks Produced by Thermal Plasma: the Influence of the Reactor Geometry on the Product Morphology*, *Plasma Chem Plasma Process*, 2010, *30*, 267–279.

[25] Pristavita, R., Meunier, J.-L., Berk, D. *Carbon Nano-Flakes Produced by an Inductively Coupled Thermal Plasma System for Catalyst Applications*, *Plasma Chem Plasma Process*, 2011, *31*, 393–403.

[26] Wnukowski, M. *Methane Pyrolysis with the Use of Plasma: Review of Plasma Reactors and Process Products*, *Energies*, 2023, *16*, 6441.

[27] Solonenko, O. P. *Thermal plasma torches and technologies. Plasma Torches: Basic studies and design.*, Institute of Theoretical and Applied Mechanics, Siberian Branch of the Russian Academy of Sciences, Novosibirsk, 2000.

[28] Donnet, J. B., Bansal, R. C., Wang, M. J. *Carbon black: Science and technology*, Dekker, New York, 1993.

[29] Gueret C., Daroux, M. Billaudi, F. *Methane pyrolysis: Thermodynamics*, *Chemical Engineering Science*, 1997, *52*, 815–827.

[30] Roscoe, J. M., Thompson, M. J. *Thermal decomposition of methane: Autocatalysis*, *International Journal of Chemical Kinetics*, 1985, *17*, 967–990.

[31] Holmen, A., Olsvik, O., Rokstad, O. A. *Pyrolysis of natural gas: chemistry and process concepts*, *Fuel Processing Technology*, 1995, *42*, 249–267.

[32] Dean, A. M. *Detailed kinetic modeling of autocatalysis in methane pyrolysis*, *The Journal of Physical Chemistry*, 1990, *94*.

[33] Hidaka, Y., Nakamura, T., Tanaka, H., Inami, K., Kawano, H. *High temperature pyrolysis of methane in shock waves. Rates for dissociative recombination reactions of methyl radicals and for propyne formation reaction*, International Journal of Chemical Kinetics, 1990, *22*, 701–709.

[34] khan, M. S., Crynes, B. L. *Survey of recent methane pyrolysis literature*, Industrial and Engineering Chemistry, 1970, *62*, 54–59.

[35] Fincke, J. R., Anderson, R. P., Hyde, T. A., Detering, B. A. *Plasma Pyrolysis of Methane to Hydrogen and Carbon Black*, Ind. Eng. Chem. Res., 2002, *41*, 1425–1435.

[36] Lee, D. H. *Hydrogen production via the Kværner process and plasma reforming*, Compendium of Hydrogen Energy, 2015, 349–391.

[37] Lanz, W. *Hydrogen Fuel Cell Engines and Related Technologies - Module 1: Hydrogen Properties*, 2001.

[38] Davey, R. *What Chemical Elements are Found in the Human Body?*, 2023, https://www.news-medical.net/life-sciences/What-Chemical-Elements-are-Found-in-the-Human-Body.aspx, accessed: 2024.

[39] NASA. *Star basics*, https://science.nasa.gov/universe/stars/, accessed: 2024.

[40] International Energy Agency. *Net Zero Roadmap: A global pathway to keep the 1.5 °C goal in reach*, 2023, https://www.iea.org/reports/net-zero-roadmap-a-global-pathway-to-keep-the-15-0c-goal-in-reach, accessed: 2024.

[41] Nnabuife, S. G., Ugbeh-Johnson, J., Okeke, N. E., Ogbonnaya, C. *Present and projected developments in hydrogen production: A technological review*, Carbon Capture Science & Technology, 2022, *3*.

[42] International Energy Agency. *Hydrogen Production and Storage: R&D priorities and gaps*, 2006, https://iea.blob.core.windows.net/assets/e19e0c2a-0cef-4de6-a559-59d0342974c3/hydrogen.pdf, accessed: 2024.

[43] Balat, M. *Potential importance of hydrogen as a future solution to environmental and transportation problems*, International Journal of Hydrogen Energy, 2008, *33*, 4013–4029.

[44] International Energy Agency. *Global Hydrogen Review 2023*, 2023, https://www.iea.org/reports/global-hydrogen-review-2023, accessed: 2024.

[45] Ishaq, H., Dincer, I., Crawford, C. *A review on hydrogen production and utilization: Challenges and opportunities*, International Journal of Hydrogen Energy, 2022, *47*, 26238–26264.

[46] VOX. *The hydrogen color palette*, https://www.amandanorthrop.com/vox, accessed: 2024.

[47] Lanz, W. *Hydrogen Fuel Cell Engines and Related Technologies - Module 2: Hydrogen Use*, 2001.

[48] Meiling Yue, Hugo Lambert, Elodie Pahon, Robin Roche, Samir Jemei, Daniel Hissel. *Hydrogen energy systems: A critical review of technologies, applications, trends and challenges*, Renewable and Sustainable Energy Reviews, 2021, *146*.

[49] Institute for Clean Technology. *Die Bedeutung von Wasserstoff für die Energiezukunft der österreichischen Wirtschaft.*, 2022, https://jimdo-storage.global.ssl.fastly.net/file/9c49fa15-4de6-44d0-86f0-d5dbb5669d6a/Wasserstoffstudie.OE_220908.pdf, accessed: 2024.

[50] Schulze-Makuch, D., Irwin, L. N. *Life in the universe: Expectations and constraints*, Springer, New York, 2018.

[51] Falcao E. HL., Wudl, F. *Carbon allotropes: Beyond graphite and diamond*, Journal of Chemical Technology and Biotechnology, 2007, 524–531.

[52] Haygot Technologies, Ltd. *Carbon and its compounds*, https://www.toppr.com/guides/chemistry/carbon-and-its-compounds/carbon/, accessed: 2024.

[53] Shah, R. *Elements that keep us alive also give color to fireworks*, 2015, https://biobeat.nigms.nih.gov/2015/07/elements-that-keep-us-alive-also-give-color-to-fireworks, accessed: 2024.

[54] Paul M. *Diamond: The world's favourite gem*, 2017, https://www.chm.bris.ac.uk/motm/diamond/diamondh.htm, accessed: 2024.

[55] Knabl, F. *Structural characterization of carbons derived from methane pyrolysis*. Master's Thesis, Montanuniversität Leoben, 2021.

[56] Giubileo, F., Di Bartolomeo, A., Iemmo, L., Luongo, G., Urban, F. *Field Emission from Carbon Nanostructures*, *Applied Sciences*, 2018, *8*, 526.

[57] Popov, V. N. *Carbon nanotubes: properties and application*, *Materials Science and Engineering*, 2004, 61–102.

[58] Fan, Y., Fowler, G. D., Zhao, M. *The past, present and future of carbon black as a rubber reinforcing filler – A review*, *Journal of Cleaner Production*, 2020, *247*, 119115.

[59] Fulcheri, L., Rohani, V.-J., Wyse, E., Hardman, N., Dames, E. *An energy-efficient plasma methane pyrolysis process for high yields of carbon black and hydrogen*, *International Journal of Hydrogen Energy*, 2022.

[60] Mordor Intelligence. *Carbon Black Market Size & Share Analysis - Growth Trends & Forecasts (2024 - 2029)*, https://www.mordorintelligence.com/industry-reports/carbon-black-market, accessed: 2024.

[61] Yap, Y. W., Mahmed, N., Norizan, M. N., Abd Rahim, S. Z., Salimi, M. N. A., Abdul Razak, K., Mohamad, I. S., Mohd Mustafa Al-Bakri Abdullah and Yunus, M. Y. M. *Recent advances in synthesis of graphite from agricultural bio-waste material: A review*, *Materials*, 2023, *16*.

[62] Yehia M. Manawi, Ihsanullah, Ayman Samara, Tareq Al-Ansari and Muataz A. Atieh. *A Review of Carbon Nanomaterials' Synthesis via the Chemical Vapor Deposition (CVD) Method*, *Materials*, 2018, *11*.

[63] Ren, J., Lau, J., Lefler, M., Licht, S. *The Minimum Electrolytic Energy Needed To Convert Carbon Dioxide to Carbon by Electrolysis in Carbonate Melts*, *J. Phys. Chem. C*, 2015, *119*, 23342–23349.

[64] Sieradzka, M., Kirczuk, C., Kalemba-Rec, I., Mlonka-Mędrala, A., Magdziarz, A. *Pyrolysis of Biomass Wastes into Carbon Materials*, *Energies*, 2022, *15*, 1941.

[65] Belbessai, S., Benyoussef, E.-H., Gitzhofer, F., Abatzoglou, N. *Carbon nanomaterial production using waste plastic pyrolysis over a new catalyst made from mining residues: Effect of plastic type*, *Chemical Engineering Journal Advances*, 2022, *12*, 100424.

[66] Keipi, T., Tolvanen, K. E., Tolvanen, H., Konttinen, J. *Thermo-catalytic decomposition of methane: The effect of reaction parameters on process design and the utilization possibilities of the produced carbon*, *Energy Conversion and Management*, 2016, *126*, 923–934.

[67] J.J. Hutchinson, C.A. Campbell, R.L. Desjardins. *Some perspectives on carbon sequestration in agriculture*, *Agricultural and Forest Meteorology*, 2007, *142*, 288–302.

[68] Zhai, Z., Zhang, L., Du, T., Ren, B., Xu, Y., Wang, S., Miao, J., Liu, Z. *A review of carbon materials for supercapacitors*, *Materials & Design*, 2022, *221*, 111017.

[69] Rivera-Utrilla, J., Sánchez-Polo, M., Gómez-Serrano, V., Alvarez, P. M., Alvim-Ferraz, M. C. M., Dias, J. M. *Activated carbon modifications to enhance its water treatment applications. An overview*, *Journal of hazardous materials*, 2011, *187*, 1–23.

[70] Hsu, C.-Y., Rheima, A. M., Mohammed, M. S., Kadhim, M. M., Mohammed, S. H., Abbas, F. H., Abed, Z. T., Mahdi, Z. M., Abbas, Z. S., Hachim, S. K., Ali, F. K., Mahmoud, Z. H., kianfar, E. *Application of Carbon Nanotubes and Graphene-Based Nanoadsorbents in Water Treatment*, *BioNanoSci.*, 2023, *13*, 1418–1436.

[71] Rajakumar, G., Zhang, X. H., Gomathi, T., Wang, S. F., Ansari, M. A., Mydhili, G., Nirmala, G., Alzohairy, M. A., Chung I. M. *Current use of carbon-based materials for biomedical applications — A prospective and review*, Processes, 2020, *8*.

[72] kesic, S. *Overview of hydrogen production by methane pyrolysis process and possible applications of the solid carbon products*. Master's Thesis, University of Zagreb, 2022.

[73] Patlolla, S. R., Katsu, K., Sharafian, A., Wei, K., Herrera, O. E., Mérida, W. *A review of methane pyrolysis technologies for hydrogen production*, *Renewable and Sustainable Energy Reviews*, 2023, *181*, 113323.

[74] Msheik, M., Rodat, S and Abanades, S. *Methane cracking for hydrogen production: A review of catalytic and molten media pyrolysis*, 2021, *14*.

[75] McConnachie, M., Konarova, M., Smart, S. *Literature review of the catalytic pyrolysis of methane for hydrogen and carbon production*, *International Journal of Hydrogen Energy*, 2023, *48*, 25660–25682.

[76] Qian, J. X., Enakonda, L. R., Wang, W. J., Gary, D., Del-Gallo, P., Basset, J.-M., Liu, D. B., Zhou, L. *Optimization of a fluidized bed reactor for methane decomposition over Fe/Al2O3 catalysts: Activity and regeneration studies*, *International Journal of Hydrogen Energy*, 2019, *44*, 31700–31711.

[77] Amin, A. M., Croiset, E., Malaibari, Z., Epling, W. *Hydrogen production by methane cracking using Ni-supported catalysts in a fluidized bed*, *International Journal of Hydrogen Energy*, 2012, *37*, 10690–10701.

[78] Amin, A. M., Croiset, E., Epling, W. *Review of methane catalytic cracking for hydrogen production*, *International Journal of Hydrogen Energy*, 2011, *36*, 2904–2935.

[79] Schneider, S., Bajohr, S., Graf, F., Kolb, T. *State of the Art of Hydrogen Production via Pyrolysis of Natural Gas*, *Chemie Ingenieur Technik*, 2020, *92*, 1023–1032.

[80] Scheiblehner, D., Neuschitzer, D., Wibner, S., Sprung, A., Antrekowitsch, H. *Hydrogen production by methane pyrolysis in molten binary copper alloys*, *International Journal of Hydrogen Energy*, 2023, *48*, 6233–6243.

[81] Neuschitzer, D., Scheiblehner, D., Antrekowitsch, H., Wibner, S., Sprung, A. *Methane Pyrolysis in a Liquid Metal Bubble Column Reactor for CO$_2$-Free Production of Hydrogen*, *Energies*, 2023, *16*, 7058.

[82] Schultz, I., Agar, D. W. *Decarbonisation of fossil energy via methane pyrolysis using two reactor concepts: Fluid wall flow reactor and molten metal capillary reactor*, *International Journal of Hydrogen Energy*, 2015, *40*, 11422–11427.

[83] Galanov, S. I., Zherlitsyn, A. G., Medvedev, Y. V., Sidorova, O. I., Shiyan, V. P. *Production of a highly dispersed carbon material and hydrogen from natural gas in a microwave reactor with metallic catalysts*, *Russ J Appl Chem*, 2011, *84*, 997–1002.

[84] Msheik, M., Rodat, S and Abanades, S. *Methane cracking for hydrogen production: A review of catalytic and molten media pyrolysis*, *Energies*, 2021, *14*.

[85] Bellan, P. M. *Fundamentals of Plasma Physics*, 2004.

[86] Lieberman, M. A., Lichtenberg, A. J. *Principles of plasma discharges and materials processing*, Wiley-Interscience, 2005.

[87] Feng, J., Sun, X., Li, Z., Hao, X., Fan, M., Ning, P., Li, K. *Plasma-Assisted Reforming of Methane*, *Advanced science*, 2022, *9*.

[88] Mesrobian, C. *Monolith materials: Taking Methane Pyrolysis from Concept to Industrial Plant*, 2021, https://arpa-e.energy.gov/sites/default/files/2021-01/08%20OK%20-Monolith_ARPAE_MethanePyrolysis2021_v3.pdf, accessed: 2024.

[89] Indarto, A. *Methane conversion in plasma*, 2010, https://www.researchgate.net/publication/286756315_Methane_Conversion_in_Plasma, accessed: 2024.

[90] Boulos, M. I. *Thermal Plasma Processing*, IEEE Transactions on Plasma Science, 1991, *19*.

[91] Radosław D, Azzolina-Jury, F., Travert, A., Maugé, F. *A review on plasma-catalytic methanation of carbon dioxide - Looking for an efficient catalyst*, Renewable and Sustainable Energy Reviews, 2019, *116*.

[92] Daghagheleh, O., Schenk, J., Zarl, M. A., Lehner, M., Farkas, M., Zheng, H. *Feasibility of a plasma furnace for methane pyrolysis: hydrogen and carbon production*, Energies, 2024, *17, 167*.

[93] Daliah, R. *Technology Landscape: Key Players in Methane Pyrolysis*, 2021, https://luxresearchinc.com/blog/technology-landscape-key-players-in-methane-pyrolysis, accessed: 2024.

[94] Fincke, J. R., Haggard, D. C., Detering, B. A., T. Hyde, Wright, R., Bewley, R. L. Haggard, D. C., Swank, W. D. *Plasma thermal conversion of methane to acetylene*, Plasma Chemistry and Plasma Processing, 2002, *22*.

[95] Baumann, P. *Erzeugung von Acetylen nach dem Lichtbogen-Verfahren*, Angewandte Chemie, 1948, 257–288.

[96] Lynum, S., Myklebust, N., Hox, K. *Decomposition of hydrocarbon to carbon black, 6,068,827*, 2000.

[97] Lynum, S., Haugsten, K., Hox, K., Hugdahl, J. *Plasma torch device for chemical processes, 5,486,674*, 1996.

[98] Fabry, F., Fulcheri, L. *Synthesis of carbon blacks and fullerenes from carbonaceous wastes by 3-phase AC thermal plasma, 6th International Conference on Engineering for Waste and Biomass Valorisation*, 2016.

[99] Monolith materials. *Technology for A cleaner World*, https://monolith-corp.com, accessed: 2024.

[100] Moss, J. J., Noelm B. T. *DC Plasma torch electrical power design method and apparatus, WO 2017/019683 A1*, 2017.

[101] Monolith materials, INC. *Monolith process in location Creek Olive*, 2016, https://monolith-corp.com, accessed: 2023.

[102] Plenesys Plasma Energy Systems. *whitepaper-plenesys-clean-hydrogen-competitive-costs*, www.plenesys.com, accessed: 2022.

[103] Plenesys Plasma Energy Systems. *Plasma methane Pyrolysis*, https://plenesys.com/plasma-methane-pyrolysis, accessed: 2024.

[104] Boutot, T. J., Zhuomin, L., Buckle, K. R., Collins, F. X., Estey, C. A., Fraser, D. M., Claus, S. J., Whidden, T. K. *Decomposition of natural gas or methane using cold arc discharge, WO 2007/019664 AI*, 2007.

[105] Boutot, T., Bullerwell, J., Liu, Z., Niu, W., Whidden, T. K., Yang, Y. *Hydrogen and Nanostructured Carbon by Plasma Decomposition of Natural Gas*, ECS Trans., 2009, *16*, 155–166.

[106] HiiROC. *The HiiROC solution*, https://hiiroc.com/our-technology, accessed: 2024.

[107] Spark Cleantech. *Decarbonized Hydrogen*, https://www.spark-cleantech.eu, accessed: 2024.

[108] Levidian Nanosystems Limited. *Putting Waste Methane to Good Use*, https://www.levidian.com/loop, accessed: 2024.

[109] Sakowin Green Energy. *Producing Hydrogen Differently*, https://sakowin.com, accessed: 2024.

[110] Hycamite TCD Technologies. *Hycamite - Decarbonising Industry*, https://hycamite.com, accessed: 2024.

[111]   Lee, D. H., Kang, H., Kim, Y., Song, H., Lee, H., Choi, J., Kim, K.-T., Song, Y.-H. *Plasma-assisted hydrogen generation: A mechanistic review*, *Fuel Processing Technology*, 2023, *247*, 107761.

[112]   Mašláni, A., Hrabovský, M., Křenek, P., Hlína, M., Raman, S., Sikarwar, V. S., Jeremiáš, M. *Pyrolysis of Methane via Thermal Steam Plasma for the Production of Hydrogen and Carbon Black*, *International Journal of Hydrogen Energy*, 2021, *46*, 1605–1614.

[113]   Kim, K. S., Seo, J. H., Nam, J. S., Ju, W. T., Hong, S. H. *Production of hydrogen and carbon black by methane decomposition using DC-RF hybrid thermal plasmas*, *IEEE Trans. Plasma Sci.*, 2005, *33*, 813–823.

[114]   Kim, K. S., Hong, S. H., Lee, K.-S., Ju, W. T. *Continuous Synthesis of Nanostructured Sheetlike Carbons by Thermal Plasma Decomposition of Methane*, *IEEE Trans. Plasma Sci.*, 2007, *35*, 434–443.

[115]   Daghagheleh, O., Schenk, J., Zheng, H., Zarl, M. A., Farkas, M., Ernst, D., Kieush, L., Lehner, M., Kostoglou, N., Obenaus-emler, R. *Optimizing methane plasma pyrolysis for instant hydrogen and high-quality carbon production*, *International Journal of Hydrogen Energy*, 2024, *79*, 1406–1417.

[116]   Zarl, M. A., Ernst, D., Cejka, J., Schenk, J. *A new methodological approach to the characterization of optimal charging rates at the hydrogen plasma smelting reduction process part 1: method*, *Material*, 2022, *15*.

[117]   Naseri Seftejani, M., Schenk, J., Zarl, M. A. *Reduction of Haematite Using Hydrogen Thermal Plasma*, *Materials (Basel, Switzerland)*, 2019, *12*.

[118]   Ernst, D., Zarl, M. A., Cejka, J., Schenk, J. *A New Methodological Approach on the Characterization of Optimal Charging Rates at the Hydrogen Plasma Smelting Reduction Process Part 2: Results*, *Materials (Basel, Switzerland)*, 2022, *15*.

[119]   Zarl, M. A., Farkas, M. A., Schenk, J. *A Study on the Stability Fields of Arc Plasma in the HPSR Process*, *Metals*, 2020, *10*, 1394.

[120]   A. Cuesta, P. Dhamelincourt, J. Laureyns, A. Martínez-Alonso, J.M.D. Tascón. *Raman microprobe studies on carbon materials*, *Carbon*, 1994, *32*, 1523–1532.

[121]   Rosenburg, F., Ionescu, E., Nicoloso, N., Riedel, R. *High-Temperature Raman Spectroscopy of Nano-Crystalline Carbon in Silicon Oxycarbide*, *Materials*, 2018, *11*.

[122]   Kim, H., Kim, H., Kim, S., Lee, S., Kim, J. *Hydrogen Production in Methane Decomposition Reactor Using Solar Thermal Energy*, *Applied Sciences*, 2021, *11*, 10333.

"Be happy, for whoever knows the secret,

Knows that happiness draws happiness."

Rumi

10 Appendix

10.1 Publications

10.1.1 Publications used within this book

1. **Oday Daghagheleh**, Johannes Schenk, Michael Andreas Zarl, Markus Lehner, Manuel Farkas, and Heng Zheng. 2024. "Feasibility of a Plasma Furnace for Methane Pyrolysis: Hydrogen and Carbon Production" Energies 17, no. 1: 167. https://doi.org/10.3390/en17010167

2. **Oday Daghagheleh**, Johannes Schenk, Heng Zheng, Michael Andreas Zarl, Manuel Farkas, Daniel Ernst, Lina Kieush, Markus Lehner, Nikolaos Kostoglou, Robert Obenaus-Emler, "Optimizing methane plasma pyrolysis for instant hydrogen and high-quality carbon production", International Journal of Hydrogen Energy, Volume 79, 2024, 1406-1417,https://doi.org/10.1016/j.ijhydene.2024.07.129.

10.1.2 Scientific conferences and symposiums

1. **METEC & 6TH ESTAD**, Düsseldorf, Germany, June 2023: **Oday Daghagheleh** held a talk and published a paper in conference proceedings 'Hydrogen production by natural gas pyrolysis with thermal plasma – An alternative approach of CO_2-free hydrogen supply for the steel industry'.

2. **EUROMAT23**, Frankfurt, Germany, September 2023: **Oday Daghagheleh** held a talk about 'On the feasibility of a new concept for hydrogen production via CH_4 plasma pyrolysis'.

3. **Hydrogen and Carbon Summit and EUROCA-PRO**, Chania, Greece, September 2023: Discussion and information exchange with international scientists.

10.1.3 Other publications during research activities in Montanuniversität Leoben

1. Heng Zheng, Johannes Schenk, Spreitzer Daniel, Thomas Wolfinger, **Oday Daghagheleh**. 2021. "Review on the Oxidation Behaviors and Kinetics of Magnetite in Particle Scale". Steel Research International, 92. https://doi.org/10.1002/srin.202000687

2. Heng Zheng, Runsheng Xu, Jianliang Zhang, **Oday Daghagheleh**, Johannes Schenk, Chuanhui Li, and Wei Wang. 2022. "A Comprehensive Review of Characterization Methods for Metallurgical Coke Structures" Materials 15, no. 1: 174. https://doi.org/10.3390/ma15010174

3. Heng Zheng, Johannes Schenk, Runsheng Xu, **Oday Daghagheleh**, Daniel Spreitzer, Thomas Wolfinger, Daiwei Yang, Yury Kapelyushin. 2022. "Surface Morphology and Structural Evolution of Magnetite-Based Iron Ore Fines During the Oxidation" Metall Mater Trans B 53, 1644–1660. https://doi.org/10.1007/s11663-022-02475-9

4. Heng Zheng, **Oday Daghagheleh**, Thomas Wolfinger, Bernd Taferner, Johannes Schenk, Runsheng Xu. 2022. "Fluidization behavior and reduction kinetics of pre-oxidized magnetite-based iron ore in a hydrogen-induced fluidized bed". Int J Miner Metall Mater 29, 1873–1881. https://doi.org/10.1007/s12613-022-2511-7

5. Runsheng Xu, Shuliang Deng, Heng Zheng, Xiaoming Huang, **Oday Daghagheleh**, Johannes Schenk, Jianliang Zhang, Jijian Zhu. 2022. "Gasification Behaviors of Ferrocoke With and Without Water Vapor". Metallurgical and Materials Transactions B. https://doi.org/10.1002/srin.202200575

6. **Oday Daghagheleh**, Johannes Schenk, Heng Zheng, Bernd Taferner, Andreas Forstner, Gerald Rosenfellner. 2022. "longterm Reoxidation of HBI in various simulated conditions". Steel Research International, 94. https://doi.org/10.1002/srin.202200535

7. Lina Kieush, Stefanie Lesiak, Johannes Rieger, Melanie Leitner, Lukas Schmidt, and **Oday Daghagheleh**. 2024. "Reoxidation Behavior of the Direct Reduced Iron and Hot Briquetted Iron during Handling and Their Integration into Electric Arc Furnace Steelmaking: A Review" *Metals* 14, no. 8: 873. https://doi.org/10.3390/met14080873

10.2 Declaration of the use of AI-based tools

Purpose	Amount [%]	Tool/Version	Note
Improvement of linguistic readability and grammar check	10	Grammarly 6.8.261	Word Add-In